

**EXPRESSION OF BETA SUBUNIT OF EPITHELIUM SODIUM
CHANNEL AND CYSTIC FIBROSIS TRANSMEMBRANE
REGULATOR IN SMALL AIRWAYS OBSTRUCTION IN CHRONIC
OBSTRUCTIVE PULMONARY DISEASE**

by

BECKY KA MAN CHAN

B.M.L.Sc., The University of British Columbia, 2003

A THESIS SUBMITTED IN PARTIAL FULFILLMENT OF
THE REQUIREMENTS FOR THE DEGREE OF

MASTER OF SCIENCE

in

THE FACULTY OF GRADUATE STUDIES

(Experimental Medicine)

THE UNIVERSITY OF BRITISH COLUMBIA
(Vancouver)

October 2008

© Becky Ka Man Chan, 2008

Abstract

Background: Excess plugging of small airways is associated with premature death in chronic obstructive pulmonary disease (COPD). Over-expression of beta-epithelial sodium channel (β -ENaC) in airway epithelia in mice resulted in plugging of small airways while cystic fibrosis transmembrane regulator (CFTR) negatively regulated ENaC activity in cell models.

Purpose: To test the hypothesis that accumulation of mucus exudates observed with the progression of COPD is related to excess airway epithelial sodium re-absorption as a result of over-expression of β -ENaC and reduced expression of CFTR by small airway epithelia.

Methods: Small airway epithelial samples from frozen lungs from patients at different levels of COPD severity were isolated by laser capture microdissection (LCM). β -ENaC, CFTR, and β -actin (control) gene expression was determined by qRT-PCR and compared to expression in entire airways and lung parenchyma surrounding these airways. β -ENaC protein as well as epithelial mucin expression and mucus plugging were localized and quantified after immunohistochemical and periodic acid Schiff staining, respectively.

Results: β -ENaC mRNA expression had a strong positive correlation with that of CFTR ($p < 0.0001$) in airway epithelia and surrounding lung parenchyma ($p = 0.01$) but not whole airways. β -ENaC mRNA and protein expression were positively correlated ($\rho = 0.40$, $p = 0.05$) and protein expression significantly increased with GOLD stage of COPD severity. Epithelial mucin expression positively correlated with β -ENaC ($\rho = 0.38$, $p = 0.05$) and CFTR

($\rho=0.40$, $p=0.04$) mRNA and with mucus plugging ($\rho=0.43$, $p=0.0002$). CFTR mRNA also correlated positively with mucus plugging ($\rho=0.48$, $p=0.02$).

Conclusions: Strong positive correlations between β -ENaC and CFTR mRNA expression that are limited to the lung parenchyma and epithelium suggest a novel mechanism of mRNA regulation. This differs from their functional relationship where an inverse relationship between CFTR expression and β -ENaC activity has been reported. Positive correlations of epithelial mucin or mucus plugging with CFTR mRNA but not β -ENaC protein expression in the small airway epithelium suggest that CFTR may regulate mucin at this site independently of β -ENaC protein. The relationship between β -ENaC mRNA and epithelial mucin expression could be due to strong correlations between β -ENaC and CFTR mRNA expression but β -ENaC's relationship with COPD GOLD stage suggests it may nevertheless play a role in COPD.

Table of Contents

Abstract	ii
Table of Contents.....	iv
List of Figures	ix
Abbreviations.....	xii
Acknowledgements	xiv
Chapter 1: Chronic Obstructive Pulmonary Disease.....	1
1.1 History of COPD	1
1.2 Epidemiology of COPD	1
1.3 Severity of COPD as classified by four GOLD stages.....	2
1.4 Pathology of COPD	4
1.5 Diagnosis and treatment of COPD	5
Chapter 2: Ion channels and mucus in small airway obstruction in COPD.....	7
2.1 Ion channels and their activity.....	7
2.2 Relationship between ENaC and COPD	8
2.3 ENaC	8
2.3.1 ENaC genes	9
2.3.2 ENaC protein	16
2.3.3 Location and function of ENaC in the lung.....	19
2.3.4 Regulation of ENaC expression and function in the lung.....	19
2.3.5 Activity of ENaC is inhibited by amiloride.....	22
2.3.6 Clearance of ENaC by ubiquitination.....	22
2.4 CFTR.....	24
2.4.1 CFTR gene.....	24
2.4.2 CFTR protein.....	27
2.4.3 Location and function of CFTR in the lung	29
2.4.4 Regulation of CFTR	29
2.4.5 Clearance of CFTR.....	31
2.5 Relationship between ENaC and CFTR.....	32
2.6 Mucus is involved in airway obstruction in COPD.....	35
2.6.1 Genes encoding mucins expressed in the lung.....	36
2.6.2 The structure of mucins	36
2.6.3 Regulation of mucin expression in airway disease.....	38
2.6.4 Secretory mucins and COPD.....	39
Chapter 3: Basic principles of techniques used in the analyses of RNA quantity and quality measurements, and gene and protein expression	40
3.1 Agilent Bioanalyzer 2100.....	40
3.2 Gene expression.....	43
3.2.1 cDNA amplification	43
3.2.2 Taqman® real-time PCR.....	45
3.2.3 Methods of quantification by real-time PCR.....	46
3.2.2.1 Relative quantification.....	46
3.2.2.2 Absolute quantification	47
3.3 Protein expression	48
3.3.1 Immunohistochemistry	48

3.3.1.1 Direct staining method	49
3.3.1.2 Indirect staining method	49
3.3.1.2.1 Alkaline phosphatase anti-alkaline phosphatase method (APAAP)	50
3.3.1.2.2 Avidin-biotin complex (ABC) method.....	52
3.3.1.2.3 Polymeric method.....	54
Chapter 4: Research.....	56
4.1 Working hypothesis.....	56
4.2 Objective.....	56
4.3 Specific aims	56
Chapter 5: Materials and Methods.....	58
5.1 Patient population and lung tissue core production.....	58
5.2 Gene expression studies in whole small airways and lung parenchyma of COPD	59
5.2.1 Sample collection and tissue processing	59
5.2.1.1 Laser capture microdissection (LCM).....	63
5.2.2 PCR on the amplified cDNA from RNA from whole small airways and lung parenchyma of patients from three GOLD categories.....	65
5.2.2.1 RNA extraction.....	65
5.2.2.2 RNA quantity and quality measurement	65
5.2.2.3 cDNA amplification	66
5.2.2.4 TaqMan® real-time PCR	67
5.2.2.4.1 Background.....	67
5.2.2.4.2 TaqMan® probe and primers design.....	68
5.2.2.4.3 Relative PCR of β -ENaC and CFTR expression in whole small airways and lung parenchyma from patients in three different GOLD categories	70
5.2.3 Quantification of β -ENaC and CFTR mRNA expression in whole small airways and lung parenchyma.....	70
For quantifying β -ENaC and CFTR mRNA expression from 99 whole small airways and 98 lung parenchyma from each lung core, relative quantification was applied using the qBASE software [108]. The principle and calculation of this quantification are presented in the Introduction (Section 3.2.3.1).	70
5.3 Gene expression studies in epithelium of small airways of COPD patients using absolute PCR quantification.....	71
5.3.1 Tissue processing for determining amount of tissue required for gene expression analysis (preliminary studies).....	71
5.3.2 Tissue processing for gene expression studies in small airway epithelia of patients from three GOLD categories	71
5.3.3 Preparation of tissue and cells for RNA extraction.....	75
5.3.3.1 Isolation of airway epithelium by LCM.....	75
5.3.3.2 Preparation on whole lung sections with small airways for RNA extraction.	77
5.3.3.3 Preparation of lung epithelial T84 cells for RNA extraction	77
5.3.4 RNA extraction.....	78
5.3.5 RNA quantity and quality measurement	79
5.3.6 Reverse transcription (RT)	80
5.3.7 Absolute PCR quantification.....	80
5.3.7.1 Preparation of full-length human plasmid DNA as standards for absolute PCR quantification.....	80

5.3.7.1.1 Transformation of bacteria with plasmids	80
5.3.7.1.2 Identification of transformed bacteria by α -complementation	84
5.3.7.1.3 Harvesting bacteria transformed with β -ENaC, CFTR, and β -actin plasmid DNA.....	85
5.3.7.1.4 Quantification and identification of plasmid DNA	86
5.3.7.1.5 Preparation of plasmid standards for absolute PCR quantification.....	88
5.3.7.2 TaqMan® real-time PCR on patients' samples to determine the amount of tissue required for gene expression analysis and whether this expression could be detected in samples from GOLD 3/4 patients	90
5.3.8 Determination of β -ENaC and CFTR mRNA expression in epithelia of small airways from patients in three different GOLD categories by absolute PCR quantification.....	91
5.3.8.1 First PCR analysis	91
5.3.8.2 Second PCR analysis.....	91
5.4. β -ENaC and CFTR protein expression and mucin staining	92
5.4.1 Preparation of lung tissue for immunohistochemical analysis of β -ENaC and CFTR and for mucin staining.....	92
5.4.2 Immunohistochemical staining of β -ENaC protein using the polymeric method (Envision™ Detection System Peroxidase/DAB, Rabbit/Mouse).....	95
5.4.3 Immunohistochemical staining of CFTR protein.....	96
5.4.3.1 The APAAP method.....	96
5.4.3.2 The ABC method.....	97
5.4.3.3 The polymeric method (Envision™ G 2 System AP, Rabbit/Mouse [Permanent Red]).....	98
5.4.4 Quantification of β -ENaC protein staining using Image-Pro Plus	99
5.4.5 Staining of mucin with periodic acid Schiff (PAS).....	99
5.4.6 Quantification of mucin staining in the airway epithelium and mucus plugging of the airway by Image-Pro Plus.....	100
5.5 Statistical Analyses.....	101
Chapter 6: Results	103
6.1 Gene expression studies of whole small airways and surrounding lung parenchyma	103
6.1.1 Quantity and quality of RNA from whole small airways and lung parenchyma .	103
6.1.2 Gene expression in whole small airways and surrounding lung parenchyma using PCR and relative quantification.....	107
6.2 Gene expression studies of small airway epithelium	113
6.2.1 Absolute quantification	113
6.2.1.1 Verification of size of vectors, inserts, and plasmids by 0.7% agarose gel electrophoresis.....	113
6.2.1.2 Real-time PCR standard curves of β -ENaC, CFTR and β -actin	117
6.2.2 RNA quantity and quality of RNA from T84 cells	119
6.2.3 LCM of small airway epithelium	119
6.2.4 Determination of the amount of tissues required for LCM followed by RNA extraction to yield RNA of sufficient quantity to quantify for gene expression analyses (preliminary studies).....	121
6.2.5 TaqMan® real-time PCR on patients' samples to determine the amount of tissue required for LCM followed by RNA extraction and gene expression analysis and	

whether this expression could be detected in samples from GOLD 3/4 patients (preliminary studies).....	123
6.2.6 Yield and quality of RNA of epithelia from 83 small conducting airways.....	124
6.2.7 PCR results from T84 RNA and total human placenta RNA and Gene expression of β -ENaC and CFTR in small airway epithelium	129
6.2.8 Variability of background information of patients used for gene expression of small airway epithelium and whole small airways as well as lung parenchyma.....	139
6.3 Protein expression	141
6.3.1 Localization of β -ENaC protein in small conducting airways	141
6.3.2 Protein expression of β -ENaC versus GOLD category, FEV ₁ pp, and β -ENaC or CFTR mRNA expression in small airway epithelium.....	143
6.3.3 Localization of CFTR protein in small conducting airways	149
6.4 Mucin studies using PAS.....	152
6.4.1 Epithelial mucin expression in small airway epithelium.....	152
6.4.2 Epithelial mucin expression versus β -ENaC, CFTR and Muc5ac mRNA expression in whole small conducting airways	161
6.4.3 Mucus plugging in small conducting airways	163
6.5 Summary of Results	175
Chapter 7: Discussion.....	177
7.1 Results supporting the working hypothesis.....	178
7.2 Results against the working hypothesis.....	180
7.3 Novel finding from this project	186
7.4 General conclusion	187
References	189
Appendix	197
UBC research ethics board certificate of approval.....	197

List of Tables

Table 1.1: Description of stages in COPD	3
Table 5.1a: COPD patients selected for gene expression studies of whole airways and lung parenchyma.....	61
Table 5.1b: Summary of the patients in Table 5.1a.....	62
Table 5.2: The assay location and the length of amplicon of each gene analyzed by PCR...	69
Table 5.3a: COPD patients with lung cores with airways fulfilling the criterium required for gene expression studies of small airway epithelium	73
Table 5.3b: Summary of the patients in Table 5.3a.....	74
Table 5.4: Number of sections used for LCM and held by each thermoplastic cap.....	76
Table 5.5: Volume of plasmids and reagents added to each digestion with restriction endonucleases.	87
Table 5.6: COPD patients selected for immunohistochemistry and periodic acid Schiff staining.....	93
Table 5.7: Summary of the patients in Table 5.6.....	94
Table 6.1: The quantity and quality of RNA extracted from whole small airways.....	104
Table 6.2: The quantity and quality of RNA extracted from surrounding lung parenchyma.	106
Table 6.3: Quantity, quality and Ct value determined after PCR of RNA from unclassified, GOLD 0-2 and GOLD 4 patients (preliminary data).	122
Table 6.4: The quantity and quality of RNA extracted from the epithelium of 83 small airways.....	126
Table 6.5: The quantity and quality of the remaining RNA from epithelium of 36 small airways.....	130
Table 6.6: The quantity and quality of the remaining RNA from the epithelium of 32 small airways with detectable gene expression.....	132
Table 6.7: Variability of background information of patients in small airway epithelium and whole small airways as well as lung parenchyma.	140
Table 6.8: Summary of significant results.....	176

List of Figures

Figure 2.1: Nucleotide sequence of the 5' end of the human SCNN 1A gene.....	11
Figure 2.2: Nucleotide sequence of 5' end of the human SCNN 1B gene.	13
Figure 2.3: Nucleotide sequence of 5' end of the human SCNN 1G gene.....	15
Figure 2.4: Schematic diagram of the subunits comprising the ENaC protein.	17
Figure 2.5: Regulation of ENaC activity by PIP ₂ and PI(3,4,5)P ₃	21
Figure 2.6: Nucleotide sequence of 5' end of the human CFTR gene.	26
Figure 2.7: Schematic diagram of CFTR protein.	28
Figure 2.8: The interaction between ENaC and CFTR.	34
Figure 2.9: Schematic diagram of a mucin monomer.	37
Figure 3.1: An electropherogram and gel image of the RNA ladder from the Bioanalyzer pico assay.....	42
Figure 3.2: Schematic diagram of alkaline phosphatase anti-alkaline phosphatase method.	51
Figure 3.3: Schematic diagram of ABC method.	53
Figure 3.4: Schematic diagram of polymeric method.	55
Figure 5.1: Representative micrographs of the laser capture microdissection of a small airway	64
Figure 5.2: Vector diagram of pCMV6-XL6.....	82
Figure 5.3: Diagram of full-length human CFTR plasmid, pBQ6.2	83
Figure 6.1: Gene expression versus GOLD stage in whole small airways and lung parenchyma of COPD patients.	108
Figure 6.2: Gene expression versus FEV _{1pp} in whole small airways and lung parenchyma of COPD patients.....	110
Figure 6.3: Scatterplots showing the correlation between β -ENaC and CFTR mRNA expression.	112
Figure 6.4: Verification of full-length human β -ENaC cDNA in the recombinant pCMV6- XL6 plasmid using 0.7% agarose gel electrophoresis.....	114
Figure 6.5: Verification of full-length human β -actin cDNA using 0.7% agarose gel electrophoresis.....	115
Figure 6.6: Verification of full-length human CFTR cDNA using 0.7% agarose gel electrophoresis.....	116

Figure 6.7: Real-time PCR standard curves.	118
Figure 6.8: Laser capture microdissection of small airway epithelium.....	120
Figure 6.9: Frequency distribution of the amount of total RNA extracted from epithelium of 83 small airways.	128
Figure 6.10: Gene expression versus GOLD stage in small airway epithelium of 24 COPD patients.....	134
Figure 6.11: Gene expression versus FEV _{1pp} in small airway epithelium of 24 COPD patients.....	136
Figure 6.12: Scatterplot showing the correlation between β -ENaC mRNA expression and CFTR mRNA expression in small airway epithelium.....	138
Figure 6.13: Light micrographs showing β -ENaC protein expression in the small airway epithelium.	142
Figure 6.14: β -ENaC protein expression versus GOLD category in 37 COPD patients.....	144
Figure 6.15: β -ENaC protein expression versus FEV _{1pp} in 37 COPD patients.....	146
Figure 6.16: β -ENaC protein expression versus mRNA expression.	148
Figure 6.17: Light micrographs showing CFTR protein expression in the small airway epithelium	151
Figure 6.18: Light micrograph showing PAS staining of the epithelium in a small airway.	153
Figure 6.19: Epithelial mucin expression versus GOLD stage.	155
Figure 6.20: Epithelial mucin expression versus FEV _{1pp}	156
Figure 6.21: β -ENaC and CFTR mRNA expression in airway epithelium versus epithelial mucin expression.	158
Figure 6.22: β -ENaC protein expression versus epithelial mucin expression.....	160
Figure 6.23: β -ENaC, CFTR and Muc5ac mRNA expression in the whole airways versus epithelial mucin expression in COPD patients.	162
Figure 6.24: Light micrograph showing mucus plugging of small airway lumen.	164
Figure 6.25: Mucus plugging versus GOLD stage.	166
Figure 6.26: Mucus plugging versus FEV _{1pp}	167
Figure 6.27: β -ENaC and CFTR mRNA expression in small airway epithelium versus mucus plugging.	169

Figure 6.28: β -ENaC, CFTR, and Muc5ac mRNA expression in the whole airways versus mucus plugging..... 171

Figure 6.29: β -ENaC protein expression versus mucus plugging. 173

Figure 6.30: Epithelial mucin expression versus mucus plugging from 73 airways of 37 COPD patients. 174

Abbreviations

Ab	Antibody
ABC	Avidin-biotin complex
AKAPS	A-kinase anchoring proteins
AMPK	AMP kinase
AP	Activating protein
ASL	Airway surface liquid
ATF	Activating transcription factor
ATP	Adenosine-5'-triphosphate
bp	Base pair
β -2-M	Beta-2-microglobulin
CRE	cAMP response element
CLE	Centilobular emphysema
COPD	Chronic obstructive pulmonary disease
cAMP	Cyclic adenosine monophosphate
C/EBP	CCAAT-enhancer binding protein
CFTR	Cystic fibrosis transmembrane regulator
CHIP	Carboxyl terminus of Hsc70-interacting protein
CT	Computed tomography
DAG	Diacylglycerol
$2^{-\Delta\Delta Ct}$	Delta-delta Ct
ENaC	Epithelial sodium channel
FEV ₁	Force expiratory volume in one second
FRET	Föster resonance energy transfer
FVC	Force vital capacity
GOLD	Global Initiative for Chronic Obstructive Lung Disease
goi	Gene of interest
GRE	Glucocorticoid response element
IC ₅₀	Half maximal (50%) inhibitory concentration
HDAC	Histone Deacetylase
HEK-293	Human embryonic kidney cells
HPRT1	Hypoxanthine phosphoribosyltransferase 1
HRP	Horseradish peroxidase
IL-1 β	Interleukin-1beta
IPTG	Isopropylthio- β -D-galactoside
kDa	KiloDalton
LB	Luria-Bertani
LCM	Laser capture microdissection
MAPK	Mitogen activated protein kinase
MDCK	Madin-Darby canine kidney epithelial cell line

MGB	Minor groove binder
MSD	Membrane spanning domain
MUC	Mucin
NBD	Nucleotide binding domain
Nedd4	Neural precursor cell expressed, developmentally down-regulated 4
NF- κ b	Nuclear factor-kappa B
NHERF1	Na ⁺ /H ⁺ exchanger regulatory factor isoform-1
NRQ	Normalized relative quantity
OCT	Optimal cutting temperature compound
P _{2Y2}	Purinergic nucleotide receptor
PLE	Panlobular emphysema
PAS	Periodic acid Schiff
PCAF	P300/CREB binding protein associated factor
PCL	Periciliary liquid
PCR	Polymerase chain reaction
PDZ	Proline, Aspartic acid, Glutamic acid
PI3K	Phosphoinositide 3 kinase
PIP ₂	Phosphatidylinositol bisphosphate
PKA	Protein kinase A
PKC	Protein kinase C
PP2A	Protein phosphatase-2A
PY	Proline-rich sequence (PPxY)
R	Regulatory
RIN	RNA integrity number
rpm	Revolutions per minute
RT	Reverse transcription
SCNN	Sodium channel, nonvoltage-gated
sgk	Serine/threonine protein kinase
SH3	Src homology 3
SMART	Switching mechanism at 5' end of RNA template
Sp	Specificity protein
STAT	Signal transducer and activator
TGF β	Transforming growth factor beta
TNF α	Tumor necrosis factor alpha
t-SNARE	Target- soluble NSF attachment receptor
Ct	Threshold cycle
v-SNARE	Vesicle-soluble NSF attachment receptor
WW domain	Protein-protein interaction domain containing two conserved tryptophan residues
X-gal	5-bromo-4-chloro-3-indolyl- β -galactoside
YAP65	YES-associated protein-65

Acknowledgements

I would like to extend my gratitude to my two supervisors, Dr. James C. Hogg and Dr. Shizu Hayashi, for providing guidance in order to achieve my goal. Thank you to Dr. Mike Allard and Dr. Darryl Knight, my Supervisory Committee, for contributing their knowledge and expertise in this project. Thanks for Dr. W. Mark Elliott, John V. Gosselink, John E. McDonough, Agripina Suarez, Azadeh Javadifard, Lisa Aird and Luoja Yang, for their technical support. I would like to give a special thank-you to Dr. Joanna Rommens for her gift of full-length human CFTR plasmids, Dr. Pascal Barbry for his gift of rabbit polyclonal β -ENaC antibody and Dr. Norbert Kartner for his gift of L12B4. In addition, I would like to give my appreciation to my family and friends. I do not think I can move to this stage without their support and encouragement. Finally, I would like to thank the British Columbia Lung Association for funding this project.

Chapter 1: Chronic Obstructive Pulmonary Disease

1.1 History of COPD

Chronic obstructive pulmonary disease (COPD) has been described for two centuries [1]. In 1808, Badham used a word “catarrh” to refer to the chronic cough and mucus hypersecretion are symptoms of chronic bronchitis [1]. He also described chronic bronchitis as a disabling disorder. The invention of stethoscope by Laënnec in 1819 led him to describe the symptoms and physical signs of emphysema in 1827 [1, 2]. In 1846, Hutchinson invented the spirometer which provided a tool to diagnose COPD [2]. The CIBA Guest symposium in 1959 and American Thoracic Society Committee in 1962 defined that chronic bronchitis and emphysema were the components of COPD [1]. Before the acronym COPD was assigned, many terms like chronic bronchopulmonary disease, chronic airflow obstruction, diffuse obstructive pulmonary syndrome were used [1]. COPD was firstly applied by William Briscoe in the 9th Aspen Emphysema Conference in 1965 [1].

1.2 Epidemiology of COPD

COPD is currently the fourth most common cause of death in the world [3] and is predicted to be the third leading cause of mortality by 2020 [4]. It is also the fourth leading cause of death in Canada. About 1.5 million Canadians were diagnosed with having this disease in 2008 [5]. Statistics showed that there are more men with COPD compared to women worldwide [4]. However, recently the rate of COPD in women is rising faster than in men in particular age groups [6] because women are increasing their cigarette smoking habit. They are also more susceptible to the tobacco smoke and other risk factors (e.g. occupational dusts

and chemicals, outdoor and indoor air pollution and respiratory infection) [7] because they have relatively smaller lungs and airways as well as more sensitive airways to risk factors compared to men. Also, hormonal factors that influence the lung also may differ between the sexes but their significance is still unknown [8].

1.3 Severity of COPD as classified by four GOLD stages

The Global Initiative for Chronic Obstructive Lung Disease (GOLD) was established by National Heart, Lung, and Blood Institute, National Institutes of Health, USA and the World Health Organization in 1997 [3]. GOLD separates disease severity into four categories (Table 1.1). Each stage is determined by the maximum volume of air expired in one second (FEV_1) and its ratio to the maximum volume that can be forcibly expired without a time limit (FEV_1/FVC) [9]. These two parameters are determined by simple spirometry [3].

Smokers with normal lung function (formerly called GOLD 0) have a higher risk of developing COPD since they are smokers and/or have suffered from related symptoms [3, 10]. An increase in GOLD staging is an indication of increased severity of COPD. The patients will have decreased lung function since they have difficulty exhaling air.

Table 1.1: Description of stages in COPD with the FEV₁ value, the ratio of FEV₁ / FVC and other characteristics of COPD of each stage.

GOLD	FEV₁	FEV₁/FVC	Other characteristics
Smokers with normal lung function (formerly GOLD 0)	> 80% predicted	> 70%	Cough and sputum production
1	≥ 80% predicted	< 70%	With or without symptoms
2	50% ≤ FEV ₁ < 80% predicted	< 70%	With or without symptoms
3	30% ≤ FEV ₁ < 50% predicted	< 70%	With or without symptoms
4	< 30% predicted	< 70%	Or the presence of respiratory failure or right heart failure

1.4 Pathology of COPD

A previous human study [11] showed that COPD is a small airway disease because there is an increase in the small airway resistance. The increase in resistance is due to mucus occlusion and/or narrowing of the small airways. COPD is characterized by irreversible airflow limitation and therefore shortness of breath [3, 12]. Of the many risk factors that contribute to COPD, cigarette smoke is the major known environmental factor related to this disease [3, 12]. In general, COPD is the mixture of diseases including emphysema, chronic bronchitis and small airway obstruction by mucus [13].

Emphysema in Greek means “to blow into” and “air containing, inflated” [6]. Emphysema is due to the destruction of alveolar walls and the capillary feeding the alveoli due to smoking [13]. Enlargement of airspace and decrease numbers of alveoli reduce the surface area of alveoli and therefore impair gas exchange and result in the loss of lung elasticity [12, 13]. Gough distinguished centrilobular emphysema (CLE) from panlobular emphysema (PLE) in 1952 [6]. The location of CLE is in the upper lobes [14]. The characteristic of CLE is destruction of the respiratory bronchioles. On the other hand, PLE is usually in the lower lobes [14]. It is mostly associated with alpha-1 antitrypsin deficiency [13].

Chronic bronchitis is defined as the presence of a chronic productive cough for three months within the span of two years [7, 11]. It is an inflammatory process in the lung associated with airway remodelling, mucus hypersecretion, and defective mucus clearance which causes pulmonary occlusion [3, 13]. Both innate and adaptive immune responses play a role in chronic bronchitis.

Airway obstruction is seen in patients with COPD. Mostly mucus would be produced by central bronchi and aspirated into the small airways [13]. A recent human study [9] showed that there is a relationship between inflammatory exudate accumulation in the small airway lumen and the severity of COPD. This study also showed inflammatory exudates formed in the small airway lumen and caused airway obstruction.

1.5 Diagnosis and treatment of COPD

Spirometry is the gold standard for diagnosing COPD [3]. Patients with chronic cough, sputum production and history of risk factor exposure will undergo spirometric examination. As mentioned in the section 1.3, FEV₁ and FVC are two parameters measured by spirometry. If patients have moderate COPD, they will undergo further examination such as a bronchodilator reversibility test, computed tomography (CT), and arterial blood gas measurement to obtain more information to confirm the disease [3].

COPD is an incurable disease but there are several ways to reduce disease exacerbation. Smoking cessation is the most effective way to decrease the progression of COPD [10, 12]. Pharmacologic treatments such as bronchodilator medication, glucocorticosteroid administration, alpha-1 antitrysin augmentation therapy, and antibiotic usage [3] are currently being used. Non-pharmacologic treatments such as pulmonary rehabilitation, lung-volume-reduction surgery, and, for severe COPD, lung transplantation have been introduced, but the effectiveness of these treatments is not very high [12]. New treatments like mediator

antagonists, protease inhibitors, and anti-inflammatory drugs are still under development [12].

Chapter 2: Ion channels and mucus in small airway obstruction in COPD

Absorptive and secretory ion channels are important in mucus clearance [15]. However, in COPD, the rate of mucus clearance decreases due to mucus occlusion. The epithelial sodium channel (ENaC) and the cystic fibrosis transmembrane regulator (CFTR) are two ion channels that play a role in mucus occlusion in COPD [16, 17].

2.1 Ion channels and their activity

ENaC and CFTR are ion channels and they are classified as ligand-gated or ligand-activated channels [18]. The ion channel has three conformational states, closed, open and inactivated. The channel would be closed when it does not bind to adequate amounts of ligand and would be opened when sufficient amounts of ligand bind to it. The channel will be inactivated when the ligand concentration is too high [19].

Ion channel activity can be determined by the patch-clamp technique [19]. A clean glass micropipette with an open tip diameter at 1 μm is attached to the cell membrane. After applying some suction to the back of the pipette, the pipette and the cell membrane will form a tight seal that prevents ion flow between the pipette and the cell membrane. Therefore, all of the ions will flow into the pipette when the single ion channel opens. The pipette filled with some solution should match the ion composition of the medium. A silver wire contacts the solution in the pipette and conducts the electrical charge to the patch-clamp amplifier. In other words, the patch-clamp technique uses a single electrode to record the single-channel current [19].

To analyze the ion channel activity, channel open probability would be used. The channel open probability is the probability that the activated channel will be opened at any given instant. The open probability increases when the frequency of channel opening increases or the duration of opening increases [20]. The open probability is determined by integrating the area under the Gaussian curve fitted to the amplitude histogram from the patch-clamp technique. When the open probability is multiplied by the number of observed channels in the patch, the average channel activity is calculated [21].

2.2 Relationship between ENaC and COPD

Although alpha (α)-ENaC was shown to be a functional unit (see below in section 2.3), a mouse model by Mall et al. [22] demonstrated that over-expression of beta (β)-ENaC gene but not α - or gamma (γ) subunit causes airway surface dehydration, neutrophilic inflammation, goblet cell metaplasia, mucus hypersecretion and airway obstruction with mucus. The current study was undertaken because these are key pathological features shared between cystic fibrosis and COPD [22, 23] as well as evidence that there is a possible interaction between CFTR, the gene mutated in cystic fibrosis, and ENaC (see section 2.5).

2.3 ENaC

Research started to investigate ENaC because it is involved in pseudohypoaldosteronism type I. Patients having this disease fail to absorb liquid from airway surfaces because of genetic defects in ENaC [24]. ENaC belongs to the degenerins / ENaC superfamily. ENaC

contains three subunits which are alpha (α), beta (β), and gamma (γ) [25]. Rat distal colon was a starting site to isolate ENaC cDNAs because high expression of this channel could be induced by aldosterone or dexamethasone [26]. The α -subunit of rat ENaC (α -rENaC) mRNA was isolated from the rat distal colon and then transfected into *Xenopus* oocytes by Lingueglia's group in 1993 [27]. The activity of ENaC in oocytes was tested by measuring the Na^+ current. Then, the cDNA of the β - and γ - subunits of rat ENaC (β -rENaC and γ -rENaC) were isolated by Canessa's team in 1994 using functional complementation with α -rENaC from the rat colon [28]. Beta-rENaC or γ -rENaC alone was unable to induce a Na^+ current. The Na^+ channel activity could be induced when β -rENaC or γ -rENaC was coinjected with α -rENaC in *Xenopus* oocytes. Alpha-rENaC is sufficient to induce the channel activity. Addition of β -rENaC or γ -rENaC would enhance the channel activity. The cDNA of the α -, β -, and γ -subunit genes of human ENaC were cloned from the kidney by McDonald and her coworkers in 1994 [29].

2.3.1 ENaC genes

ENaCs are encoded by the sodium channel, nonvoltage-gated 1 (SCNN 1) genes [25]. As mentioned earlier, ENaC belongs to the degenerins / ENaC superfamily. Scientists were first able to identify the degenerin gene family in *C. elegans* [25]. Then, the cloning of ENaC cDNAs from rat colon or human kidney and expression in *Xenopus* oocytes allowed the isolation of the cDNA coding the α - [30], β - and γ -subunits [26]. The α -subunit of the human ENaC (α -ENaC) is encoded by SCNN 1A gene which is on the p arm of chromosome 12 (12p13) [28, 31]. The β -subunit (β -ENaC) and γ -subunit of ENaC (γ -

ENaC) are encoded by the SCNN 1B and SCNN 1G genes, respectively. Both genes are located on chromosome 16 (16p12-13) and are only 400 kilo nucleotides apart [28, 31, 32].

All three subunits of human ENaC genes have a translation start codon in exon 2 [33]. The human α – ENaC gene (Figure 2.1) has two alternative 5' exons (1A and 1B) with two transcription start sites that are 52 nucleotides apart from each other [34]. Exon 1A and exon 2 are spliced together after removal of a 665-nucleotide intron 1 to form the 5' end of the mature mRNA of α -ENaC. Exon 1B is within intron 1 and continues unspliced into exon 2 [34]. Sequences further upstream function as a promoter for exon 1A. Sequence within exon 1A acts as a promoter for exon 1B. The α – ENaC gene (Figure 2.1) does not have a TATA or CCAAT box, but has some putative transcription factor binding sites, including those for AP (activating protein)-1, Sp (specificity protein) 1, NF κ -B (nuclear factor-kappa B), and three glucocorticoid response elements (GRE) [25, 35].

```

-240 cctctggttg cccacattcc tgcaactctg tgaccacagc aggggagatt acacattc
-180 agcctggcag ccaacagtgt aaaaaggaae agaatgtcct agggccccgc ctagccccca
-120 gcttcacctg ggcccctccc gggcttgagc aaggttgagc ggggtggcga ggaatcagca
-60 gaaagagga gggaccagga ggaggcagac gcatcccacc tgagtgcgct gctcccactt
  1 agtgagcggg gaggagacct gcagagacct cttctctctt ctctgca ga cctgaagatg
  60 aggetgacct gtgggtgccc ttggagggct gcccaacttgc tgagcctcta gctcctggaa
 120 gcacacttgg gactcccccc ttgctctcct tcctggagac agactccctt tggctgtggc
 240 tccttctatt tgccccccacc actgcccccc acctgectct actcactcag tgccccctct
 300 ccatccctat ctctctgtcc ttgctgttcc ctctctattg tctccctctt tctgcccctc
 360 tgctctcccg gttccccacc aggcctctct agcctggctg gcccttctc cttgtgttgc
 420 cctcctagct gtgggctcag gatccttcta cttgttcaga tctttgccc tcacctgcca
 480 tcctgtcccc cagcctcctt gcctgtctgc gtctaaagcc cctgcccaga gtccgccttc
 540 tcaggtccag tactcccagt tcacctccct cgggagccct ccttccctcg gaaaactccc
 600 ggctctgact cctcctcagc ccctcccccc gccctgctca cctttaattg agatgctaat
 660 gagattcctg tegtctccat ccctggccgg ccagcgggag ggctcccag ccaggccgct
 720 gcacctgtca ggtgagggg aggagaggtt tgctgccag attcaactgg aaaggaacca
 780 gtcccagtc agccgcaacc tgggagtggg aagctggagg cagcccagac ctcttgaggc
 840 cctgcagtc tggggcagag acagaatcag gacacagctc gaggtcaggg ccagagggctg
 900 gagctgaggg cctagagtga gagggggcaa ggcaaggggg ggagaggaag agaggcagga
 960 tttagagagag gaggcagccc agaaagagga gagcaggaga gacccaaaga gaaacagaag
1020 gcagatagag agggagttag aggcaggagc tgagacacag atcctggagg aagaagacca
1080 aaggaagggg gcagagacag aaagggaggt gctaggacaa aactcgaaag gtggccctat
1140 cagggaaagca gaggagaggg cgttctaggg aagcccagct ccggcacttt tggccccaac
1200 tcccgcaggt ctgctggctc caggaaaggt ggaggagggg gggaggagtg ggagaatgtg
1260 ggcgcagggg gggacatggg catggccagg ggcagcctca ctcggttcc aggggtgatg
1320 ggagagggca ctcagggccc agagctcagc cttgaccctg acccttgctc tccccaatcc
1380 actccggggc tcattgaagg gaacaagctg gaggagcagg accctagacc tctgcagccc
1440 ataccaggtc tcattgaggg gaacaagctg gaggagcagg actctagccc tcacagtcc
1500 actccagggc tcattgaagg gaacaagcgt gaggagcagg ggctgggccc cgaacctgcg
1560 gcgccccagc agcccacggc ggaggaggag gcctgatcg agtccaccg ctccctaccga
1620 gagctcttcg agttcttctg caacaacacc accatccacg gcgccatccg cctggtgtgc
1680 tcccagcaca accgcatgaa gacggccttc tgggcagtgc tgtggctctg cacctttggc
1740 atgatgtact ggcaatcgg cctgcttttc ggagagtact tcagctaccc cgtcagcctc
1800 aacatcaacc tcaactcgga caagctcgtc tccccgcag tgaccatctg caccctcaat
1860 ccctacag

```

Figure 2.1: Nucleotide sequence of the 5' end of the human SCNN1A gene. SCNN1A is located on chromosome 12p13. Nucleotide #1 represents the transcription start site of exon 1. Exon 1A, 1B (in orange font from nucleotide 1-721 and from nucleotide 784-1398) and 2 (in blue font) along with the 5' flanking sequence in black intron 1 which includes the sequence in black font after exon 1A are shown in this figure. GRE, Sp1, AP-1 are highlighted in light blue, magenta, and bright green, respectively. NF-κB element is in a magenta box. The translation start codon is highlighted in yellow.

The human β -ENaC gene (Figure 2.2) also has two alternative 5' exons (1A and 1B) which are 1,559 nucleotides apart from each other. The transcription start sites are 46,322 nucleotides and 44,601 nucleotides upstream of exon 2, respectively [33]. Human β -ENaC contains two distinct promoters in its 5' flanking region. The upstream one (before exon 1A) does not have a TATA box while the downstream one has a TATA box. There are some transcription factor binding sites like those for Sp1, AP-1 and -2, and GRE and cAMP response element (CRE) in these two promoters (Figure 2.2).

```

-480 tccaccttgg tggaggtgga agagggcggag ggaagaacgt tctctgggaaa agtggctgca
-420 tatgtccccc taaagtcacc aacttgccca gagqacactg tgtctgcagg ggtgtggatg
-360 tgatgggggg ggcctctgtac tgggtgagcgc gatgcttcgc ctagggtgaa gggacaggta
-300 cacgcgtggg gtgggatgga gtgttcatat atgtggcttg tgatatatac tagagggagc
-240 tgggggtacac tcggatgagg ggtctgtgga catattcgtg gcgcatgtgg gtatcgctgg
-180 tgtcccggag tggggaggga gaatgcggag cgcgtacgtg cggggggcgt ccagtgtccc
-120 tgaacctggc gtgtgggggc tggagcttat tgggagggca gggaggtggt caggggagcc
-60 gggaccgtgc gtgtggccag gccggtagcg cccagtaagc tccaccgcgc ggcgctcccc
1 gtgcttccc gcccctgaac ctgctccctc ccagtcggtc tcgccgcgct cgccgggtgt
61 cccagtgctca ccaacactcg gccgcgcgcg ccagcttggc gcgcaccgcc gcctccgcc
121 ccgcccagac cgcgcatcct ccgtgtccc gctcagccc ccgagcagc atgacggcga
181 accctggctc gcacccggtc tcccgcgcgc tgcccggagt ccttgccgc gcgccttctc
241 ctgcccaccc ccggcccgcg agctcctgtc ccggcctcag ttcccacgg gaggcgctt
301 ggggtcctgt ctgagggcgc tgggacccgg cctggggact gaacgggttg gggcgagg
361 ggagagctgg aggctgggaa aagccccag ggtgcagaag gcagacggg ccagggtccc
421 cggcgtgtct gggacctcag agacggcggc aaagtccctg catagagtgg cgggggcaag
481 aagtgttcca agaggtgaca acaatgaaac tcgagagcgc tttctactg ctgggcacag
541 ctcagcagag cgccttgctc aaacgacctc acttcgctca cagggcatcc ctgtgggtg
601 gttctcttgc tgtccccatt ttgcagaggt gcaaactgag ggtcagaggg tgggaaagct
661 tccctacgct ccaggaacaa gttgctgagc tcagatttga acccaggcag tccgacctg
721 gagcctacct cgtgggctgt cagtggcgtc cggggaacgt gggtttctt tgggggtgatg
781 tggtgaggga ggccagatcc gaaccccctg cagttgtctg cgtgaggat tctcaagtgc
841 taagttgatg tctggacaat gtcatatgac ttaggtgtgc tgtggagggg aagggtctgg
901 gatatagtac agggacattc tcactctagc gtggaggggg aaaaatgagg acagagttta
961 gggaggaagc agcagagacc tccagtcacc aaaaggcaca tcttcccact cacctccacc
1021 agggagtagg ggcagaacaa ccaagactgg ctttggctcc tggcagccca gctctcaca
1081 agccgggtgg atgggtctga aagctcccag agacctgagc accctatctc tagatcccag
1141 catccgtgag cagcccacc tgctaccaca ttgagctgtg taattccatg cagaacaacag
1201 ggatccatc tcttctctct gtaatcttc accctggcc tccagctcc ccaaaggtaa
1261 acaccttcat aatttgaggt gtttccttct agacccttcc cccacactac acagtcatat
1321 atacagagcc atagaaaata tgtaaaatac ttagtaatgt agtaatgttg taggtggata
1381 tttaatagaa atgatgcaac ccttgggagg ctgaggaagg ccggtcactt gaggtcagga
1441 gtttgagacc agcccagcct acatggtgaa accccatttc tacaaaaaaa aaaaaaaaaa
1501 tttagcgggc atagtggat gtcgctgtaa tcccagctac tcaggaggc taaccagggtg
1561 gatcgcttga acccaggagg tggaggttgc agtgagctga gatggcacca ttgactcta
1621 gccgagctca aagagcaaga ctctgtttca gaaaaataga actagaagta gaaatggtac
1681 aaccaccta tgtcattctg caacttgagc cctctcatca ccagttaacc atgctgctgc
1741 atataaaccc agcttattta tttaaactgc tgcattggatt cccgctgtgg ataatgccta
1801 ccgatgggaa ttttaggtgac aaaaattttc aggttggttt ttatttcagc atcttctata
-----intron 1B (44,460 nucleotides)-----
46321 aggtgccact atgcacgtga agaagtacct gctgaagggc ctgcatcggc tgcagaaggg
46381 ccccggctac acgtacaagg agctgctggt gtggactgac gacaacacca acacccacgg
46441 ccccagcgc atcatctgtg aggggcccac gaagaaagcc atgtggttcc tgetcacctc
46501 gctcttgcgc gccctctgtc gctggcagtg ggcattcttc atcaggacct acttgagctg
46561 ggaggtcagc gtctccctct ccgtaggctt caagaccatg gacttcctg ccgtcacctt
46621 ctgcaatgct agcccttca a

```

Figure 2.2: Nucleotide sequence of 5' end of the human SCNN 1B gene. SCNN 1B is located on chromosome 16p12.2-p12.1. Exon 1A and B (in orange font), exon 2 (in blue font), and the 5' flanking sequence, parts of intron 1 (in black font) are shown in this figure. GRE, Sp1, AP-2, AP-1 binding sites, CRE and TATA box are highlighted in light blue, magenta, red, bright green, grey and dark blue, respectively. Nucleotide #1 represents the transcription start site of exon 1. The translation start codon is highlighted in yellow.

The human γ -ENaC gene (Figure 2.3) has a single transcription start site at the 5' end of an untranslated exon which is 3,510 nucleotides upstream of exon 2 [36]. It does not have a TATA or CCAAT box but has two GC-rich boxes required for the promoter activity [36]. Human γ -ENaC gene has some putative transcription factor binding sites such as those for Sp1 and AP-2, and a CRE (Figure 2.3) [36].

```

-360 ttactgctgg tgctagggca ggcacctgcc atctggacgg gagtggaagg aagtcgcggg
-300 gcagtaatag ggggcagcag gcgctttgag gcgccttggg gtaagtgccg cagagaccca
-240 ggatggaatgc aggatggcag ggcggcctcg ggcggcagc aggcactgcg cggtagccca
-180 ggaagacgca gcgcggccgg gctggggcgc agggcggcctt cggggcgcca gggggcgttg
-120 tgaagtcctg gcccgcctcg ggcggtctca ggtgcctggc ggctgggga aagcacctgg
-60 gcaggtgggggg ggcgggggg gggaggcggg tccctagggg ggcggggg ggcggggg
1 aagagcctgc ggcgggggg ccaggggatg ctagccgag ggcgggggg ggagcagcgc
61 acccgcacga gccttggacc ctttggaacc gaaaggtgag ttcagccggg ttgggtcggg
121 ccagctcggg ggttctgggc actggagcgg atgccggggc ccagggcgtc ggacgcgcgc
181 agcgcgggggg gtggcgagc cagcatcagc cggtggcggc ttcccggtgc ccgggatgct
241 gggacacctt gcccggcgg tagcggccag ctctcccggg tctaggcgg ggcggggg
.....intron 1 (3180 nucleotides).....
3481 tcacctgctt ctcttctttg cccctccagc acgcccgtcc tcagagtccc gtcctcaaag
3541 tcccatcctc gccatggcac ccggagagaa gatcaaagcc aaaatcaaga agaatctgcc
3601 cgtagcgggc cctcagggcg cgaccattaa agagctgatg cggtggtagt gcctcaacac
3661 caacacccat ggctgtcgcc gcctcgtggt gtcccggcgc cgctgcgcgc gctcctctg
3721 gategggttc acactgactg ccgtggcctt catcctctgg cagtgcgccc tctcgtctt
3781 ctccttctat actgtctcag tttccatcaa agtccacttc cggagctgg atcttctctg
3841 agtcaccatc tgcaacatca accctataa

```

Figure 2.3: Nucleotide sequence of 5' end of the human SCNN 1G gene. SCNN 1G is located on chromosome 16p12. Exon 1 (in orange font), exon 2 (in blue font), and the 5' flanking sequence, the 5' and 3' ends of intron 1 (in black font) are shown in this figure. Sp1, AP-2 binding sites and CRE are highlighted in magenta, bright green and grey, respectively. The GC-rich box is shown in the red box. Nucleotide #1 represents the transcription start site of exon 1. The translation start codon is highlighted in yellow.

The length of the human α -, β -, and γ -ENaC mRNAs are 3171, 2597 and 3516 nucleotides, respectively and they share more than 80% identity with the respective mouse mRNAs [32].

The introns of all three ENaC genes are in the similar relative positions. The exon-intron structure of these three genes are highly conserved [37] indicating they may have a common evolutionary origin.

2.3.2 ENaC protein

The α -, β -, and γ -ENaC proteins contain 669, 640, and 649 amino acids, respectively [38]. The molecular weights of the non-glycosylated forms of each subunit are 75, 70, and 70 kDa, respectively [26, 39] whereas N-glycosylated forms of each subunit are 85, 85 and 80 kDa, respectively [39]. Although their gene structures, as discussed above, are similar, the proteins only share 26-32% sequence identity. The α and β or γ protein subunits share 26-28% identity while β and γ protein subunits share 32% identity [37].

As mentioned earlier, expression of β -or γ - ENaC alone will not create any change in Na^+ currents. However, expression of α -subunit is able to generate some Na^+ current. A large current is generated when these three subunits are co-expressed together [26, 29]. In order to generate a functional channel, two α -, one β - and one γ -subunits are required [25] (Figure 2.4).

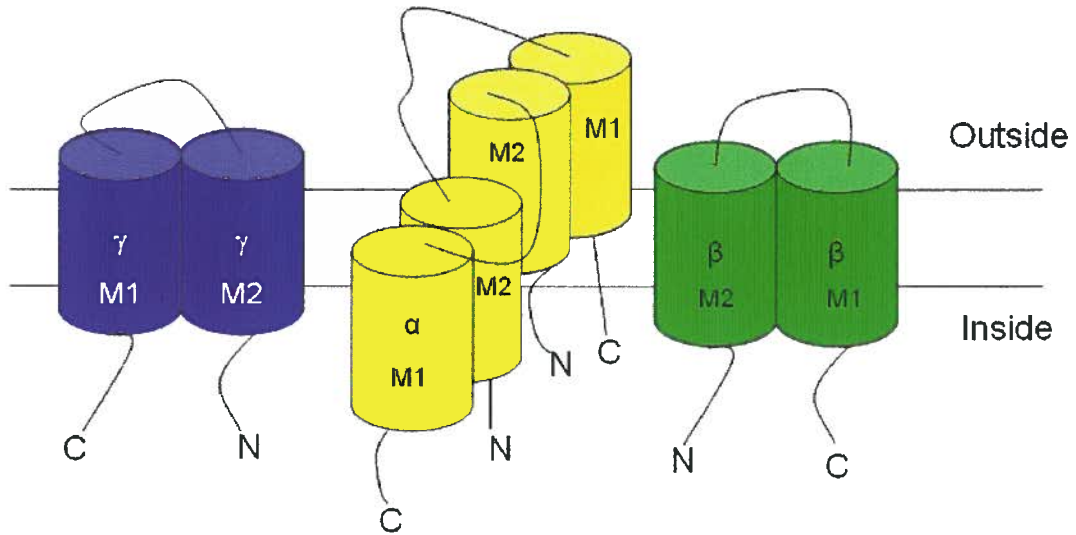


Figure 2.4: Schematic diagram of the subunits comprising the ENaC protein. The two parallel lines represent the bilayer plasma membrane. N and C represent the N-terminus and C-terminus of the ENaC subunits. M1 and M2 represent the membrane spanning domains 1 and 2.

Each subunit of ENaC is composed of four different domains (Figure 2.4). The first domain is the cytoplasmic amino (N)-terminal domain. The second domain is the large extracellular loop. The third domain is two hydrophobic membrane spanning domains (M1 and M2). The last domain is the cytoplasmic carboxyl (C)-terminal domain [31, 38]. The N-terminal domain is involved in subunit assembly, gating, endocytic retrieval and degradation. The lysine residues in this domain may participate in ubiquitination, endocytosis and channel degradation. The N-terminus is important for subunit delivery to the plasma membrane. The extracellular loop located between two membrane spanning domains has two highly conserved cysteine-rich residues which help to bring each subunit to the cell surface. The extracellular loop also has an amiloride binding site that allows amiloride to inhibit ENaC activity. The two membrane spanning domains are important for channel gating. The C-terminal domain is important in channel regulation. Some studies show that the tyrosine, serine and threonine residues in carboxyl tails of the β or γ subunits could be phosphorylated by protein kinase C (PKC) [40, 41]. PKC could decrease the channel open probability in *Xenopus oocytes*. A proline-rich motif is found in C-terminus of all subunits [31]. This motif in C-terminus domain can bind to Nedd4 (neuronal precursor cell expressed developmentally down-regulated gene 4) which allows ubiquitination of ENaC. The details of ubiquitination of ENaC are elucidated in section 2.3.6.

2.3.3 Location and function of ENaC in the lung

ENaC is located in the apical membrane of the polarized epithelium of airways and type II pneumonocytes [25]. As mentioned earlier, two α -, one β - and one γ -subunits are required for making a functional unit of ENaC.

ENaC in the lung is involved in controlling Na^+ transport across the membrane and therefore maintains the ion composition and volume of the luminal fluid [25]. The expression of all three subunits is high in small and medium sized airways while more α - and γ -subunits are expressed in type II pneumonocytes [25, 42, 43].

2.3.4 Regulation of ENaC expression and function in the lung

Expression of ENaC in the lung is transcriptionally regulated by glucocorticoids [28]. Champigny et al. showed that, in primary cultures of rat lung epithelial cells, the three subunits of ENaC are regulated similarly by dexamethaxone [28, 44]. The same group revealed that binding of aldosterone and dexamethaxone to their receptors is required to upregulate mRNA expression of ENaCs in both lung cells and total lung of the rat [44, 45].

Serum and glucocorticoid-regulated serine/threonine protein kinase (sgk1) mRNA levels increase when dexamethasone is administered. This increase in sgk1, in turn, increases ENaC function by increasing the number of ENaC channels assembled at the cell surface [46].

Actinomycin D (a general inhibitor of transcription) decreased the glucocorticoid-regulated expression of β - and γ -ENaC in H441 cells (human lung adenocarcinoma epithelial cell line) [46]. However, the GRE in 5' flanking region of γ -ENaC is not yet identified. Therefore, the mechanism of glucocorticoid-mediated γ -ENaC mRNA expression is still unknown [46].

IL-1 β binds to IL-1 β type I receptor and activates the p38 mitogen activated protein kinase (MAPK) pathway. Activation of this pathway inhibits the activity of the α -ENaC promoter and therefore decreases α -ENaC mRNA and protein expression in both rat and human alveolar type II cells [45].

Physiological regulation is another type of regulation that takes place on the surface of airway to regulate ENaC open probability and control Na⁺ absorption. P_{2Y2} receptors (purinergic receptor) couple via G_{q/11}-coupled receptors to stimulate protein lipase C (PLC β). PLC β hydrolyzes phosphatidylinositol bisphosphate (PIP₂) to generate diacylglycerol (DAG) and inositol 1, 4, 5-triphosphate. DAG activates PKC and therefore down-regulates ENaC activity [47] (Figure 2.5). On the other hand, direct interaction of ENaC with PI(3,4,5)P₃ increases the number and activity of ENaC [48] (Figure 2.5). Studies [49, 50] to determine the putative phosphatidylinositide binding sites in ENaC showed that the cytosolic portion of the N-terminus of β -ENaC is important for PIP₂ or PIP₃ regulation.

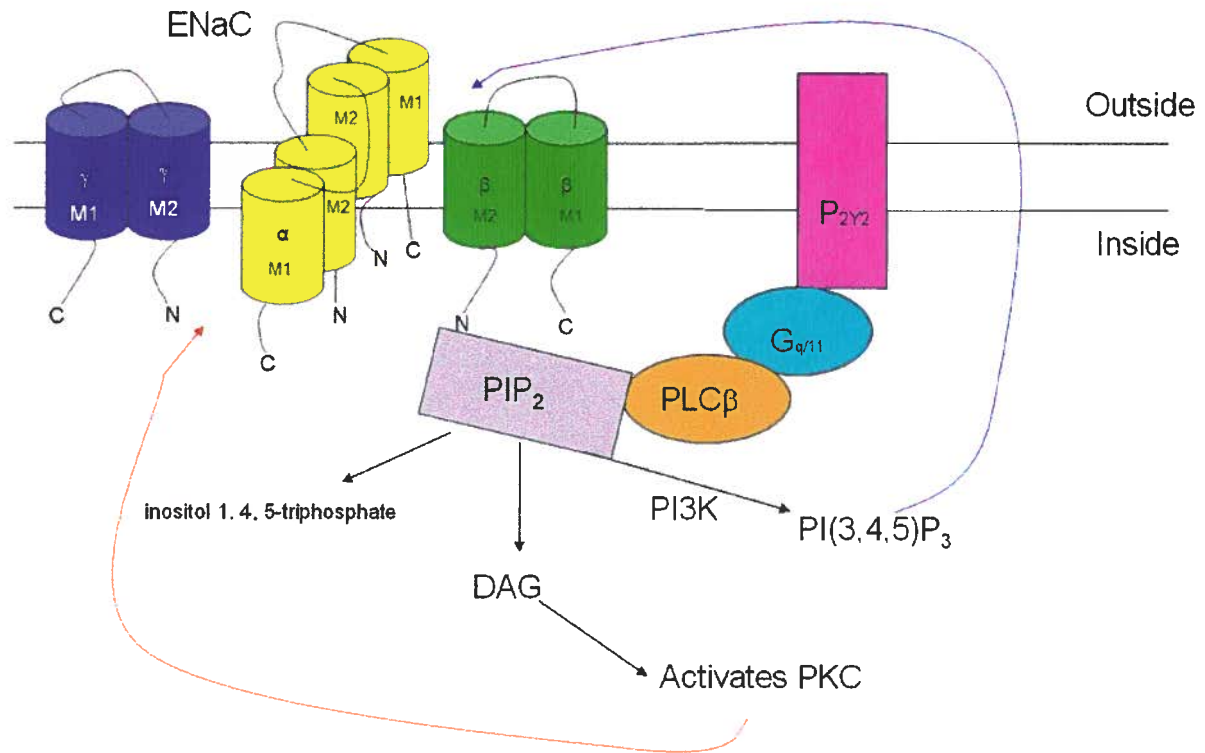


Figure 2.5: Regulation of ENaC activity by PIP₂ and PI(3,4,5)P₃. P₂Y₂ receptors (magenta rectangle) coupled via G_{q/11}-coupled receptors (light blue oval) to stimulate protein lipase C (PLCβ) (orange oval). PLCβ hydrolyzes phosphatidylinositol bisphosphate (PIP₂) (purple rectangle) to generate diacylglycerol (DAG) and inositol 1, 4, 5-triphosphate. DAG further activates protein kinase C (PKC) to decrease ENaC activity (red arrow). Phosphorylation of PIP₂ by PI3K (phosphoinositide 3 kinase) forms PI(3,4,5)P₃. PI(3,4,5)P₃ is able to increase the activity of ENaC (blue arrow).

Neutrophil elastase is a serine protease that is shown to increase Na⁺ current in near-silent ENaC channels in NIH-3T3 cells (mouse embryo fibroblast) [51]. The patch-clamp experiment done in NIH-3T3 cells showed neutrophil elastase increased Na⁺ current by increasing the open probability of near-silent (inactive) ENaCs. Although, the mechanism of the increased open probability of near-silent ENaC by neutrophil elastase is still unknown, previous studies suggested that channel-activating proteases may cleave the anti-inhibitory domain and activate near-silent ENaCs and therefore increase the channel activity [52, 53]

2.3.5 Activity of ENaC is inhibited by amiloride.

Amiloride (3,5-diamino-N-aminoiminomethyl-6-chloropyrazinecarboxamide) was first identified in 1964 after screening for non-steroidal saluretic agents with antikaluretic properties in rats [31]. The IC₅₀ (concentration of a substance that provides 50% inhibition to a certain reaction) of ENaC inhibition by amiloride is about 5 μM [25]. The biological half life of this drug in humans is about 6 to 9 hours. Amiloride is found to have a direct blocking effect on ENaC in the plasma membrane [54, 55]. It binds to the channel pore and to the amiloride receptor in the extracellular loop of ENaC [31, 55] and therefore interferes with the transepithelial Na⁺ transport.

2.3.6 Clearance of ENaC by ubiquitination

The assembly, trafficking and turnover of the three ENaC subunits are not fully understood. Studies using rat ENaC expressed in *Xenopus* oocytes, Madin-Darby canine kidney (MDCK)

cells and NIH-3T3 fibroblast cells showed that ENaC is a short-lived protein where its two subunits, α and γ , have a half life of 1 hour [56]. Rat β -ENaC has a longer half life (more than 3 hours) compared to the α - and γ -subunits [56].

ENaC is retrieved from the plasma membrane via clathrin-mediated endocytosis. After internalization of ENaC, it can be degraded by two different pathways. The assembled ENaC is mono-ubiquitinated and degraded through endosomal and lysosomal pathways [56, 57]. Some mono-ubiquitinated ENaC would extend to form poly-ubiquitinated ENaC for proteasome degradation [57]. However, this degradation system mostly deals with the unassembled or misfolded ENaC in the intracellular pool which is poly-ubiquitinated [57, 58]. Immunohistochemical staining of rat ubiquitin-protein ligase, Nedd4, in the epithelial lining of the lung showed that this protein co-localizes with ENaC [59]. Nedd4 is transported to the apical membrane of the epithelium when the intracellular calcium ion concentration increases [60]. The WW domains (protein-protein interaction domain containing two conserved tryptophan residues) of Nedd4 associate with the proline-rich PY motifs within the C-terminus of each ENaC subunit [58, 60, 61]. Wiemuth et al. showed that Nedd4 decreases the expression of α -ENaC on the cell surface and in the intracellular pool which suggests that Nedd4 is able to control both lysosomal and proteasomal pathways [57].

Rao et al. used HEK-293 cells expressing human ENaC subunits to show that high molecular weight ENaC subunits undergo ubiquitination [39]. The high molecular weight of ENaC is due to covalent modifications such as N-glycosylation [39].

Syntaxin 1A is one of the t-SNARE proteins where t refers to target membrane and SNARE refers to soluble NSF attachment receptor where NSF is an N-ethylmaleimide sensitive fusion protein. Syntaxin 1A decreases the expression of ENaC by inhibiting the insertion of ENaC into the plasma membrane [62]. The heterotrimeric SNARE complex is made of t-SNARE proteins and v (vesicle)-SNARE proteins and mediates the fusion of cellular vesicles with the cell membrane [63]. A model of SNARE protein-mediated insertion of ENaC suggested that the interaction between the t-SNARE protein at the plasma membrane and v-SNARE protein on the internal vesicle regulates channel insertion. Over-expression of Syntaxin 1A disrupts the stoichiometric interactions among the components of the heterotrimeric SNARE complex required for membrane fusion [62]. The direct binding of syntaxin 1A to ENaC prevents the insertion of ENaC into the plasma membrane.

2.4 CFTR

CFTR is the gene mutated in cystic fibrosis and was firstly cloned by Riordan's group in 1989 [64]. CFTR belongs to ATP Binding Cassette Transporter Family because it is able to bind and hydrolyze ATP. Also, CFTR is known as the cAMP regulated chloride channel in epithelial cells [15, 65].

2.4.1 CFTR gene

The gene for CFTR is located on the q arm of chromosome 7 (7q31.2) [15]. Its gene contains 27 exons to give a mature CFTR mRNA of 6129 nucleotides excluding the poly A

tail at the end of 3' untranslated region [64]. Based on NCBI sequence, the major transcription start site is 133 nucleotides upstream of the translation start codon found in exon 1 (Figure 2.6). The 6129 nucleotide mRNA contains a 4440-nucleotide open reading frame that codes for a 1480 amino acid protein. The CFTR promoter region (Figure 2.6) does not have a TATA box, but has a high GC content and Sp1 and AP-1 protein binding sites [66]. There are some other elements found in the promoter region like the inverted CCAAT element as well as CRE and GRE [67].

```

-1800 ttcttaatcc ctttattttc acttgcttgt tgataacaaa gaagaactaa ttattaattt
-1740 atttcaaaat gcatgtatta tatttgatgg gccacactaa cagttataaa ccaacaaca
-1680 gattgggaat ggggaagtgg atgtggtgag ttcaatcaca tgcttgggaa aagtcaatag
-1620 tgaagacaga gtctcacaat tttttgtcat aatggagaga tgaaaacaca ggtagaggat
-1560 ttcaaacacac agagtggatg gtgagttaaa aatgctgaaa ttctttcctg gtgtctaact
-1500 taatgcaatg tggtttatct ctctgctctt ttctctacta ttcaaattta ggataataaa
-1400 gattaaatgt ttctaaatct tactttacaa tatcaagaaa aaaaggtatg cttttgccca
-1380 cgaagaggca aagcagagct atgaaaacct gctgaacaca ttctttattt tcaacacagg
-1320 ttcttgcctt tccatcatga aatgcacatt ttatttgtac tgtatttggg tgaccacaag
-1260 tcaacaacaa gataattcac aagacccttg ccttagatgt gtcggcaata aagtaatcag
-1200 gccaaaattt ttactttcct ttgaattttt caattcaaac acaatgatg cttgctttta
-1140 cacagtaggg ttcaggattg agagggttgg ctcttataaa accgtcaqag acacaggcaa
-1080 tcctacacaa aattctcaga aggaaggcgc ctacgcctgg gaatgccag atgccccca
-1020 gagagttgaa gatggcgttt ctctgagtca ggtcaaagt aacacattac cttcgcttca
-960 aagactgctt ggcttccttt cgggtgatta gtcaagatgt tttgctgact gagactagga
-900 aatctatagg agggcgggtt agtttacatt gttccttgtc attatcgcta aaacctcca
-840 aagcctcctt taaaaatgcg cactgggcta aaaaggatag acaaggaaca catcctgggc
-780 cggaatttac gcaaagcatt atctcctctt acctccttgc agattttttt ttctctttca
-720 gtacgtgtcc taagatttct gtgccaccct tggagtccac tcacctaaac ctgaaactaa
-660 taaagcttgg ttctttttct cgacacgcaa aggaagcgct aaggtaaa caccagaccc
-600 acactgcctc ggaacttttc ggctctctaa ggctgtattt tgatatacga aaggcacatt
-540 ttcttccctt ttcaaaatg caccttgcaa acgtaacagg aacccgacta ggatcatcgg
-480 gaaaaggagg aggaggagga aggcaggctc cggggaagct ggtggcagcg ggtccgggg
-420 agggcggacc ctgacgcgaa ggagggtcta ggaagctctc cggggagccg gttctcccgc
-360 cggtggtctc ttctgtcctc cagcgttacc aactggacct aaagagaggc cgcgactgtc
-300 gccacctgc gggatgggcc tgggtctggc cgtatagga acggacctgg aaggagcgcg
-240 cgcgaggagg ggaggctg ggtcgaatc gggaaaggga ggtgcgggc gtcgaggagg
-180 cgaaggagga gaggaggaag gagcgggagg ggtgctggcg ggggtgcgta gtgggtggag
-120 aaagccgcta gagcaaatc ggggccggac caggcagcac tcggctttta acctgggcag
-60 tgaaggcggg ggaaagagca aaaggaaggg gtggtgtgcg gaggtagggg ggtgggggg
1 aattggaagc aatgacatc acagcaggtc agagaaaaag ggttgagcgg caggcaccca
61 gagtagtagg tctttggcat taggagcttg agcccagacg gccttagcag ggaccaccagc
121 gcccgagaga ccatgcagag gtcgcctctg gaaaaggcca gcgtgtgtctc caaacttttt
181 ttcag

```

Figure 2.6: Nucleotide sequence of 5' end of the human CFTR gene. CFTR is located on chromosome 7 (7q31.2). Exon 1 in blue font is shown in this figure. GRE, Sp1, AP-1 and CRE are highlighted in light blue, magenta, bright green and grey, respectively. The GC-rich box, the inverted CCAAT element, and NF- κ B element are shown in the red, blue, and magenta boxes, respectively. Nucleotide # 1 represents the transcription start site. The translation start codon is highlighted in yellow.

2.4.2 CFTR protein

The CFTR protein contains 1480 amino acids [64]. CFTR is N-glycosylated with a molecular weight of 180 kDa. It is a monomeric transmembrane protein (Figure 2.7) [68] and is composed of five functional domains including two membrane spanning domains (MSD1 and MSD2), two nucleotide binding domains (NBD1 and NBD2) and a regulatory (R) domain [64, 68]. Each MSD contains six consecutive transmembrane spanning regions and they are responsible for forming a functional chloride (Cl^-) channel which allows the Cl^- ion to move through this channel. Cl^- movement is driven by the force generated by the Cl^- concentration gradient. NBD1 is located between MSD1 and the R domain closer to N-terminus while NBD2 is close to the C-terminus. Both NBDs contain ATP binding sites that are important for ATP hydrolysis. Hydrolysis of ATP regulates the opening and closing of this channel. The R domain is unique to CFTR compared with other proteins in ATP Binding Cassette Transporter Family. Some research suggested that the R domain is important for phosphorylation-dependent channel regulation [69].

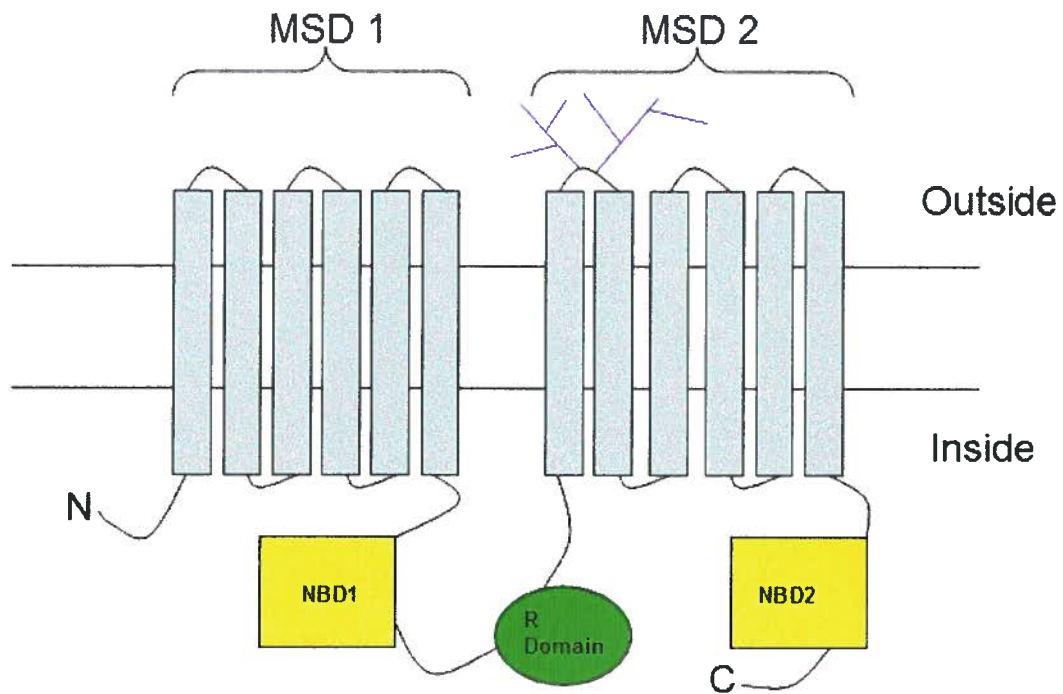


Figure 2.7: Schematic diagram of CFTR protein. This protein is composed of five domains. Two consecutive membrane spanning domains (MSD1 and 2) are within the plasma membrane (two parallel lines). The blue lines on top of the MSD2 represent N-glycosylation sites. Two nucleotide binding domains (NBD1 and 2) and regulatory domain (R domain) as well as N- and C-terminus are in the cytoplasm.

2.4.3 Location and function of CFTR in the lung

In the lung, CFTR is highly expressed in serous cells of the submucosal glands [70]. It is also found in the apical area of plasma membrane of epithelial cells of the small airway [71]. CFTR is also located in Type I and II alveolar cells [42].

CFTR is important for mucus clearance and host defense from airborne microorganisms and particles [15, 64, 68]. CFTR is functional as the cAMP-regulated Cl⁻ channel which controls Cl⁻ transport across the plasma membrane. It also regulates the function of other transport proteins in the membrane such as the K⁺ channel, ENaC, and Cl⁻/HCO³⁻ exchanger [65, 72] through protein kinase A (PKA) / PKC phosphorylation [68]. Studies showed that loss of ENaC regulation by CFTR could increase Na⁺ re-absorption [15].

2.4.4 Regulation of CFTR

Regulation of CFTR is achieved either by controlling its expression or function. Sp1 and AP-1 binding sites (Figure 2.6) are involved in increasing transcription of the CFTR gene. On the other hand, removal of an inverted CCAAT element between nucleotide position -132 to 119 upstream of the translational start site decreases CFTR transcription. The inverted CCAAT element, CRE, and GRE in the CFTR promoter region play a role in regulating its gene expression [67]. CCAAT-enhancer binding protein (C/EBP) and ATF/cAMP (activating transcription factor/cyclic-AMP) form complexes with the inverted CCAAT element which is required for cAMP activation of CFTR transcription [67]. CCAAT displacement protein (CDP/cut protein) is a transcription repressor which also binds to the

inverted CCAAT element. The C-terminus of CDP/cut protein associates with histone deacetylase (HDAC) which changes chromatin to a transcriptionally inactive state [73]. When CDP/cut protein competes with transcriptional activators (ATF and human histone acetyltransferase, hGCN5) to bind to the inverted CCAAT element, CDP/cut protein recruits HDACs to the CFTR promoter and therefore represses transcription [73]. The activity of CDP/cut protein is regulated by p300/CREB binding protein-associated factor (PCAF). CDP/cut protein associates with CREB binding protein (CBP) and p300, two transcriptional coactivators that associate with PCAF. PCAF has histone acetyltransferase activity which acetylates the C-terminus of CDP/cut protein. This acetylation inhibits the binding of CDP/cut protein to nucleosomal DNA which impairs the recruitment of HDAC to nucleosomes. In other words, PCAF corresponds to the inhibition of CDP/cut-mediated repression of gene transcription [74]. IL-1 β , a proinflammatory peptide, is shown to activate NF- κ B protein. NF- κ B proteins binds to the κ B element in the promoter region (Figure 2.6) and therefore increases CFTR mRNA levels [67].

With respect to CFTR function, PKA, Ezrin (an actin binding protein), and NHERF1(Na⁺/H⁺ exchanger regulatory factor isoform-1) play a role in activating CFTR activity [75]. Binding of PKA to Ezrin and binding of CFTR to NHERF1 enhance the phosphorylation of CFTR by PKA [75]. Phosphorylation of CFTR by PKA could enhance the binding of ATP to NBDs of CFTR and therefore accelerate the rate of CFTR opening [68]. Two main protein kinases (PKA and PKC) may play a role in R domain regulation of CFTR [68].

Patch-clamp studies showed that the opening of the CFTR channel is regulated by the PKA signalling pathway [47]. Adenosine from ATP binds to A_{2B} receptors which couple to a Gs protein. This G protein could stimulate adenylate cyclase and therefore converts ATP to cAMP which phosphorylates the PKA-II isoform. The regulatory domains of the phosphorylated PKA interact with A-kinase anchoring proteins (AKAPS) and therefore regulate CFTR by phosphorylation [47].

On the other hand, protein phosphatase 2C could deactivate CFTR in airway and intestinal epithelia [68]. Also, protein phosphatase-2A (PP2A) inhibits the protein expression and activity of CFTR by dephosphorylating the C-terminus of CFTR [75]. AMP kinase (AMPK) also negatively regulates CFTR activity by phosphorylating serine residues found between amino acids 1420-1457 (S¹⁴²⁶, S¹⁴³⁵, S¹⁴⁴², S¹⁴⁴⁴, S¹⁴⁵⁵ and S¹⁴⁵⁶) in CFTR.

2.4.5 Clearance of CFTR

The half life of wild type CFTR protein is more than 48 hours as shown in the pig kidney epithelial cells transfected with wild type human CFTR cDNA. This half life was determined by up-regulating surface CFTR expression by pretreatment of cells with sodium butyrate and low temperature, then treating cells at room temperature for up to 48 hours with cycloheximide (an inhibitor for protein biosynthesis) followed by surface biotinylation, extraction of biotinylated proteins with streptavidin and quantitative immunoblot analysis of biotinylated proteins [76]. PKA is activated by c-AMP that controls the exocytosis and clathrin-mediated endocytosis of CFTR and therefore regulates the expression of CFTR in

the apical membrane [62]. Syntaxin 1A inhibits the insertion of CFTR to the plasma membrane [62, 75]. The possible mechanism is similar to the inhibition of insertion of β -ENaC mentioned in section 2.3.6.

A large portion of CFTR (~75%) is degraded in the endoplasmic reticulum and the remaining is transported to Golgi apparatus [77, 78]. Aberrant forms of CFTR are ubiquitinated in the endoplasmic reticulum and regulated by Hsc70 co-chaperone CHIP (carboxyl terminus of Hsc70-interacting protein) [79] and degraded in proteasomes [78]

2.5 Relationship between ENaC and CFTR

Both ENaC and CFTR are located on the ciliated epithelial cells [80]. Many laboratories used MDCK cells, NIH-3T3 fibroblasts, and *Xenopus* oocytes co-transfected with ENaC and CFTR to show negative regulation of ENaC activity by CFTR [72, 81, 82]. Although this regulatory mechanism is still unknown, some results suggested that there is an indirect interaction between ENaC and CFTR. Some evidence showed that the open probability of ENaC but not the number of active channels is inhibited by CFTR. This could be shown in A6 cells which are the epithelial cells derived from the kidney of *Xenopus laevis*. [31, 83]. However, other studies suggested that this negative functional regulation is due to a direct protein-protein interaction. For example, the C-terminus of α -rENaC, β -rENaC and/or N-terminus of γ -rENaC interact with the region between N-terminus site of NBD1 and intracellular R domain of CFTR which are important for negative functional regulation of ENaC by CFTR [41, 84].

There is another means of interaction between CFTR and ENaC (Figure 2.8). CFTR binds to the PDZ1 domain of NHERF1 (see section 2.4.4 on the regulation of CFTR activity by NHERF1). The YES-associated protein-65 (YAP65) binds to the PDZ2 domain of NHERF1. The WW domain of YAP65 binds to the PY motif in the C-termini of the three ENaC subunits. Because the Src-homology-3 (SH3) domain of YAP65 interacts with the non-receptor tyrosine kinase c-YES, a member of the c-Src kinase family, and because c-Src is a potent inhibitor of ENaC, it is possible that c-YES mediates the CFTR inhibition of ENaC-channel activity [75].

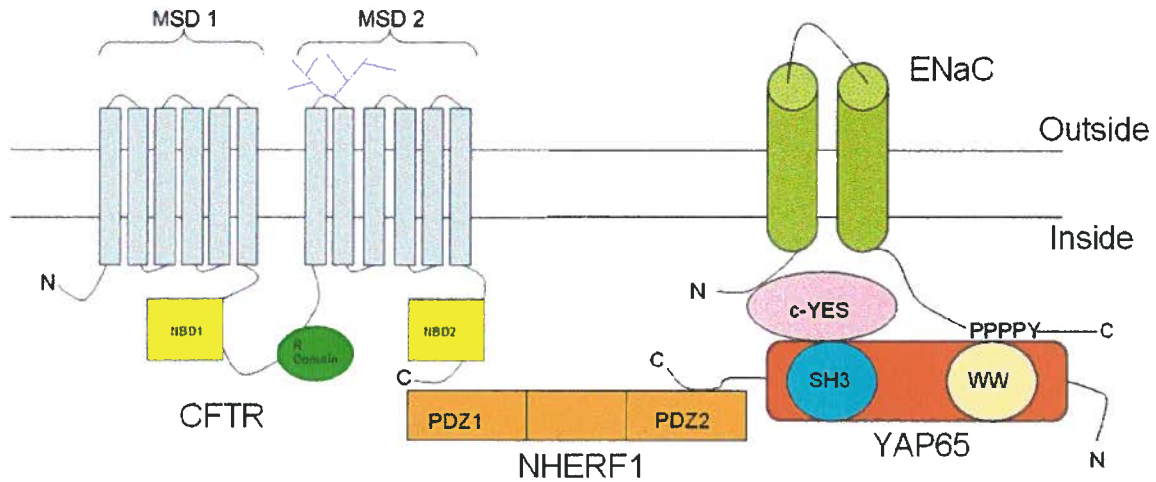


Figure 2.8: The interaction between ENaC and CFTR. CFTR binds to the PDZ1 domain of Na⁺/H⁺ exchanger regulatory factor isoform-1 (NHERF1) (orange rectangle). The YES-associated protein-65 (YAP65) (red rectangle) binds to the PDZ2 domain of NHERF1. The WW domain of YAP65 (yellow oval) binds to the PY motif in the C-termini of the three ENaC subunits. The Src-homology-3 (SH3) domain (light blue oval) of YAP65 interacts with the non-receptor tyrosine kinase c-YES (pink oval), a member of the c-Src kinase family, and because c-Src is a potent inhibitor of ENaC, it is possible that c-YES mediates the CFTR inhibition of ENaC channel activity.

2.6 Mucus is involved in airway obstruction in COPD

In the lung, mucus clearance is an innate immune response for preventing foreign particles from accumulating in the airway which, in the case of bacteria, cause infection. This clearance system includes epithelial water and ion transport, mucus, cilia beating and cough [80]. Mucin is secreted by goblet cells. The mucus layer and periciliary liquid layer (PCL) together form the airway surface liquid (ASL) which lies on top of the airway surface [83]. Mucus has viscoelastic properties [80]. It lubricates the airway lumen and traps foreign airborne particles such as dust and bacteria. PCL is a low viscosity solution which allows cilia to beat efficiently and to move mucus along the airway [85]. ASL contains not only saltwater but also proteases/antiproteases, oxidants/antioxidants, antibodies and antiseptic enzymes (defensin and lysozyme) to inactivate pathogens [83]. The hydration of ASL is regulated by epithelial water and ion transport.

Mucus dehydration, mucin hypersecretion, and sputum production can be seen apparently in patients with asthma, cystic fibrosis and COPD [80, 86, 87]. Mucin hypersecretion by goblet cells or ASL dehydration due to abnormal Na^+ absorption and/or Cl^- secretion cause mucus adhesion to the airway surface and mucus obstruction in the small airway in COPD [80]. These factors impair mucus transport and this results in the accumulation of foreign particles in the small airway and therefore exacerbate the disease. Hogg et al. [9] found that occlusion of the lumen of small conducting airways by inflammatory exudates containing mucus increases as lung function decreases. This mucus occlusion causes premature death in patients with COPD after lung volume reduction surgery [88]. These patients may have problems clearing some airborne bacteria [88].

2.6.1 Genes encoding mucins expressed in the lung

MUC1 is the first membrane-bound mucin cDNA cloned from breast cancer tissue. This gene is located on the q arm of chromosome 1 [87]. MUC 4 is the membrane-bound mucin as well and its gene is located at the q arm of chromosome 3 [87, 89]. MUC2 is the first secreted mucin cDNA cloned from intestinal epithelium [90]. MUC2, MUC5AC and MUC5B are major secreted mucin genes expressed in the airways. These three secreted mucin genes are located at the p arm of chromosome 11 (11p15) [87].

2.6.2 The structure of mucins

Mucus consists of secreted mucins, water, ions, cells, and cellular debris [87, 90]. Mucin is a glycoprotein (Figure 2.9) and is the main component of mucus. Of the two different types of mucins, the membrane bound mucins are located on the surface of the plasma membrane. They are important for cellular adhesion, pathogen binding, and signal transduction. On the other hand, secreted mucins are stored in secretory granules which transport them to the cell surface where the mucins contribute to the formation of the mucus layer in the lumen of the airways. The mucin monomer (Figure 2.9) has a protein backbone with repeated structures. Repeated structures represent serine and threonine residues. They form glycosidic linkages with oligosaccharides. The cysteine-rich domains in secreted mucins polymerize with those of other mucin monomers to make secreted mucin more viscous [87].

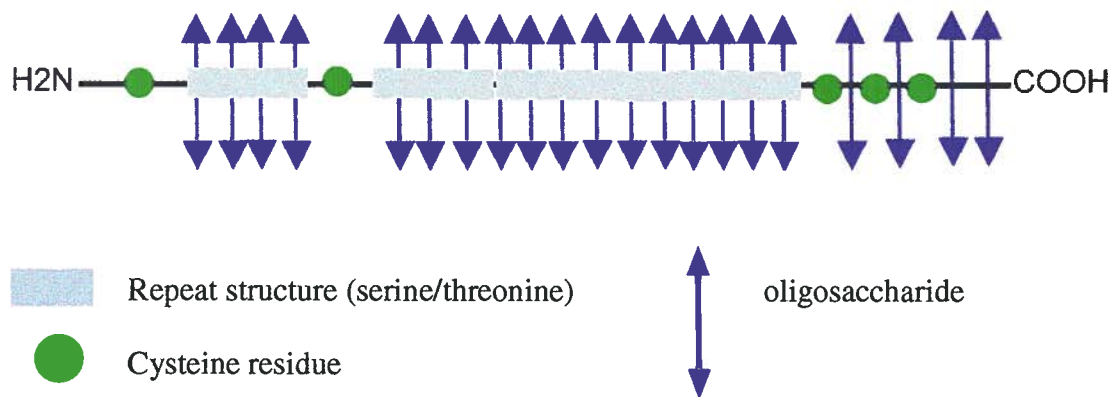


Figure 2.9: Schematic diagram of a mucin monomer. The black horizontal line with H₂N (N-terminus) on the left side and COOH (C-terminus) on the right side is the protein backbone. The serine/threonine residues are the repeat structure shown as the blue rectangular boxes. The cysteine residues are shown as green circles. The oligosaccharides are shown as vertical blue lines with arrow heads.

2.6.3 Regulation of mucin expression in airway disease

In the healthy state, MUC1 and MUC4 are highly expressed in lung. MUC2 and MUC5AC are mainly expressed by goblet cells of the airway epithelium. MUC5B is expressed in mucosal cells of the submucosal glands [90].

Toxic agents, airway inflammatory mediators including cytokines and chemokines and bacteria (e.g. *Pseudomonas aeruginosa*) are shown to up-regulate the expression of certain mucin genes in the airways [89, 90]. Tobacco smoke, ammonia vapor and nitric oxide are examples of toxic agents that stimulate mucin release. Studies suggested that IL-13 could stimulate signal transducer and activator (STAT) 6, one of the transcription factors in the STAT family that binds to the MUC5AC promoter and therefore increases mucin production [87]. Studies using cycloheximide show that activation of p38 MAPK by IL-13 requires STAT6 activation and subsequent de novo protein synthesis. Indirect phosphorylation of p38 MAPK by IL-13 could upregulate MUC5AC mRNA expression [91]. Cell surface receptors like epithelial growth factor receptor, P_{2Y2} receptor and Toll-like receptor 2 also play a role in mucin gene regulation. These receptors may stimulate the p38 MAPK pathway. Therefore, activation of several transcriptional factors by this p38 MAPK system could up-regulate MUC2 and MUC5AC gene expression [90, 91]. On the other hand, TNF- α , neutrophil elastase, IL-8 and transforming growth factor - β are responsible for regulating several MUC genes post-transcriptionally. Colonization and accumulation of mucoid *Pseudomonas aeruginosa* in the airways are responsible for up-regulation of MUC5AC in the 4 kb DNA fragment upstream of the MUC5AC transcription start site [92].

2.6.4 Secretory mucins and COPD

Human studies [86, 87] demonstrated that there was no goblet cell hyperplasia in bronchiolar epithelium in COPD patients. However, more periodic acid Schiff (PAS) positive mucin staining was seen in bronchiolar lumen of patients with COPD than smokers and non-smokers with normal lung function. Immunohistochemical staining of bronchioles [86] showed that MUC5AC protein expression was higher in COPD patients than in non-smokers and smokers without COPD. This protein was predominant in goblet cells, the cilia, and cytoplasm of the airway epithelial cells. Both MUC5AC and MUC5B proteins were found in the airway lumen. The same study revealed that more MUC5AC protein expression was seen in the current smoking group of the COPD patients than smokers and non-smokers with normal lung function, suggesting that cigarette smoking may trigger the expression of this protein in these patients.

Chapter 3: Basic principles of techniques used in the analyses of RNA quantity and quality measurements, and gene and protein expression

3.1 Agilent Bioanalyzer 2100

The Agilent Bioanalyzer 2100 has been available since 1999. It is the first lab-on-a-chip system in the world [93-95]. The Agilent Bioanalyzer 2100 is an instrument connected to a computer to provide one-step RNA separation and quantification [94]. Basically, an RNA 6000 LabChip kit is provided with 12-well microfluidic chips, syringe, spin filter, sample buffer, gel matrix and fluorescent dye [96]. Two types of chips, nano and pico, are available to measure RNA concentration and quality [94, 97]. Nano assay provides a linear range of quantification between 25 ng/ μ l to 500 ng/ μ l while pico assay provides a linear range between 200 pg/ μ l to 5000 pg/ μ l [94, 97]. An RNA ladder is available from Ambion, Inc [96].

The Agilent Bioanalyzer 2100 works in the similar way as the combination of a gel electrophoresis apparatus and a UV spectrophotometer. The instrument has twelve platinum electrodes which connect to a high power voltage supply. The voltage setting controls the precision of the RNA separation [95, 96]. Eleven samples and an RNA ladder in the pico or nano chip are separated through a single separation channel sequentially. The fluorescence from the dye bound to the nucleic acids is monitored between 670 nm and 700 nm [96]. An electropherogram and/or gel like image (Figure 3.1) is displayed on the computer screen. RNA concentration is based on comparing the samples under investigation to RNA ladder fragments and the unit of [RNA] is in ng/ μ l. The RNA ladder produces six peaks representing different size RNA fragments (0.2, 0.5, 1.0, 2.0, 4.0, and 6.0 kilonucleotides in

the output from the RNA ladder (Figure 3.1). The total concentration of RNA ladder is 1000 pg/ μ l in the pico assay and 150 ng/ μ l in the nano assay [96].

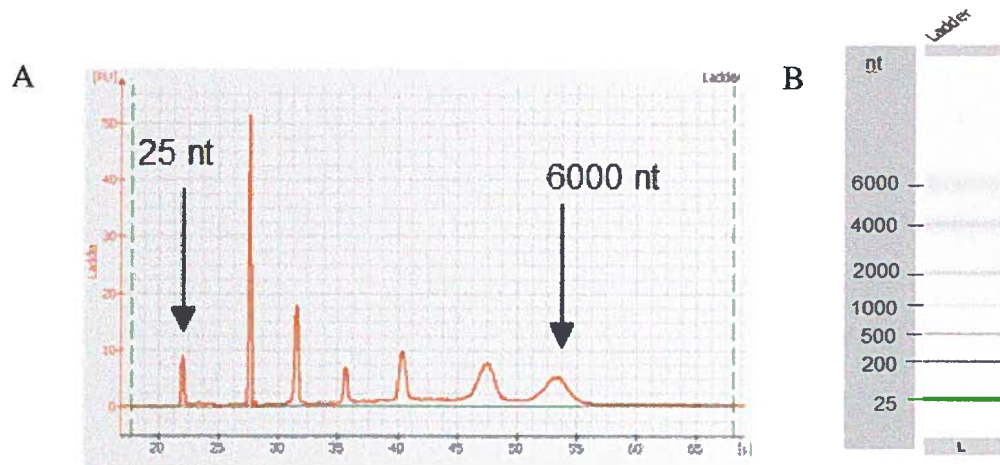


Figure 3.1: An electropherogram and gel image of the RNA ladder from the Bioanalyzer pico assay. A) The electropherogram shows 7 peaks. The first peak on the left is the RNA marker which is 25 nucleotides (nt) long followed by the 200, 500, 1000, 2000, 4000, and 6000 nt fragments of the RNA ladder. B) The gel image showing the RNA marker size and 6 corresponding bands of RNA ladder plus the 25 nt fragment of RNA marker.

Compared to traditional gel electrophoresis and spectrophotometry which require relatively large amounts of sample, only 1 μ l (200 pg RNA for pico chip and 25 ng RNA for a nano chip) of RNA sample is loaded in a chip [97]. Also, since the laser excites the fluorescent dye which is intercalated into the RNA in the sample, this technique is more sensitive compared to the traditional gel electrophoresis and UV spectrophotometer [97]. The data for each RNA sample is analyzed in real-time. The results from Bioanalyzer give information regarding the RNA quality using RNA integrity number (RIN) [98]. RIN is based on the height, width, and number of peaks in different quadrants of an electropherogram of each RNA sample [99]. This categorization of RNA integrity had been created using about 1300 RNA samples with different levels of integrity from 3 different mammalian species [98]. The electropherogram with different peak distributions of each sample is classified by a predefined RIN system where a value of 1 represents degraded RNA and 10 represents intact RNA [98, 99]. The instrument can provide results within 25 minutes [96]. The disadvantage of using Agilent Bioanalyzer is that the injection and separation steps may be difficult to reproduce consistently [97]. The separation of the sample is based on electrophoretic migration. Slight differences between the electrophoretic mobilities of the components in the sample would produce greater intra-plate and inter-plate variation.

3.2 Gene expression

3.2.1 cDNA amplification

cDNA amplification is based on two processes, first strand cDNA synthesis [100] and long-distance PCR amplification [101]. cDNA synthesis using a technique called SMART™

(Switching Mechanism at 5' End of RNA Template) applies two properties of the Moloney murine leukemia virus reverse transcriptase. The first is the addition of non-template oligonucleotides to the 3' end of the newly made cDNA when the enzyme reaches the 5' end of the mRNA template (terminal transferase activity). The second feature of this enzyme is its ability to switch to another template [102]. In the SMART technology (BD BioSciences Clontech), oligo dT₃₀ is inserted in the 3' BD SMART™ CDS Primer IIA: 5'-AAGCAGTGGTATCAACGCAGAGTACT₍₃₀₎VN-3'. V can be A, G, or C while N can be A, T, G or C. Oligo dT of the primer binds to the poly A tail of the mRNA template and reverse transcriptase initiates the 1st strand cDNA synthesis. When this enzyme reaches the 5' end of the mRNA template, its terminal transferase activity adds deoxycytidines to the 3' end of the newly synthesized cDNA. Universal template amplification BD SMART™ IIA oligonucleotide, 5'-AAGCAGTGGTATCAACGCAGAGTACGCGGG-3', binds to the deoxycytidine added onto the first strand cDNA. This allows the reverse transcriptase to switch templates. Compare to traditional reverse transcription, the first strand cDNA sequence has additional 5' and 3' universal priming sites for long-distance PCR amplification.

In long-distance PCR amplification, a BD SMART IIA oligonucleotide (23 nucleotides long) 5'-AAGCAGTGGTATCAACGCAGAGT-3' was used (BD BioSciences Clontech). Taq DNA polymerase and a small amount of proofreading DNA polymerase amplify different size DNA fragments [101] This combination allows amplification of the full-length cDNA with less error rate in base pairing and yields more longer products compared to traditional PCR [101]. TaqStart™ antibody (1.1 µg/µl) is mixed with the above polymerases in the

PCR reaction to improve the efficiency and specificity of PCR reaction by reducing the non-specific amplification product synthesis [103]. TaqStart™ antibody is a neutralizing antibody which recognizes Taq polymerase, inhibits enzymatic activity during PCR set-up at room temperature [103]. The inhibitory process is reversible. The Taq polymerase gains its activity back when the antibody is inactivated by the high temperature used during amplification.

3.2.2 Taqman® real-time PCR

Real-time PCR is a gold standard for detection and quantification of nucleic acid molecules because of high sensitivity and specificity, good reproducibility, and large linear range of detection [104, 105]. Taqman real-time PCR is based on the use of the 5' exonuclease activity of Taq polymerase which hydrolyzes the probe bound to the template (Section 5.2.2.4.1).

PCR is separated into four different phases, linear ground phase, early exponential phase, exponential phase, and plateau phase. A PCR cycle at which a significant increase in reporter fluorescence detected during the exponential phase of amplification is called threshold cycle (Ct). Ct is determined by the point at which the amplification plot of fluorescent signal versus cycle number crosses a threshold of the fluorescent signal that is set within the exponential phase of the amplification.

3.2.3 Methods of quantification by real-time PCR

3.2.2.1 Relative quantification

Relative quantification is based on determining the relative change in mRNA level. For this quantification, it is not necessary to have a calibration curve based on standards of known concentration. Relative quantification could be calculated with or without correction for PCR efficiency [106, 107]. Under the optimal conditions, the target DNA doubles during each PCR cycle. For the efficiency correction model, PCR efficiency is equal to $10^{-1/\text{slope}}$ [106]. The slope is that of the PCR standard curve which represents the relationship between Ct value and input quantity of total RNA or cDNA.

The delta-delta-Ct method ($2^{-\Delta\Delta Ct}$ method) is a mathematical model to calculate the changes in gene expression as a relative fold change between an experimental sample and a calibrator [106]. In the classic $2^{-\Delta\Delta Ct}$ method, only one reference gene could be applied. Hellemans et al. modified the classic $2^{-\Delta\Delta Ct}$ method to allow more than one stably expressed reference gene to be applied in the gene expression studies and this improved normalization [108]. Q-base is an open source program developed by Hellemans team that applies the modified $2^{-\Delta\Delta Ct}$ method for automatic analysis of gene expression [107].

According to Hellemans [108]:

$$NRQ = \frac{E_{goi}^{\Delta Ct, goi}}{\sqrt[f]{\prod_0^f E_{ref_o}^{\Delta Ct, ref_o}}}$$

Where

NRQ = the normalized relative quantity,

E = the base for exponential amplification, also referred to as the efficiency of the PCR reaction and calculated as

$E = 10^{\left(\frac{-1}{slope}\right)}$ where the slope is that of a standard curve generated from the Ct and quantity values of a dilution series for the amplicon of interest,

$\Delta Ct = Ct$ of the reference sample – Ct of the sample for the target gene or gene of interest (goi),

Denominator = the sample specific normalization factor which is calculated from the geometric mean of the normalized relative quantities of the reference genes.

3.2.2.2 Absolute quantification

Absolute quantification is based on a standard curve made from serially diluted standards [106]. The linear relationship between Ct and the starting amount of the standards in the standard curve is used to determine the copy number or total RNA concentration in the samples under investigation [106, 109]. The absolute quantification method assumes that

standards and samples have similar amplification efficiencies. The standards can be made of either RNA or DNA. Recombinant RNA derived from the PCR fragment containing the T7 promoter sequence can be prepared by *in vitro* transcription with a T7 Transcription Kit [110]. The RNA standards would be reverse transcribed to cDNA standards. DNA standards are prepared from purified recombinant plasmid DNA carrying the cDNA of interest, purified PCR product or commercially synthesized oligonucleotides [106] [109].

The standard curve made of DNA standards is better than RNA standards because DNA is more stable and reproducible [106]. Recombinant plasmid DNA is able to resist contaminating RNAase activity and multiple freezing and thawing during long term storage.[110]. Using recombinant plasmid DNA can mimic the actual mRNA in the samples to be measured because the recombinant plasmid DNA has the full-length cDNA which corresponds to the size of the respective mRNA in the sample. The disadvantage is that it is time consuming to generate plasmid DNA standards. Also, because plasmid DNA standards do not require a reverse transcription step, it cannot be used to account for any differences in the efficiency of reverse transcription [106, 110].

3.3 Protein expression

3.3.1 Immunohistochemistry

Immunohistochemistry is used to localize proteins in tissue sections using labeled antibodies to locate the interaction between antigen and antibody [111]. The antigen-antibody complex

can be visualized by the label on the primary antibody which can be a fluorescent dye, enzyme activity, radioactive isotope or colloidal gold.

Coons and his colleagues first used a fluorescent dye to study Pneumococci in 1941 [112]. Nakane and Pierce developed an indirect staining technique (see section 3.3.1.2) using non-fluorescent primary (1°) and secondary (2°) antibodies (Ab) and horseradish peroxidase (HRP) in 1966 [113]. Mason and Sammons in 1978 suggested alkaline phosphatase (AP) as another choice for labelling.[114].

3.3.1.1 Direct staining method

In the direct staining method [111], antibody labelled with a fluorescent dye (for example, fluorescent isothiocyanate labelled Ab detects an antigen on a section or smear of tissue. This process is short because only one Ab is involved. However, the fluorescent signal is low because only one molecule of Ab with fluorochrome binds to one antigen recognition site [111]. Also, the binding site of Ab could be blocked by the conjugated fluorochrome which leads to decreased sensitivity of detection [111]. Therefore, this staining method is not optimal.

3.3.1.2 Indirect staining method

In the indirect staining method, 1° and 2° Ab are used. The unlabelled 1° Ab detects antigen on the tissue and the labelled 2° Ab binds to the 1° Ab. This method is more sensitive

because more than one molecule of 2° Ab could bind to one molecule of 1° Ab; therefore, the signal is amplified.

3.3.1.2.1 Alkaline phosphatase anti-alkaline phosphatase method (APAAP)

In the APAAP method (Figure 3.2), an extra Ab, besides to two used in the usual indirect methods, is involved and is coupled with AP. This complex immunologically binds to 2° Ab. The use of many 2° Ab and anti-alkaline phosphatase conjugated with AP together could amplify the signal without using additional 1° Ab [21].

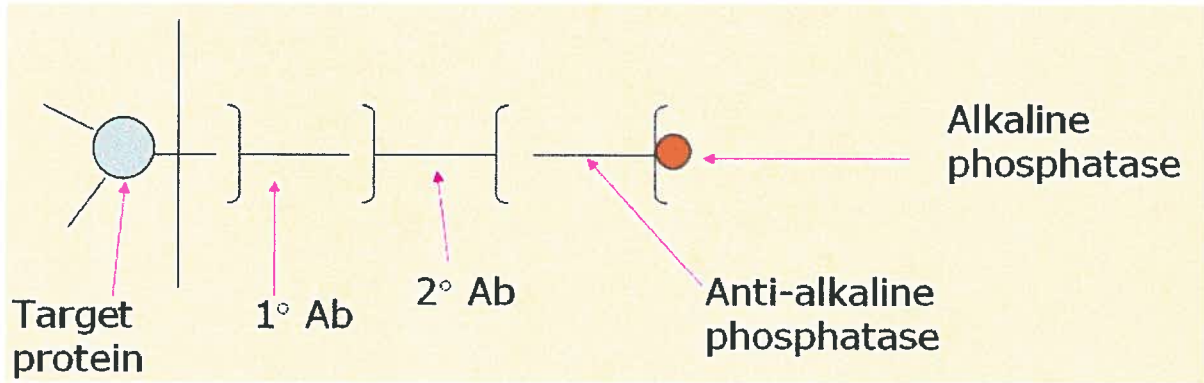


Figure 3.2: Schematic diagram of alkaline phosphatase anti-alkaline phosphatase method.

3.3.1.2.2 Avidin-biotin complex (ABC) method

In the ABC method (Figure 3.3), avidin, a glycoprotein of egg white is used. It consists of four identical subunits. Each subunit can bind to one biotin. Biotin is a vitamin that forms the coenzyme or prosthetic group of some enzymes that transfer carboxyl groups [111]. This avidin-biotin complex can bind to biotinylated 2° Ab and biotinylated peroxidase or phosphatase, as either HRP or AP, respectively. Each avidin provides four binding sites for the biotinylated Ab or enzyme to bind and therefore amplifies the staining intensity [115, 116]. The enzyme converts a colourless substrate to a coloured product [115, 116].

The Naphthol AS-BI (2-Naphthalenecarboxamide, 7-bromo-N-(2-methoxyphenyl)-3-(phosphonoxy)-, disodium salt) phosphate and New Fuchsin mixture is one of the substrates used in the APAAP and ABC process along with biotinylated AP. The Naphthol AS-BI phosphate is a naphthol salt that acts as a coupling agent while New Fuchsin is a hexazonium salt that acts as a trapping agent [21, 111]. AP catalyzes the hydrolysis of naphthol AS-BI phosphate. The intermediate, naphthol AS couples with New Fuchsin and finally forms an insoluble red product which could be viewed under the light microscope. The whole reaction takes place at alkaline pH.

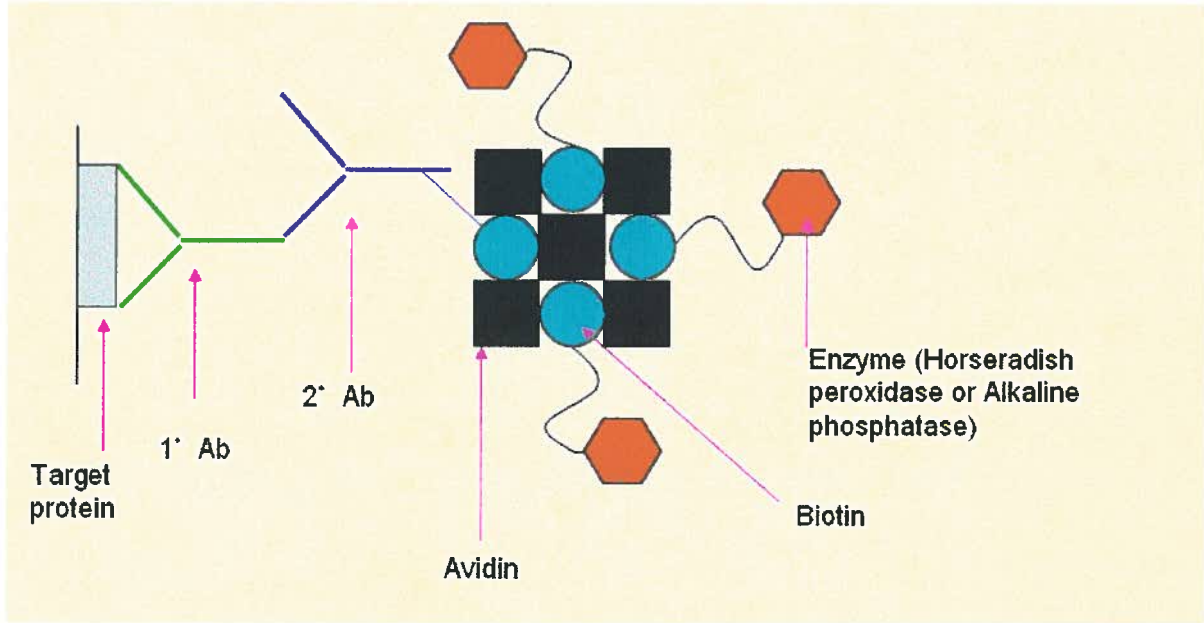


Figure 3.3: Schematic diagram of ABC method. The 1° Ab binds to the target protein. The biotinylated 2° Ab is able to bind to the 1° Ab. An avidin has four binding sites for biotin. Therefore, the avidin is able to link the biotinylated 2° Ab and the biotinylated enzymes.

3.3.1.2.3 Polymeric method

The polymeric method (Figure 3.4) uses an unlabelled 1°Ab as well. The difference between this and the ABC method is that the 2° Ab is replaced with a dextran polymer backbone which is covalently bound to twenty 2° Ab and one hundred enzymes (HRP or AP) at the same time. This system increases the signal intensity and sensitivity because of the high density of active enzyme bound to the dextran polymer [117, 118]. In the polymeric method, Vector® VIP substrate (Vector Laboratories, Burlington, Ontario, Canada), a substrate for HRP, is converted to an insoluble violet product in the tissue sections. Permanent red substrate (Dako, Mississauga, Ontario, Canada), a substrate for AP, is converted to an insoluble red product in the tissue sections.

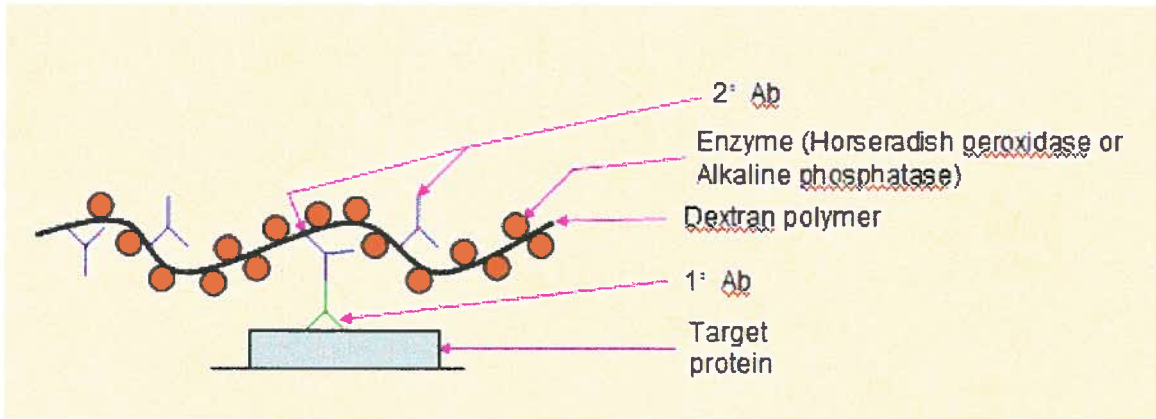


Figure 3.4: Schematic diagram of polymeric method.

Chapter 4: Research

4.1 Working hypothesis

The accumulation of mucus exudates observed with progression of COPD is related to excess airway epithelial sodium re-absorption as a result of over-expression of β -ENaC and reduced expression of CFTR by small airway epithelial cells.

4.2 Objective

The main objective for this project is to quantify expression of β -ENaC and CFTR mRNA and protein in small airways epithelia from COPD and control patients and relate these to lung function and mucus plugging.

4.3 Specific aims

Based on this objective, the research is divided into the following parts:

- a. to quantify β -ENaC and CFTR mRNA expression in whole small airways and lung parenchyma from patients of each of the GOLD categories using real time PCR and relative quantification.
- b. to laser capture small airways epithelia from lung tissue sections from COPD patients.
- c. to measure the quality and quantity of the RNA extracted from the captured tissue.
- d. to evaluate number of lung tissue sections needed to obtain adequate RNA for qualitative PCR of two mRNAs of interest, namely β -ENaC and CFTR and a control mRNA, that of β -actin, in small airway epithelium.

- e. to quantify β -ENaC and CFTR mRNA expression in small airway epithelium from control and COPD patients using real time PCR and absolute quantification.
- f. to localize and quantify the expression of β -ENaC and CFTR proteins in small airway epithelium from these patients using immunohistochemistry and Image Pro Plus.
- g. to localize and quantify epithelial mucin and mucus plugging in small airways of these patients using periodic acid Schiff and Image-Pro Plus.
- h. to correlate the mRNA and protein expression of β -ENaC and CFTR to lung function and mucus plugging.

Chapter 5: Materials and Methods

5.1 Patient population and lung tissue core production

The patients who require surgical removal of small, peripheral lung tumors were invited to enroll in the lung registry and lung tissue bank in St. Paul's Hospital, Vancouver [9, 119]. The background information of patients (gender, age, pre-operational lung function tests, thoracic CT scan, and smoking and occupational histories) is saved in the lung registry. All studies based on the patient samples stored in the lung registry and lung tissue bank have to be approved by the Structure/Function oversight committee that meets weekly [119]. The progress of the studies based on the lung registry and lung tissue bank samples is monitored by the presentations by scientists in Research in Progress seminars to the oversight committee. These studies are also approved by the University of British Columbia/Providence Research Ethics Board. After removing areas of lung for other research purposes and pathologic diagnosis, the rest were inflated with a supporting medium. Since 1993, the resected lung specimens (n=145) have been inflated with Optimal Cutting Temperature compound (OCT) (Tissue-Tek, Sakura Finetek, USA Inc., Torrance, CA, USA) or 50% cryomatrix compound (Shandon, Pittsburgh, PA, USA) to allow cutting the frozen sections [119]. These inflated lungs were then frozen over liquid nitrogen. Two cm thick frozen lung slices were cut on a band saw, and the lung slices cut with a power-driven hole-saw to get tissue cores that are 1 cm in diameter and 2 cm in length. Finally, the frozen lung cores were labelled and stored at -70°C [119].

5.2 Gene expression studies in whole small airways and lung parenchyma of COPD patients using amplified cDNA and relative PCR quantification

Amplified cDNA used for my gene expression studies of whole small airways and lung parenchyma was provided by a technician, John Gosselink, who studied the expression of over 50 other genes and therefore the necessity to amplify the cDNA. Laser capture microdissection, RNA extraction, RNA quantity and quality measurements, and cDNA amplification of the RNA from the whole airways and lung parenchyma that are described below were done by John Gosselink [120].

5.2.1 Sample collection and tissue processing

Small conducting airways with a diameter less than or equal to 2 mm were used for these studies because they are the site of the airway disease in COPD [3]. Two 10 µm thick sections cut from each frozen lung tissue core from each patient were stained with hematoxylin & eosin for selection of cores with small airways that meet this criterion. Ninety-nine frozen cores with conducting airways satisfying the above criterion were obtained from 16 GOLD 0, 17 GOLD 2 and 12 GOLD 3/4 patients (Table 5.1a and 5.1b). Each core provided one conducting airway. Whole small conducting airways included the epithelium, smooth muscle and connective tissues. From these cores twenty-two 10 µm serial consecutive sections were cut on a cryotome (Thermo Shandon, Waltham, MA, USA) at - 25°C. Frozen sections (10 µm thick) placed on pre-cleaned microscopic slides were dehydrated once with 70% ethanol and nuclear stained with RNase-free hematoxylin followed by dehydration with 70% ethanol. Then these sections were stained with RNase-

free eosin followed by dehydration once in each of 80%, 90% and 95% ethanol, and twice with 100% ethanol. The residual ethanol was removed with xylene. All these lung sections were then used for laser capture microdissection of the whole small airways (see below).

Table 5.1a: COPD patients selected for gene expression studies of whole airways and lung parenchyma showing GOLD category, number of cores, FEV₁pp, FEV₁/FVC, age and pack years.

Case	GOLD	# of cores	FEV ₁ pp	FEV ₁ /FVC	Age	Smoking History (Pack Years)
1979	0	3	86	81	66	17
2299	0	1	99	85	53	38
2415	0	2	109	76	57	37
2416	0	3	96	77	73	26.5
2431	0	2	81	77	70	40
2753	0	2	93	78	62	42
3381	0	1	91	82	69	49
3491	0	2	95	77	76	40
5503	0	4	97	74	64	71
5771	0	2	104	77	58	50
5783	0	1	106	82	57	9
5907	0	3	96	74	71	15
5968	0	2	97	70	70	69
6043	0	2	112	83	45	30
6091	0	2	86	75	70	36
6104	0	3	91	83	73	24
1200	2	2	75	70	65	37
2076	2	3	61	63	67	60
2086	2	1	61	52	64	65
2142	2	1	63	62	50	55.5
2427	2	2	69	54	69	40.5
2891	2	2	61	65	63	22
3145	2	1	66	61	70	140
3377*	2	3	57	63	67	76.5
3380	2	2	68	52	75	60
3395	2	3	75	68	62	50
3469	2	3	77	61	53	23.5
5972	2	2	64	52	62	52
6097	2	2	73	58	66	81
6102	2	2	68	54	48	9
6282	2	3	57	54	55	30
6438	2	1	55	49	56	39
6696	2	3	65	61	41	21
2751	3/4	1	46	60	75	60
3467	3/4	3	46	57	59	37
5760	3/4	1	32	57	59	46
5914	3/4	3	24	23	61	N/A
5916	3/4	3	20	24	57	N/A
5918	3/4	2	28	44	59	30
5919	3/4	3	18	37	54	74
5921	3/4	3	16	31	52	48
5922	3/4	2	18	27	58	N/A
5934	3/4	1	16	46	60	N/A
5935	3/4	3	23	44	55	N/A
6034	3/4	3	46	42	66	50

The patients listed, except those highlighted in pink, are the same as those in Table 5.3.

* One of the cores in this case was not available for gene expression studies of lung parenchyma

Table 5.1b: Summary of the patients in Table 5.1a listed by GOLD category with total number of patients and lung cores used as well as average lung function, age and smoking history.

GOLD	# of patients	# of cores*	FEV₁pp (Mean±SD)	FEV₁/FVC (Mean±SD)	Age (Mean±SD)	Smoking History (Pack Years) (Mean±SD)
0	16	35	96.2±8.5	78.2±4.1	64.7±8.5	37.0±17.4
2	17	36	65.6±6.7	58.8±6.2	60.8±9.0	50.7±30.6
3/4	12	28	27.7±12.0	46.0±12.8	60.0±6.0	49.3±14.5
Total	45	99				

* Only one airway per core was used

5.2.1.1 Laser capture microdissection (LCM)

LCM is a modern technique developed by Emmert-Buck's group in 1996 [121]. It is used for isolating pure populations of morphologically similar cells for molecular analysis [121-123].

Of the 22 serial sections from cores containing small airways that were stained with RNase-free hematoxylin & eosin, the first and last of these sections were reserved for archival purposes. The intervening frozen lung tissue sections (Figure 5.1) were placed on the stage of the LCM microscope (Acturus, CA, USA). A thermoplastic cap was placed on top of the section. A laser beam (60-100 mW) activated precise spots (15-30 μm in diameter) on the special thermoplastic film as the small airway was traced. Pre- and post-dissection images were taken and saved in the computer either in TIFF or JPEG format. The captured airway (Figure 5.1) from each section from each core was transferred to thermoplastic caps, and as each cap has the capacity to hold airways from 3 to 4 serial sections [124], a total of seven caps were used for each airway. These thermoplastic caps with the capture airways were placed on seven 0.5 ml microcentrifuge tubes containing 50 μl lysis buffer (Qiagen RNeasy® Mini Kit, Mississauga, Ontario, Canada). The tubes were inverted for at least 15 minutes to allow digestion of the captured airway. Airways captured into tubes were pooled together to give the final volume of 350 μl for RNA extraction. After the whole airways were isolated, the remaining lung parenchyma (Figure 5.1) from 16 of those consecutive sections from 98 of 99 frozen cores (Table 5.1a) were scraped off from the slides and immersed in 350 μl of lysis buffer. The pooled airway lysates and lung parenchymal lysates were stored at -70°C until RNA extraction.

Figure 5.1 has been removed due to copyright restrictions.

The information removed is representative micrographs of the laser capture microdissection of a small airway from a section of a frozen core of lung tissue (A) before, (B) after capture and (C and D) the captured airway where (D) represents an enlargement of the red box area of part (C) and bar length equals 100 μm . (Courtesy of J.V. Gosselink [124])

5.2.2 PCR on the amplified cDNA from RNA from whole small airways and lung parenchyma of patients from three GOLD categories

5.2.2.1 RNA extraction

One volume of 70% ethanol was added to the pooled airway lysates and lung parenchymal lysates. Lysis buffer contained guanidine isothiocyanate and 1% β -mercaptoethanol which are used to inactivate RNase in the lysates. The pooled airways and lung parenchyma from above in the lysis buffer and ethanol mixture were loaded into RNeasy® MiniElute Spin columns (Qiagen, Mississauga, Ontario, Canada). The RNA from the pooled airways and lung parenchyma was washed with the RW 1 buffer (Qiagen) followed by DNase I digestion (Qiagen) and RPE buffer (Qiagen) wash. The RNA was then washed with 80% ethanol. RPE buffer contains a low concentration of salt which is responsible for removing protein and carbohydrates away from RNA samples. Eighty % ethanol is able to remove residual salts from RNA samples. The RNA was then eluted from the RNeasy® MiniElute Spin columns with 30 μ l RNase-free water (Qiagen). The extracted RNA was stored at -70°C .

5.2.2.2 RNA quantity and quality measurement

The quantity and quality measurement of the RNA isolated from pooled airways and lung parenchyma were measured by Agilent Bioanalyzer 2100. Two μ l of the RNA from the extracted RNA in 30 μ l of RNase-free water was incubated in the heat block (VWR International, Mississauga, Ontario, Canada) at 70°C for 2 minutes and immediately chilled on ice for 5 minutes. RNA 6000 pico dye concentrate supplied with the RNA 6000 Pico Assay (Agilent Technologies, Palo Alto, CA, USA) was spun down for 10 seconds before

adding 1 μ l of it to 65 μ l of filtered RNA 6000 pico gel matrix. The gel matrix and dye were mixed and spun down at room temperature at 13,000xg for 10 minutes. Nine μ l of the gel dye mix was dispensed into a well on the pico chip with G marked on it. This well carries the gel that is used for capillary electrophoresis. The plunger was used to add pressure to inject the gel into the capillary of the chip which sat on the chip priming station. Five μ l of RNA 6000 pico marker was added into a well for the RNA ladder and the 11 sample wells. Pico marker is a tracing dye that traces the migration of sample in the gel. One μ l of 1 ng/ μ l RNA ladder (Ambion Inc, Austin, TX, USA) was loaded into its respective well. One μ l of each previously heated RNA sample was then added into the sample wells. The chip was vortexed by the vortex mixer (Agilent Technologies) at 2400 rpm for 1 minute. This step allowed mixing the RNA and solution in each well thoroughly. The quantity and quality of RNA were analyzed by Agilent 2100 Bioanalyzer based on RNA ladder (1 ng/ μ l) and RIN.

5.2.2.3 cDNA amplification

The optimal PCR cycle number is determined before the actual experiment. Basically, 25 ng reversed transcribed commercial placenta or lung RNA and the above primers (Section 3.2.1) were used in the long- distance PCR reaction following first strand synthesis as described above (Section 3.2.1). The reaction was allowed to run for 27 cycles in a PCR Express thermocycler (Hybraid, Middlesex, UK). Five μ l aliquots were retrieved at 15, 18, 21, 24 and 27 cycles. These aliquots were then analyzed by 1.2 % agarose / ethidium bromide gel electrophoresis and visualized with an Eagle Eye gel documentation system (Stratagene, La

Jolla, CA, USA) to check which cycle number was required for the amplification to reach the plateau phase [124]

Fifty ng of total RNA from each whole conducting airway or lung parenchymal lysates were used in first strand cDNA synthesis and cDNA amplification using the Clontech Super SMART™ cDNA Amplification kit (BD Sciences, San Jose, CA, USA) following manufacturer's instructions [124]. The principle of this amplification is presented in the Introduction (Section 3.2.1).

5.2.2.4 TaqMan® real-time PCR

5.2.2.4.1 Background

TaqMan® real time PCR is similar to traditional PCR that uses non-fluorescent labelled forward and reverse primers. The difference in TaqMan® is that a fluorescent labelled probe is applied. Each TaqMan® probe is labelled with 5' FAM™ reporter fluorophore and 3' TAMRA quencher. In the intact probe, the proximity of the quencher reduces the fluorescence emitted by the reporter by Förster resonance energy transfer (FRET) [125]. When Taq polymerase encounters the probe hybridized to the DNA template during amplification, it cleaves the 5' nucleotide of the probe that carries the reporter dye away from the quencher to allow fluorescence emission which is detected in real time [126]. Therefore, accumulation of fluorescence increases with each amplification cycle if amplification is successful.

5.2.2.4.2 TaqMan® probe and primers design

According to the respective NCBI sequence (refer to Table 5.2), the β -ENaC, CFTR, β -actin, β -2-microglobulin (β -2-M) and hypoxanthine phosphoribosyltransferase 1 (HPRT1) mRNAs are 2597, 6129, 1793, 987 and 1435 nucleotides long, respectively. The β -ENaC, CFTR, β -actin, β -2-M, and HPRT1 TaqMan® MGB (3'- minor groove binder) probe target sequence, forward and reverse primers (Applied Biosystems, Foster City, CA, USA) have been chosen from the Applied Biosystems inventory (Table 5.2) and purchased from Applied Biosystems. Similarly probes and primers for Muc5ac (Table 5.2) were chosen and reserved for studies involving whole small airways analyses of mucin expression and mucus plugging.

Table 5.2: The assay location and the length of amplicon of each gene analyzed by PCR.

Gene Name	Genebank accession number	Length of mRNA (nucleotide)	Applied Biosystems Assay ID	5' Probe location in the mRNA	Length of amplicon (bp)
β -ENaC	NM_000336	2597	Hs00165722_m1	1011	66
CFTR	NM_000492	6129	Hs00357011_m1	3597	93
β -actin	NM_001101	1793	Hs99999903_m1	36	171
β - 2-M	NM_004048	987	Hs99999907_m1	413	75
HPRT1	NM_000194	1435	Hs99999909_m1	562	100
MUC5AC	AJ298317	7382	Hs01370716_ml	4048	76

5.2.2.4.3 Relative PCR of β -ENaC and CFTR expression in whole small airways and lung parenchyma from patients in three different GOLD categories

Five μ l of Universal PCR master mix (Applied Biosystems), 0.5 μ l of 5' FAM-labeled MGB probe of β -ENaC, CFTR, β -actin, β -2-M or HPRT1 with their respective primers pairs (Applied Biosystems) were added into each well of a 384-well microplate. Five μ l of 10X diluted amplified cDNA were used to perform Taqman® real-time PCR analysis of β -ENaC and CFTR expression with β -actin, β -2-M and HPRT1 (Table 5.2) as reference genes. For a PCR negative control, RNase-free water was used instead of amplified cDNA. Each sample was run in triplicate for each target gene while the PCR negative control was run once. The thermal cycling conditions were as follows: 95°C for 10 minutes, followed by 40 cycles at 95°C for 15 seconds and 60°C for 1 minute. The PCR reaction was run in the ABI Prism 7900 HT Sequence Detection System (Applied Biosystems).

5.2.3 Quantification of β -ENaC and CFTR mRNA expression in whole small airways and lung parenchyma

For quantifying β -ENaC and CFTR mRNA expression from 99 whole small airways and 98 lung parenchyma from each lung core, relative quantification was applied using the qBASE software [108]. The principle and calculation of this quantification are presented in the Introduction (Section 3.2.3.1).

5.3 Gene expression studies in epithelium of small airways of COPD patients using absolute PCR quantification

5.3.1 Tissue processing for determining amount of tissue required for gene expression analysis (preliminary studies)

Because I was next interested in restricting the analysis of the expression of the genes of interest to the epithelial layer of the airway and using absolute quantification it was necessary to determine the amount of total RNA required for these gene expression studies. Thirty, sixty and ninety serial consecutive sections from the respective three frozen lung cores with small airways from each of three patients of undetermined GOLD category were cut and stained and dehydrated in the same way mentioned in section 5.2.1. Similarly, sixty sections from each of two lung cores from one GOLD 0 patient and one core from each of two GOLD 2 patients were cut and treated as above. All these lung sections, except for first and last sections from each core that were reserved for archival purposes, were then prepared for LCM of the small airway epithelium. Because of the limited availability of lung tissue from GOLD 3/4 patients, twelve consecutive 50 µm whole lung sections without further processing from cores with small conducting airways were used from 3 of these patients.

5.3.2 Tissue processing for gene expression studies in small airway epithelia of patients from three GOLD categories

Seventy-eight frozen lung tissue cores with 83 airways satisfying the above criterion were obtained from 14 GOLD 0, 13 GOLD 2 and 12 GOLD 3/4 patients (Table 5.3a and b). Sixty

10 μm serial consecutive sections were cut and processed as above (section 5.2.1) in preparation for LCM.

Table 5.3a: COPD patients with lung cores with airways fulfilling the criterium required for gene expression studies of small airway epithelium, showing GOLD category, number of lung cores and airways used, FEV₁pp, FEV₁/FVC, age and smoking history.

Case	GOLD	# of cores	# of airways	FEV ₁ pp	FEV ₁ /FVC	Age	Smoking History (Pack Years)
1979*	0	2	2	86	81	66	17
2299*	0	3	3	99	85	53	38
2415*	0	1	1	109	76	57	37
2416	0	1	1	96	77	73	26.5
2431*/**	0	2	2	81	77	70	40
2753*/**	0	3	3	93	78	62	42
3381*/**	0	2	2	91	82	69	49
3491*	0	2	3	95	77	76	40
5503*	0	2	2	97	74	64	71
5771*/**	0	2 (1)	4	104	77	58	50
5907*	0	2	2	96	74	71	15
5968*/**	0	2 (1)	2	97	70	70	69
6091*	0	2	2	86	75	70	36
6104*	0	2	2	91	83	73	24
1200*/**	2	3 (1)	4	75	70	65	37
2076*/**	2	2 (1)	2	61	63	67	60
2086	2	2	2	61	52	64	65
2427*/**	2	2 (1)	2	69	54	69	40.5
2891*	2	2	2	61	65	63	22
3380*/**	2	2	2	68	52	75	60
3395*	2	2	2	75	68	62	50
3469*/**	2	2	2	77	61	53	23.5
5972*/**	2	2 (2)	2	64	52	62	52
6097*/**	2	2	2	73	58	66	81
6102*/**	2	2 (2)	2	68	54	48	9
6438*/**	2	2 (1)	2	55	49	56	39
6696*/**	2	2 (1)	2	65	61	41	21
2751*/**	3/4	1 (1)	1	46	60	75	60
3467*/**	3/4	2 (1)	2	46	57	59	37
5760*/**	3/4	2 (1)	2	32	57	59	46
5914*/**	3/4	2	2	24	23	61	N/A
5916*/**	3/4	2	2	20	24	57	N/A
5918*/**	3/4	2	3	28	44	59	30
5919*/**	3/4	2 (1)	2	18	37	54	74
5921*/**	3/4	2	2	16	31	52	48
5922*/**	3/4	2 (1)	2	18	27	58	N/A
5934*/**	3/4	2 (1)	2	16	46	60	N/A
5935*/**	3/4	2 (1)	2	23	44	55	N/A
6034*	3/4	2	2	46	42	66	50

* patients involved in first PCR analysis (see section 5.3.8.1).

** patients involved in second PCR analysis (see section 5.3.8.2).

Blue color indicates that lung cores provided more than one airway.

() # of cores that were also used in the in gene expression studies of whole airways and lung parenchyma.

Table 5.3b: Summary of the patients in Table 5.3a listed by GOLD category with total number of patients, lung cores and airways used as well as average lung function, age and smoking history.

GOLD	Cases	# of cores	# of airways	FEV₁pp (Mean±SD)	FEV₁/FVC (Mean±SD)	Age (Mean±SD)	Smoking History (Pack Years) (Mean±SD)
0	14	28	31	94.4±7.3	77.6±4.0	66.6±6.8	39.6±16.7
2	13	27	28	67.1±6.7	58.4±6.8	60.8±9.2	43.1±20.7
3/4	12	23	24	27.8 ±12.0	41.0±12.9	59.6±6.0	49.3±14.5
Total	39	78	83				

5.3.3 Preparation of tissue and cells for RNA extraction

5.3.3.1 Isolation of airway epithelium by LCM

A laser beam (70-80 mW) activated precise spots (7.5 mm in diameter) on the special thermoplastic film as the epithelium of the small airway was traced on lung sections prepared for LCM. Epithelial cell layers of each airway from sections from each core were transferred to seven thermoplastic caps as described above. However, unlike the maximum capacity of the thermoplastic caps for holding three to four whole airways (Section 5.2.1.1) since, in comparison to whole airways, the epithelium of the small airways takes up less space, this limitation of 3 to 4 serial sections per cap did not apply and consequently more sections could be accommodated per cap. For airway epithelium from 30, 60, 90 consecutive sections from frozen lung cores from patients unclassified according to GOLD categories, number of sections used for LCM and number of sections carried by each thermoplastic cap are shown in Table 5.4.

Table 5.4: Number of sections used for LCM and held by each thermoplastic cap from patients unclassified according to GOLD categories (see section 5.3.1).

Total # of sections	# of sections for LCM	# of sections per cap
30	28	4
60	58	9 (first 6 caps), 4 (last cap)
90	88	13 (first 6 caps), 10 (last cap)

For the 58 sections from each of two lung cores from one GOLD 0 patient and one core from each of two GOLD 2 patients described in section 5.3.1 as well as 58 sections obtained from each of the airways from the lung cores from patients in the three different GOLD categories described in section 5.3.2, LCM was performed in the same way as above and the captured airway epithelium was distributed to the caps as described for the 60 sections from the unclassified GOLD patients (Table 5.4). Epithelial cells from each airways captured into seven tubes containing 50 μ l lysis buffer were pooled together to give the final respective volume of 350 μ l for RNA extraction.

5.3.3.2 Preparation on whole lung sections with small airways for RNA extraction

Twelve 50 μ m whole lung sections from one core from each of the three GOLD 3/4 patients were placed in 350 μ l lysis buffer immediately after sectioning. A tissue homogenizer (Tissue-Terror™, BioSpec Products, Inc. Bartlesville, OK, USA) was used to homogenize lung tissue after the tissues were in the lysis buffer.

5.3.3.3 Preparation of lung epithelial T84 cells for RNA extraction

RNA from T84 cells served as a positive control of the reverse transcription (RT) step of RT-PCR of CFTR. The T84 cell line (American Type Culture Collection [ATCC] cell line CCL248; Manassas, VA, USA) is a transplantable human carcinoma cell line derived from a lung metastasis of a colon carcinoma. T84 cells are epithelial cells and constitutively express CFTR on the cell surface [127]. One ml of T84 cells (9.4×10^6 cells/ml) was added to 5 ml

ATCC complete medium (1:1 mixture of Dulbecco's modified Eagle's medium and Ham's F12 medium for a final concentration of 1.2 g/L sodium bicarbonate, 2.5 mM L-glutamine, 15 mM HEPES [pH 7.4], 0.5 mM sodium pyruvate and 0.5% fetal bovine serum). Cells in this medium were transferred to a 25 cm² flat culture flask (Sarstedt, Newton, NC, USA) and were incubated in a Series II CO₂ water jacketed incubator (Thermo Fisher Scientific, Waltham, MA, USA) with 5% CO₂ at 37°C. After T84 cells were 90% confluent, they were washed twice with 2.5 ml warm phosphate buffered saline. Then 0.5 ml of 0.1% trypsin was added to the flask and the culture was incubated for 15 minutes in order to detach cells from the surface of the flask. This was followed by addition of 4.5 ml of ATCC complete medium to stop trypsinization. Five ml of the detached cells mixed with 10 ml of ATCC complete medium were transferred to a 75 cm² flat culture flask (Sarstedt). The flask was incubated at 37°C until cells were about 90% confluent. For total cell counts, 12 µl of the 15 ml of cells detached as above from the 75 cm² flask were added to the hematocrit followed by putting on a cover slip. The cell count was done under the light microscope (Nikon, Japan).

5.3.4 RNA extraction

RNA extraction of the pooled airway epithelial cell lysates or the minced whole lung tissues were performed in the same way as outlined in Section 5.2.2.1.

For extracting RNA from the T84 cells using RNeasy® Mini Kit (Qiagen), only 3 x 10⁶ cells is the recommended starting amount of cells for loading onto a RNeasy® MiniElute Spin column of the RNeasy® Mini Kit, otherwise the RNA binding capacity of this column will

be exceeded. The cells in the culture medium were aliquoted into twelve 1.5 ml microcentrifuge tubes and spun at 300 x g for 5 minutes. The supernatant was removed before adding 350 µl lysis buffer into each microcentrifuge tube. The T84 cell lysate was extracted with RNeasy® Mini Kits (Qigaen) following the manufacturer's instructions. The RNA of T84 cells was eluted with 50 µl RNase-free water and pooled to give a final total volume of this RNA sample of 600 µl.

5.3.5 RNA quantity and quality measurement

The quantity and quality measurement of the RNA isolated from epithelial layers and whole lung sections were measured by Agilent Bioanalyzer 2100 as described in section 5.2.2.2.

One ng/µl total human placenta RNA (BD Clontech, Mountain View, CA, USA) was used as a positive control of the RT step of RT- PCR of β-ENaC. The amount of this RNA was confirmed and the quality of this RNA was measured by using Agilent Bioanalyzer 2100.

The quantity of the total RNA from the T84 cells was measured by Spectronic BioMate 3 UV-Vis Spectrophotometer at OD₂₆₀ (Thermo Fisher Scientific) while the quality of this RNA was measured using Agilent Bioanalyzer 2100. The extracted RNA of T84 cells in 600 µl RNase-free water was stored at -70 °C for later use.

5.3.6 Reverse transcription (RT)

RNA from isolated small airway epithelia, whole lung tissue sections, human placenta and T84 cells was converted into cDNA by reverse transcription. Twenty-five μl of RNA (50 ng) was incubated with 2.5 μl of 10 mM dNTP (Invitrogen, Burlington, Ontario, Canada) and 2.5 μl of 50 ng/ μl random hexamers (Invitrogen) at 65°C for 5 minutes to denature the secondary structure of the RNA followed by incubation on ice for more than 1 minute. Then 5 μl of 10X RT buffer (Invitrogen), 5 μl of 0.1 M dithiothreitol (Invitrogen), 5 μl of 50 mM MgCl_2 , 2.5 μl of 40 U/ μl RNaseOUT (Invitrogen) were added. The samples were placed in the thermal cycler (ThermoHybaid, USA), and were incubated at 25 °C for 2 minutes. Then 2.5 μl of 200 U/ μl Superscript II reverse transcriptase (Invitrogen) was added to the samples giving a final volume of 50 μl . The samples were incubated at 25°C for 10 minutes, 42°C for 50 minutes and 70°C for 15 minutes and stored at -20°C. RNA from human placenta and T84 cells was used as a positive control for the RT reaction. For the negative control, Superscript II was replaced by RNase-free water.

5.3.7 Absolute PCR quantification

5.3.7.1 Preparation of full-length human plasmid DNA as standards for absolute PCR quantification

5.3.7.1.1 Transformation of bacteria with plasmids

Three μl (~40 ng) of full-length human β -ENaC cDNA in the pCMV6-XL4 vector (Figure 5.2) (Origene, Rockville, MD, USA), or pBQ6.2 [64], the full-length human CFTR cDNA in the pBluescript (KS+) vector (Figure 5.3) (a generous gift from Dr. J. Rommens, Toronto,

Ontario, Canada), or the full-length human β -actin cDNA in pCMV6-XL4 (Origene) were added to 50 μ l of Subcloning Efficiency™DH5 α ™ competent cells (Invitrogen). Fifty μ l of competent cells with 10 μ l 1X Tris-EDTA (TE) buffer in the absence of plasmid acted as a negative control while 17.5 ng of pUC19 added to competent cells served as a positive control. These bacteria were incubated on ice for 30 minutes followed by heat shock for 45 seconds at 37°C. The tubes were then cooled on ice for 2 minutes before 950 μ l of 37°C SOC medium (2% tryptone, 0.5% yeast extract, 10mM sodium chloride, 2.5 mM potassium chloride, 10 mM MgCl₂, 10 mM magnesium sulphate, and 20 mM glucose) were added to each tube. The tubes were then incubated in a shaker incubator (New Brunswick Scientific, Edison, NJ, USA) at 37°C at 225 rpm for an hour before 20 μ l of these bacteria were spread on pre-formed culture plates (see below).

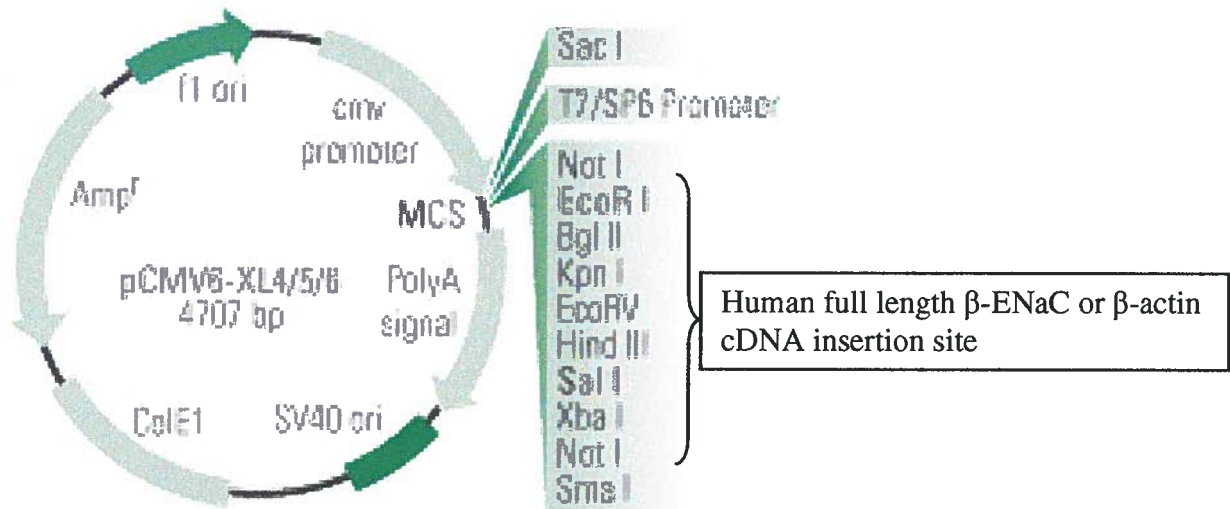


Figure 5.2: Vector diagram of pCMV6-XL6 (adapted from Origene 2007) with the full-length human β -ENaC or β -actin cDNA inserted between two Not I sites.

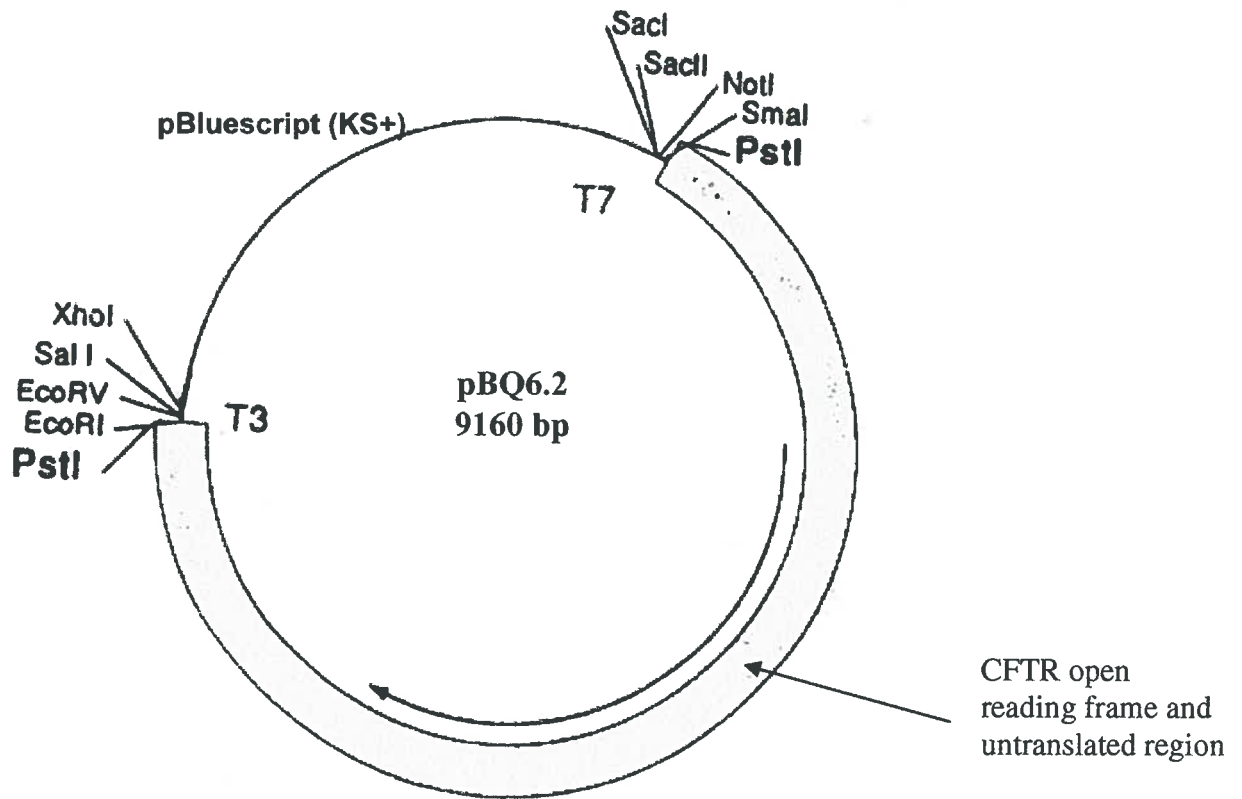


Figure 5.3: Diagram of full-length human CFTR plasmid, pBQ6.2 (With permission from Dr. J. Rommens). The single arc represents the vector, pBluescript (KS+). The full-length human CFTR cDNA is inserted into the Pst site of this vector. The arrow indicates the direction of transcription.

5.3.7.1.2 Identification of transformed bacteria by α -complementation

Alpha-complementation is a method used to identify cells transformed with recombinant plasmids. The plasmid vector has, as part of the multi-cloning region, an intact lac-Z gene that produces an α fragment of β -galactosidase. On the other hand, *E. coli* has been engineered to possess a lac-Z gene encoding the omega (ω) fragment of β -galactosidase. These two fragments assemble to form an active complex of β -galactosidase when *E. coli* is transformed with plasmids which express an intact lac-Z gene. This process is called α – complementation [128]. Active β -galactosidase turns the chromogenic white substrate 5-bromo-4-chloro-3-indolyl- β -galactoside (X-gal) into one with a blue colour. Therefore, *E. coli* transformed with plasmids (i.e. pUC19) with an intact lac-Z gene would generate blue colonies when X-gal is present. However, *E. coli* transformed with plasmids in which the multi-cloning site is disrupted by insertion of recombinant DNA do not produce active β -galactosidase and, therefore, the colonies would be white [129].

Before spreading the bacteria from above on Luria-Bertani (LB) agar plates (10 g tryptone, 5 g yeast extract, 5 g sodium chloride, and 15 g Bacto™ agar [Becton, Dickinson & Company, Sparks, MD, USA] in one litre distilled water), 40 μ l of a solution containing 20 mg/ml X-gal (Calbiochem-Novabiochem, La Jolla, CA, USA) in dimethylformamide (Sigma-Aldrich, St Louis, MO, USA) and 200 mg/ml of isopropylthio- β -D-galactoside (IPTG) (Sigma-Aldrich) were spread on LB agar plates with and without 100 μ g/ml ampicillin (Sigma-Aldrich). Bacteria transformed with plasmid carrying the gene for ampicillin resistance will survive in the presence of ampicillin while untransformed bacteria are eliminated. Plates were dried in an Isotemp incubator (Fisher Scientific, Ottawa, Ontario, Canada) at 37°C for

at least 4 hours. X-gal is a substrate for β -galactosidase and IPTG inactivates the lac repressor which when active, represses ω peptide synthesis. With this inactivation of the lac repressor by IPTG, the ω peptide is synthesized and assembles with the α fragment from the vector to form the active β -galactosidase that is capable of changing white X-gal to give a blue product [129]. Therefore, X-gal with IPTG is used to distinguish colonies that contain the non-recombinant vectors from recombinant plasmids. After the plates were dried, 20 μ l of bacteria were spread on LB agar plate containing 100 μ g/ml ampicillin. For testing the viability of cells that had been heat shocked, 20 μ l of competent cells heat shocked after adding 1X TE buffer without plasmid were spread on the LB plates without ampicillin. The plates were then incubated overnight at 37°C.

5.3.7.1.3 Harvesting bacteria transformed with β -ENaC, CFTR, and β -actin plasmid

DNA

Once colonies of bacteria treated with the recombinant plasmids became visible on LB agar plates containing 100 μ g/ml ampicillin, single white colonies were picked and transferred to a 14-ml plastic incubation tube (VWR) which had 3 ml LB medium containing 100 μ g/ml ampicillin. The bacteria were incubated in the shaker incubator (New Brunswick Scientific, Edison, NJ, USA) at 300 rpm at 37°C for 8 hours, transferred to 100 ml LB medium containing 100 μ g/ml ampicillin, and incubated further at 300 rpm at 37°C for 16 hours. Finally the transformed bacteria were spun down by centrifugation at 7500 rpm at 4 °C for 15 minutes.

5.3.7.1.4 Quantification and identification of plasmid DNA

β -ENaC, CFTR, and β -actin plasmid DNA was purified using the HiSpeed® Plasmid Midi Kit (Qiagen) under the manufacturer's direction. The plasmid purification kit is based on the principle of alkali lysis. Plasmid was first extracted from the bacteria using sodium dodecyl sulfate (SDS) and NaOH. SDS denatures bacterial proteins and NaOH denatures chromosomal and plasmid DNA. Potassium acetate neutralizes this mixture to allow covalently closed plasmid DNA to re-anneal rapidly while the proteins and linear DNA are precipitated and the lysate is cleared by filtration. The plasmid is then bound to the anion-exchange resin under low salt and pH 7 condition. Remaining RNA, protein, and other impurities were washed away using medium salt buffer. Plasmid DNA was then eluted with high salt buffer and finally precipitated and desalted with isopropanol. About 500 μ l of each β -ENaC, CFTR, and β -actin plasmid DNAs were obtained using this purification kit. Concentration of β -ENaC, CFTR, and β -actin plasmid DNA was then measured at OD₂₆₀ using Spectronic BioMate 3 UV-Vis Spectrophotometer (Thermo Fisher Scientific). The ratio of OD₂₆₀ and OD₂₈₀ was used to determine the purity of plasmid DNA. After measuring the concentration of plasmid DNA, restriction enzyme (RE) digestion was performed to determine if the purified products had the expected restriction fragment sizes of the β -ENaC, CFTR, or β -actin cDNAs, respectively.

The details of the components of the digestion of the plasmids carrying the cDNAs of interest by restriction endonucleases in 1.5 ml microcentrifuge tubes are given in table 5.5. According to manufacturer's specifications, one unit (U) of restriction enzyme is able to digest 1 μ g of bacterial virus lambda DNA in a 50 μ l reaction in 1 hour.

Table 5.5: Volume of plasmids and reagents added to each digestion with restriction endonucleases.

Plasmid DNA				Buffer	Restriction Enzymes*	Tris-EDTA	Total volume
	concentration	volume	input amount				
β-ENaC	792.85 µg/ml	5 µl	3.96 µg	2 µl of 10x REact 3**	0.5 µl 15 U/µl Not I	12.5 µl	20 µl
β-actin	367.2 µg/ml	20 µl	7.34 µg	5 µl of 10x REact 3**	0.5 µl 15 U/µl Not I	24.5 µl	50 µl
CFTR	651.45 µg/ml	1 µl	0.65 µg	1 µl of 10x REact 2***	0.5 µl 10 U/µl Pst I	7.5 µl	10 µl

* NotI (Invitrogen), PstI (GibcoBRL®).

** 1x REact 3: 50mM Tris-HCl, pH8.0, 10mM MgCl₂, 100mM NaCl (Invitrogen).

*** 1X REact 2: 50mM Tris-HCl, pH8.0, 10mM MgCl₂, 50mM NaCl (GibcoBRL®,

Burlington, Ontario, Canada).

The volume of restriction enzyme used above was replaced by 1X TE buffer as a negative control. The tubes were incubated in a 37°C water bath (Precision Scientific, Chicago, IL, USA) for two hours. Plasmid DNA either digested or not was loaded into a 0.7% agarose gel stained with 0.5 µg/ml ethidium bromide. Gel electrophoresis was performed using the Bio-Rad® PowerPAC 300 (Bio-Rad Laboratories, Hercules, CA, USA) as a power source and the gel image was taken using Gene Flash™ (TopoGEN, Port Orange, FL, USA).

5.3.7.1.5 Preparation of plasmid standards for absolute PCR quantification

To prepare real-time PCR standard curves, 10 times serial dilutions giving 2×10^6 , 2×10^5 , 2×10^4 , 2×10^3 , 2×10^2 , and 2×10^1 copies were made to give six standards for each of β-ENaC, CFTR, and β-actin plasmid DNAs based on the following criteria. The mass of a single molecule of plasmid DNA is based on the length in base pairs (bp) where one bp has a molecular weight of approximately 650 g:

$$\text{Mass of single molecule of plasmid (g)} = \frac{\text{plasmid size (bp)} \times 650 \text{ g / mol / bp}}{6.02 \times 10^{23} \text{ molecules /mol}}$$

The input copy numbers of plasmids was used together with the mass of single molecule of plasmid DNA to give the total mass of plasmid DNA required for that standard as follows:

$$\text{Mass of plasmid DNA needed (g)} = \text{Copy number of interest} \times \text{Mass of single plasmid (g)}$$

Since the volume of the plasmid DNA standards to be added to the PCR reaction was arbitrarily set at 5 μ l, DNA needed to give the required mass for the highest copy number standard in this 5 μ l volume was calculated and further serial dilutions were made from this highest copy number preparation for the remaining standards.

5.3.7.1.6 TaqMan® Real-time PCR efficiency of β -ENaC, CFTR, and β -actin mRNA

Together with the probes and primers for TaqMan® real-time PCR of the β -ENaC, CFTR and β -actin targets from above (Section 5.2.2.4.2), the serially diluted plasmid DNA was used to create a standard curve for each of the genes of interest. Five μ l of Universal PCR master mix (Applied Biosystems), 0.5 μ l of 5' FAM-labeled MGB probe of β -ENaC or CFTR or β -actin with their primer pairs (Applied Biosystems) were added respectively into each well of a 384-well microplate. Five μ l of each of the plasmid DNA standards of each gene were added. For a PCR negative control, RNase-free water was used instead of plasmid DNA. Each standard of the genes was run in triplicate while the PCR negative control was run once. Therefore, nineteen wells were used to generate each of the standard curves. The thermal cycling conditions were as follows: 95°C for 10 minutes, followed by 40 cycles at 95°C for 15 seconds and 60°C for 1 minute. The slope of the standard curve of the Ct values against the plasmid copy number was used to calculate the real-time PCR efficiency ($10^{-1/\text{slope}}$).

5.3.7.2 TaqMan® real-time PCR on patients' samples to determine the amount of tissue required for gene expression analysis and whether this expression could be detected in samples from GOLD 3/4 patients

Five μ l of the 50 μ l of cDNA from the RNA isolated from small airways epithelia of 28, 58 and 88 sections from each lung core from each of three patients of unclassified GOLD class as well as 58 sections from each of two cores from one GOLD 0 patient and one core from each of two GOLD 2 patients and RNA from twelve whole 50 μ m sections from lung cores with a small airway from three GOLD 3/4 patients were used for TaqMan® real-time PCR. Five μ l of Universal PCR master mix (Applied Biosystems), 0.5 μ l 5'FAM-labeled β -ENaC or CFTR or β -actin probe with their primer pairs (Applied Biosystems), plus cDNA from each patient were loaded into each well of a 384-well microplate. Each sample was run in triplicate for each target. The RT positive control (human placenta RNA and T84 cells) was performed in triplicate while the RT negative and PCR negative controls for each target were performed once. The thermal cycling conditions were as follows: 95°C for 10 minutes, followed by 40 cycles at 95°C for 15 seconds and 60°C for 1 minute. The PCR reaction was run in ABI Prism 7900 HT Sequence Detection System (Applied Biosystems).

5.3.8 Determination of β -ENaC and CFTR mRNA expression in epithelia of small airways from patients in three different GOLD categories by absolute PCR quantification

5.3.8.1 First PCR analysis

Based on the results from the analysis to determine the number of sections of airways required for gene expression analysis (Section 5.3.1 and 5.3.7.2) and the determination of the minimal amount of RNA required for reliable PCR analysis of the three mRNAs of interest (Section 5.3.1 and 5.3.7.2), only RNA from epithelium isolated from 64 out of 83 small airways (Table 5.3a) qualified for further gene expression studies. The 64 airways were from 37 patients. For quantifying β -ENaC and CFTR mRNA expression in epithelial layers from each of 64 small airways of COPD patients (Table 5.3a) in this first PCR analysis, absolute quantification was used. This quantification was based on the use of serial dilutions of β -ENaC, CFTR, and β -actin plasmid DNA to generate three standard curves as described in sections 5.3.7.1.5 and 5.3.7.1.6. The mRNA expression of β -ENaC and CFTR was determined by absolute PCR quantification as described in section 5.3.7.2 and was normalized with β -actin expression in the same samples.

5.3.8.2 Second PCR analysis

Since expression of these genes could not be detected in most of the samples analyzed above (see section 5.3.8.1), the remaining RNA from the isolated small airway epithelium of lung tissue cores from these patients was considered for use in the second PCR analysis. To determine which samples qualified, the remaining RNA was re-analyzed using the

Bioanalyzer. Only 36 out of the 64 small airway epithelial samples had sufficient amounts of remaining RNA for a second PCR analysis (Table 5.3a) (see Results section 6.2.6 for minimal amount required). All of the available remaining cDNA in these 36 samples was used in the second PCR analysis.

5.4. β -ENaC and CFTR protein expression and mucin staining

5.4.1 Preparation of lung tissue for immunohistochemical analysis of β -ENaC and CFTR and for mucin staining

Five frozen sections (10 μ m thick) with small airways from each of 72 lung cores from 37 patients spread over the three GOLD categories (Table 5.6) were cut, placed on HistoBond® adhesion microscopic slides (Paul Marienfeld GmbH & Co, Lauda-Königshofen, Germany) and then stored at -70°C.

Table 5.6: COPD patients selected for immunohistochemistry and periodic acid Schiff staining showing GOLD category, FEV₁pp, FEV₁/FVC, age and pack years. (These patients are the same as those listed in Table 5.3a, except cases 2415 and 2416 were not involved in the immunohistochemistry and periodic acid Schiff staining studies.)

Case	GOLD	# of cores	# of airways	FEV ₁ pp	FEV ₁ /FVC	Age	Smoking History (Pack Years)
1979	0	2	2	86	81	66	17
2299	0	2	2	99	85	53	38
2431 [#]	0	2	2	81	77	70	40
2753 [#]	0	2	2	93	78	62	42
3381 [#]	0	2	2	91	82	69	49
3491	0	2	2	95	77	76	40
5503*	0	2	2	97	74	64	71
5771 [#]	0	2	2	104	77	58	50
5907	0	2	2	96	74	71	15
5968 [#]	0	2	2	97	70	70	69
6091	0	2	2	86	75	70	36
6104	0	2	2	91	83	73	24
1200 [#]	2	3	4	75	70	65	37
2076 [#]	2	2	2	61	63	67	60
2086	2	1	1	61	52	64	65
2427 [#]	2	1	1	69	54	69	40.5
2891	2	2	2	61	65	63	22
3380 [#]	2	2	2	68	52	75	60
3395	2	2	2	75	68	62	50
3469 [#]	2	2	2	77	61	53	23.5
5972 [#]	2	2	2	64	52	62	52
6097 [#]	2	2	2	73	58	66	81
6102 [#]	2	2	2	68	54	48	9
6438 [#]	2	2	2	55	49	56	39
6696 [#]	2	2	2	65	61	41	21
2751 [#]	3/4	1	1	46	60	75	60
3467 [#]	3/4	2	2	46	57	59	37
5760 [#]	3/4	2	2	32	57	59	46
5914 ^{#*}	3/4	2	2	24	23	61	N/A
5916 [#]	3/4	2	2	20	24	57	N/A
5918 [#]	3/4	2	2	28	44	59	30
5919 [#]	3/4	2	2	18	37	54	74
5921 [#]	3/4	2	2	16	31	52	48
5922 [#]	3/4	2	2	18	27	58	N/A
5934 [#]	3/4	2	2	16	46	60	N/A
5935 ^{#*}	3/4	2	2	23	44	55	N/A
6034	3/4	2	2	46	42	66	50

COPD patients also used in the second PCR analysis in the gene expression studies of small airway epithelium.

* COPD patients used for establishing the color segmentation profile for Immunohistochemistry of β -ENaC. COPD patients used for establishing the color segmentation profile for periodic acid Schiff staining (highlighted in blue)

Two airways per core for one of the three cores was used (highlighted in red).

Table 5.7: Summary of the patients in Table 5.6 listed by GOLD category with total number of patients, lung cores and airways used as well as their average lung function, age and smoking history.

GOLD	Cases	# of cores	# of airways	FEV₁pp (Mean±SD)	FEV₁/FVC (Mean±SD)	Age (Mean±SD)	Smoking History (Pack Years) (Mean±SD)
0	12	24	24	93.0±6.4	77.8±4.3	66.8±6.6	40.9±17.6
2	13	25	26	67.1±6.7	58.4±6.8	60.8±9.2	43.1±20.7
3/4	12	23	23	27.8 ±12.0	41.0±12.9	59.6±6.0	49.3±14.5
Total	37	72	73				

5.4.2 Immunohistochemical staining of β -ENaC protein using the polymeric method

(Envision™ Detection System Peroxidase/DAB, Rabbit/Mouse)

One frozen section (10 μ m thick) from each of 72 lung cores with the 73 small airways listed in table 5.6 and summarized in table 5.7 and stored until used as described in section 5.4.1 was fixed with cold methanol for 5 minutes and washed with 100 μ l 1X TBS-Tween 20 pH 7.6 (0.05M Tris, 0.9% NaCl, 0.05% Tween 20) followed by 3% H₂O₂ (Surgipath Medical Industries, Winnipeg, Manitoba, Canada) treatment of endogenous peroxidases and a universal protein block (Dako) for 10 minutes and 20 minutes, respectively. Sections were then incubated for 60 minutes with the primary polyclonal rabbit anti-human β -ENaC antibody (a generous gift from Dr. P. Barbry, France) diluted 1:800 with 1X TBS, containing 0.05 mM PMSF, 0.01 μ g/ml aprotinin, and 0.01 μ g/ml leupeptin. Polyclonal rabbit anti- β -ENaC is the antibody against the last 17 cytoplasmic residues of human β -ENaC [130]. Next sections were incubated with Envision™ detection system (Dako) for 30 minutes, stained with freshly made Vector® VIP substrate (Vector Laboratories, Burlington, Ontario, Canada) for 15 minutes and washed with running tap water for 5 minutes. Sections were counterstained with pre-warmed methyl green (Vector Laboratories) for 15 seconds followed by washing with distilled water to remove excess stain. Sections were finally dipped in 0.05 % acetic acetone (200 μ l glacial acetic acid in 400 ml acetone) for 10 to 15 times. All the blocking and immunostaining were performed in Dako Autostainer Staining System. Frozen human kidney section (5 μ m) was used as a positive control. For the negative control, sections (a frozen kidney section and sections from each of 72 lung cores from above in section 5.4.1) were incubated with 1000x rabbit pre immune serum (a generous gift from Dr. P. Barbry) instead of polyclonal rabbit anti-human β -ENaC antibody.

5.4.3 Immunohistochemical staining of CFTR protein

5.4.3.1 The APAAP method

Two frozen lung sections (10 µm thick) from each of two lung cores with small airways, one from a GOLD 2 and the other, an unclassified patient, were used to compare the immunostaining of CFTR using the following methods. These four sections were fixed with room temperature acetone for 10 minutes. Sections were washed with 100 µl 1X TBS-Tween 20 pH 7.6 (0.05M Tris, 0.9% NaCl, 0.05% Tween 20). Then, two sections (one from the GOLD 2 and one from the unclassified patient) were incubated with a 1:50 dilution of the 1° Ab L12B4 (a generous gift from Dr. N. Kartner, Toronto, Canada) (diluted with 1X TBS containing 1% BSA, 0.5 mM PMSF, 0.01 µg/ml aprotinin, 0.01 µg/ml leupeptin, 5% normal rabbit serum and 5% human serum from blood type AB) for 60 minutes. L12B4 is the mouse monoclonal antibody against human CFTR [131]. It detects the nucleotide binding domain 1 (residue 386-412) of CFTR. Sections were then incubated with a 1:40 dilution of the rabbit anti-mouse IgG (Dako)(diluted with 1X TBS containing 1% BSA) for 30 minutes. Sections were incubated with a 1:100 dilution of APAAP (Dako) (diluted with 1X TBS containing 1% BSA) for 30 minutes, stained with freshly made New Fuchsin for 20 minutes and counterstained with Gill's hematoxylin (Surgipath Medical Industries, Winnipeg, Manitoba, Canada) for 2 minutes. The other two frozen lung sections were treated in the same way as mentioned above except the mouse monoclonal antibody against human CFTR was replaced with 500X dilution of mouse IgG (Dako). All the blocking and immunostaining were performed in Dako Autostainer Staining System.

5.4.3.2 The ABC method

Eight frozen sections (10 μm thick) from a lung core of a GOLD 2 patient with a small airway were used in this study. These slides were separated into two groups in which four slides were either fixed with room temperature acetone for 10 minutes or room temperature 10% formalin for 15 minutes. Sections were washed with 100 μl 1X TBS-Tween 20 pH 7.6 (0.05M Tris, 0.9% NaCl, 0.05% Tween 20) followed by incubation with avidin biotin block (Dako) for 15 minutes. Three different dilutions (50X, 100X, and 500X) of polyclonal goat anti-CFTR antibody (Santa Cruz Biotechnology Inc, Santa Cruz, CA, U.S.A) were used in each group. The antibody was diluted with 1X TBS containing 0.05 mM PMSF, 0.01 $\mu\text{g/ml}$ aprotinin, 0.01 $\mu\text{g/ml}$ leupeptin, 5% normal rabbit serum and 5% human serum from blood type AB. Each section was incubated with the designated concentrations of goat anti-CFTR antibody for 60 minutes. Polyclonal goat anti-CFTR antibody is directed against the C terminus of human CFTR. Sections were then incubated with 300X dilution of biotinylated rabbit anti-goat IgG (Dako) for 30 minutes, then with avidin biotin complex alkaline phosphatase (Dako) for 30 minutes before staining with freshly made new fuchsin for 20 minutes followed by counterstained with Gill's hematoxylin (Surgipath Medical Industries) for 2 minutes. The positive controls were eight frozen kidney sections (5 μm) processed in the same way as the frozen lung sections mentioned above. For the negative control, one frozen lung section and one kidney section treated with each of the two fixatives were incubated with 2000X dilution of goat IgG instead of polyclonal goat anti-CFTR antibody. All the blocking and immunostaining were performed in Dako Autostainer Staining System.

5.4.3.3 The polymeric method (Envision™ G|2 System|AP, Rabbit/Mouse [Permanent Red])

Twelve frozen sections (10 µm thick) from a lung core of an unclassified COPD patient with a large airway and a small airway was used in this study. These twelve slides were separated into 3 groups fixed with three different fixatives. Four slides were fixed with room temperature acetone for 10 minutes, another four with cold methanol for 5 minutes, the last four with room temperature 10% formalin for 10 minutes. Sections were washed with 100 µl 1X TBS-Tween 20 pH 7.6 (0.05M Tris, 0.9% NaCl, 0.05% Tween 20). Three different dilutions of polyclonal goat anti-CFTR antibody (200X, 400X and 2000X) (Santa Cruz Biotechnology Inc) were used in each group. The antibody was diluted with 1X TBS containing 0.05 mM PMSF, 0.01 µg/ml aprotinin, 0.01 µg/ml leupeptin, 5% normal rabbit serum and 5% human serum from blood type AB. Each slide was incubated with the designated dilution of goat anti-CFTR antibody for 30 minutes. Since the EnVision™ detection system (Dako) only detects either rabbit or mouse antibodies, sections were incubated with 300X dilution of biotinylated rabbit anti-goat IgG (Dako) for 30 minutes. Sections were washed with 1X TBS and then incubated with tertiary antibody, rabbit/mouse (LINK) (Dako), for 30 minutes. Rabbit/mouse (LINK) is a dextran coupled with secondary antibodies against rabbit and mouse immunoglobulins. Sections were then washed with 1X TBS and incubated with alkaline phosphatase (Dako) for 30 minutes before staining with freshly made permanent red chromogen (Dako) for 10 minutes and counterstained with Gill's hematoxylin (Surgipath Medical Industries) for 2 minutes. For the negative control, one frozen section from each of the fixation groups was incubated with 4000X dilution of

goat IgG instead of polyclonal goat anti-CFTR antibody. All the immunostaining were performed in Dako Autostainer Staining System.

5.4.4 Quantification of β -ENaC protein staining using Image-Pro Plus

A light microscope (Nikon Eclipse E800, Japan) with SPOT Flex™ camera attachment (Diagnostic Instrument Inc., Sterling Heights, MI, USA) was used to capture images of each small airway from the lung sections that were stained for β -ENaC. All the images were captured at 4X magnification. The epithelium of the airway was first traced for measurement using an image analysis software called Image-Pro Plus (Media Cybernetics Inc). A segmentation profile was determined in order to allow the software to detect and distinguish the positive staining from the background staining. To avoid inclusion of background staining in the measurement, three sections (refer to table 5.6) with strong positive staining were used for colour segmentation. The software calculates the area of staining within the small airway epithelium highlighted by segmentation as well as the perimeter of the basement membrane of the small airway that had been traced and divides them to quantify β -ENaC protein expression in the small airway epithelium.

5.4.5 Staining of mucin with periodic acid Schiff (PAS)

One frozen section (10 μ m thick) from each of 72 lung cores (Section 5.4.1) with small airways listed in table 5.6 and summarized in table 5.7 was used for mucin staining. The tissue sections were dried in air followed by oxidizing them for 5 minutes in 0.5% periodic

acid. The sections were rinsed with distilled water for 3 times, immersed in Schiff's reagent (Surgipath) for 5 minutes, and rinsed in warm running tap water for 5 minutes followed by counterstaining with diluted Gill's hematoxylin (Surgipath) for 30 seconds. Saturated lithium carbonate was applied to make the hematoxylin stain look blue. The mucin was stained in magenta. The sections were then rinsed with running tap water, dried in the air overnight and coverslipped.

5.4.6 Quantification of mucin staining in the airway epithelium and mucus plugging of the airway by Image-Pro Plus

The same instrumentation and procedure used to quantify β -ENaC staining above (Section 5.4.4) was used to quantify mucin staining with the periodic acid Schiff reagent. This included creating a segmentation profile using two sections specified in table 5.6 with strong positive staining. Similarly, the software calculated the area of pink mucin staining in the airway epithelium highlighted by the segmentation process which is then divided by the perimeter of the basement membrane of the small airway that had been traced to quantify the expression of epithelial mucin.

In many cases, the walls of the small airways have folds when observed after tissue processing. In order to calculate the size of the mucus plug relative to the size of airway lumen correctly, the ratio of plug area to the expanded luminal area of the airway was obtained. Image-Pro Plus measured the area of the mucus plug after the mucus plug was traced. The area of expanded lumen (A_{P1}^*) was calculated from the area enclosed by a circle

formed by the full length of basement membrane (A_{P2}^*) minus the area of epithelium (A_E) [9]. A_{P2}^* was calculated using the length of the basement membrane of the small airway (P2).

The equation of calculating A_{P1}^* is as follows:

$$A_E = A_{P2} - A_{P1}$$

$$A_{P1}^* = A_{P2}^* - A_E$$

$$A_{P1}^* = A_{P2}^* - (A_{P2} - A_{P1})$$

$$A_{P1}^* = (P2)^2 / 4\Pi - (A_{P2} - A_{P1})$$

where A_E = Area of the epithelial layer

A_{P1} = Area within the airway lumen (from measurement)

A_{P2} = Area within basement membrane (from measurement)

A_{P1}^* = Area of fully expanded lumen

A_{P2}^* = Area within basement membrane after the luminal area is fully expanded

P2 = Length of basement membrane (from measurement)

Once the area of the expanded lumen is calculated, the extent of mucus plugging of the airway lumen could be obtained by dividing the area of the mucus plug by the area of the expanded lumen.

5.5 Statistical Analyses

The non-parametric Kruskal-Wallis test was used to analyze the difference in the median normalized β -ENaC or CFTR mRNA expression among the three GOLD categories. Linear regression analysis was used to determine the correlation between the median of normalized

β -ENaC or CFTR mRNA expression and the FEV_{1pp} (according to Results section 6.1.2 and 6.2.7) of the corresponding patient as well as the correlation between the normalized β -ENaC and CFTR mRNA expression of each airways (Results section 6.1.2 and 6.2.7). The non-parametric Kruskal-Wallis test was used to analyze the difference in the median β -ENaC protein expression, epithelial mucin expression, or mucus plugging and GOLD category (Result section 6.3.2, 6.4.1, 6.4.3). The correlation between β -ENaC protein expression, epithelial mucin expression, or mucus plugging and the FEV_{1pp} (Results section 6.3.2, 6.4.1, 6.4.3) as well as the relationship between β -ENaC protein and mRNA expression of β -ENaC or CFTR (Results section 6.3.2) were analyzed by Spearman's rank correlation coefficient. Spearman's rank correlation coefficient was also used to determine the correlation between β -ENaC protein expression and epithelial mucin expression (Results section 6.4.1) as well as the correlation between epithelial mucin expression and β -ENaC, CFTR mRNA or Muc5ac mRNA expression (Results section 6.4.1 and 6.4.2). The correlation between mucus plugging and β -ENaC, CFTR or Muc5ac mRNA expression (Results section 6.4.3) as well as the relationship between mucus plugging and β -ENaC protein expression (Results section 6.4.3) were analyzed by Spearman's rank correlation coefficient. The correlation between mucus plugging and epithelial mucin expression was analyzed by Spearman's rank correlation coefficient (Results section 6.4.3). Student's t test was used to compare background history of patients providing the two lung sample types (Results section 6.2.8). Bonferroni correction was used to adjust for multiple comparison. All statistical analyses were done using JMP IN 5.1 (SAS Institute Inc, Cary, NC, USA) and GraphPad Prism 5 (GraphPad Software, La Jolla, CA, USA). P-values ≤ 0.05 were considered significant.

Chapter 6: Results

6.1 Gene expression studies of whole small airways and surrounding lung parenchyma

6.1.1 Quantity and quality of RNA from whole small airways and lung parenchyma

Table 6.1 shows the average values of the quantity and quality of the total RNA extracted from small conducting airways captured from 22 consecutive serial sections from the cores of lung tissue from COPD patients in the different GOLD categories. The average amounts of extracted RNA from GOLD 0, 2 and 3/4 were 270, 228 and 432 ng, respectively. The average RIN of airways in GOLD 0, 2, and 3/4 was 4.8, 5.0 and 4.0, respectively. The Kruskal-Wallis analysis showed a significant increase between the RNA yield from GOLD 0 to 3/4 ($p=0.004$) and from GOLD 2 to 3/4 ($p=0.0002$). It also showed a significant decrease in RIN from GOLD 0 to 3/4 ($p=0.03$).

Table 6.1: The quantity and quality of RNA extracted from whole small airways.

GOLD category	# of cases	# of airways	Average quantity of extracted RNA (ng) ±SD (range)	Average RIN ±SD (range)
0	16	35	270±255 (51-957)	4.8±1.5 (2.4-7.7)
2	17	36	228±237 (48-1008)	5.0±1.8 (2.4-7.9)
3/4	12	28	432±309*† (225-1350)	4.0±1.1* (2.1-6.5)

Total RNA was extracted from isolated whole small airways of 22 consecutive serial sections (10 µm thick) of 35 airways from 16 GOLD 0 patients, 36 airways from 17 GOLD 2 patients, and 28 airways from 12 GOLD 3/4 patients. The average quantity of total RNA extracted is represented in ng while the average RNA quality is expressed as RIN, where n= 99 airways. The Kruskal-Wallis test was used to analyze the difference in average yield and RIN between the different GOLD stages.

* p=0.004 or 0.03 for the comparison of average RNA quantity or RIN to GOLD 0 patients

† p=0.0002 for the comparison of average RNA quantity or RIN to GOLD 2 patients.

Table 6.2 shows the average values of the quantity and quality of total RNA extracted from the lung parenchyma that remained after the whole airways had been removed from 16 of the consecutive lung sections from the cores from above, except for one core from a GOLD 2 patient which was not included since the corresponding sample was missing. The average quantity of extracted RNA from surrounding lung parenchyma from GOLD 0, 2, and 3/4 was 2040, 2040 and 2520 ng, respectively, and the average RIN was 4.8, 4.7, and 4.2, respectively.

Table 6.2: The quantity and quality of RNA extracted from surrounding lung parenchyma.

GOLD category	# of cases	# of airways	Average quantity of extracted RNA (ng) ±SD (range)	Average RIN ±SD (range)
0	16	35	2040±1620 (183-5568)	4.8±1.5 (1.0-7.2)
2	17	35	2040±1470 (321-5301)	4.7±1.4 (1.0-6.6)
3/4	12	28	2520±1500 (555-6930)	4.2±1.5 (1.0-6.7)

Total RNA was extracted from the tissue remaining on the first 16 consecutive serial sections (10 µm thick) of 35 lung cores from 16 GOLD 0 patients, 35 lung cores from 17 GOLD 2 patients, and 28 lung cores from 12 GOLD 3/4 patients after the whole airways had been captured. The average quantity of total RNA extracted is represented in ng while the average RNA quality is expressed as RIN, where n= 98 lung parenchymal samples. The Kruskal-Wallis test showed no significant difference between the yields or RIN from different GOLD stages.

6.1.2 Gene expression in whole small airways and surrounding lung parenchyma using PCR and relative quantification

Ten times amplified cDNA from each of 99 whole small airways and each of 98 surrounding lung parenchymal tissue of 45 COPD patients were used in these studies. Figure 6.1 shows the median mRNA expression of β -ENaC or CFTR normalized to that of β -actin, β -2-M and HPRT1 in the two tissue types from patients of the three GOLD categories. The Kruskal-Wallis test used to analyze the difference in median mRNA expression in these GOLD categories showed that there is no significant change in mRNA expression of β -ENaC or CFTR among the three GOLD categories in either tissue type.

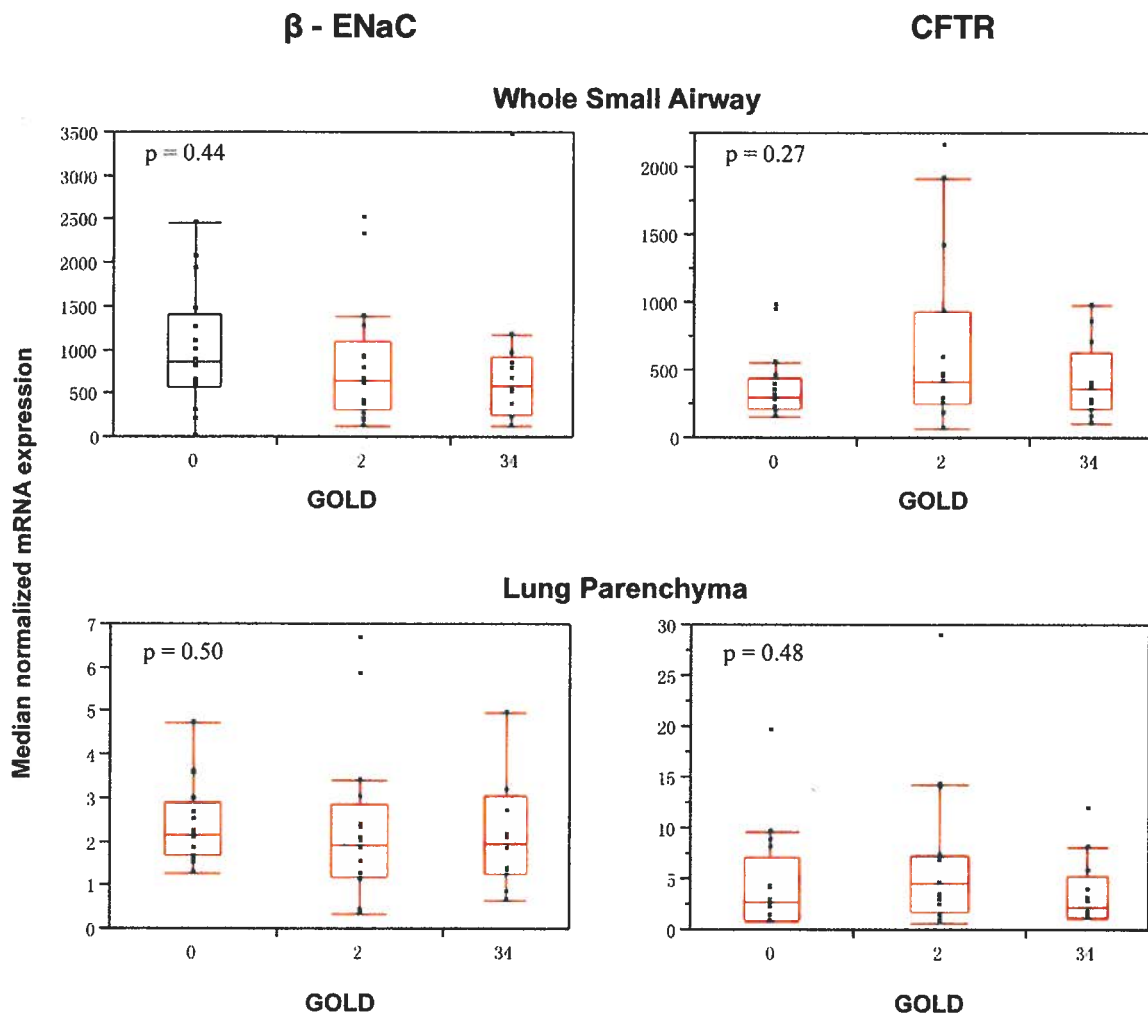


Figure 6.1: Gene expression versus GOLD stage in whole small airways and lung parenchyma of COPD patients. The median mRNA expression for each patient was normalized to that of β -actin, β -2-M, and HPRT1. The median normalized mRNA expression for each patient is on the y-axis and the different GOLD categories are on the x-axis. The data are expressed as box plots. The red line inside the box represents median mRNA expression in each GOLD stage and the boxes denote the lower and higher quantiles while the tails represent the range of the data with the exception of data outside the tails that are possible outliers. P values are from the Kruskal-Wallis test used to analyze the difference in mRNA expression among three GOLD stages.

The correlation between the median of the normalized mRNA expression of β -ENaC or CFTR in whole small airways and lung parenchyma of 45 COPD patients and the FEV_{1pp} of these patients (Table 5.1a) is shown in Figure 6.2. Linear regression used to analyze the correlation showed no significant correlation between mRNA expression and FEV_{1pp} in these two tissue types.

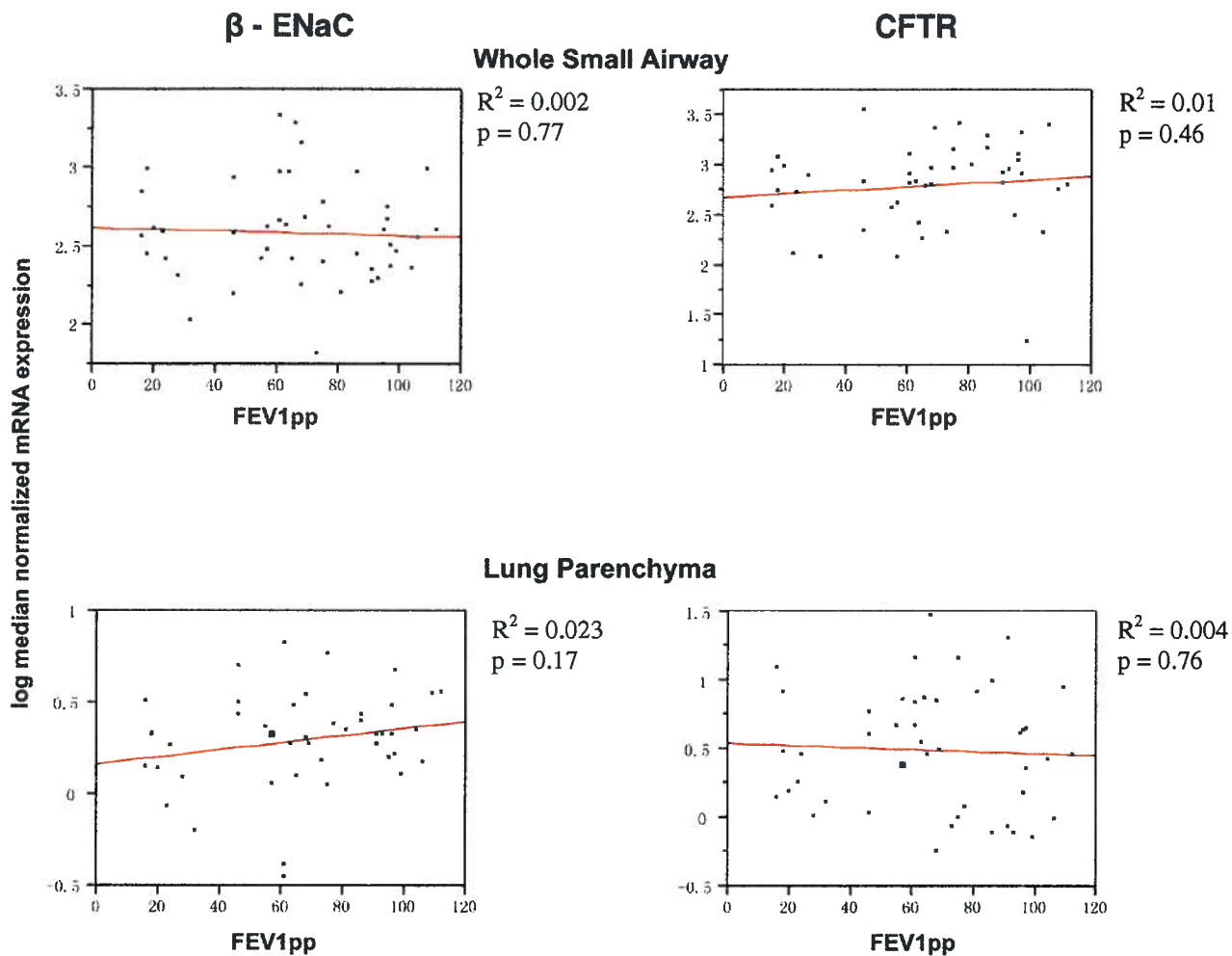


Figure 6.2: Gene expression versus FEV_{1pp} in whole small airways and lung parenchyma of COPD patients. The median mRNA expression of β -ENaC and CFTR normalized with that of β -actin, β -2-M, and HPRT1 for each patient is transformed into a log scale. FEV_{1pp} measures lung function as a percentage of the predicted value. Linear regression (red line) was used to analyze the correlation between gene expression and FEV_{1pp}.

The same individuals whole small airways (n=99) and lung parenchyma (n=98) were used to analyze the correlation between the normalized β -ENaC and CFTR mRNA expression in these tissues (Figure 6.3). In this case, linear regression showed a significant positive correlation between β -ENaC and CFTR mRNA expression in the lung parenchymal samples ($R^2 = 0.06$, $p = 0.01$).

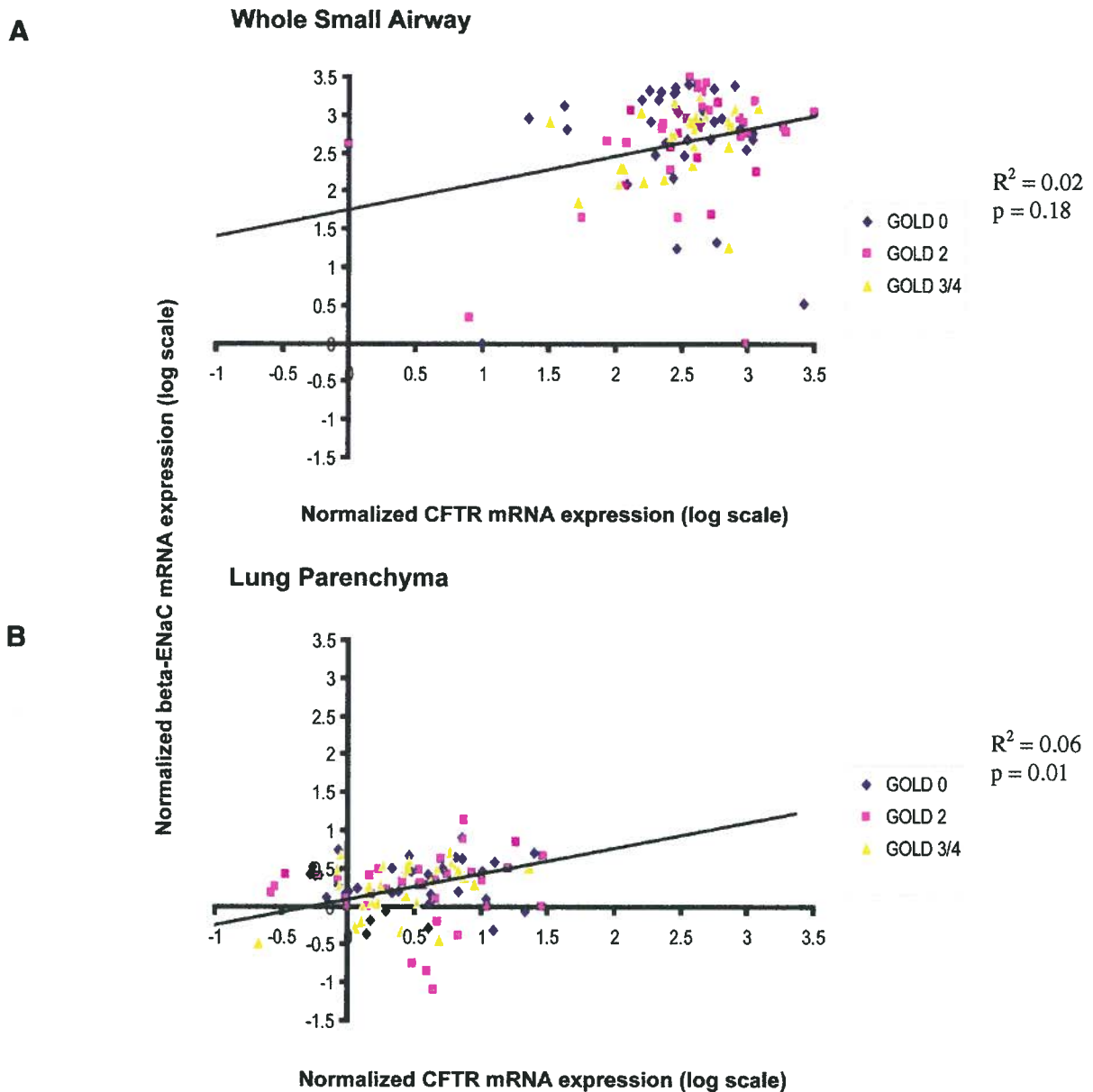


Figure 6.3: Scatterplots showing the correlation between β -ENaC and CFTR mRNA expression. Log transformed the normalized β -ENaC are plot against that of the respective CFTR mRNA expression in A) 99 whole small conducting airways from 45 COPD patients and B) 98 surrounding lung parenchyma from the same patients. These samples are coded according to GOLD categories the patient represent with GOLD 0 (◆), GOLD 2 (■), and GOLD 3/4 (▲). The linear regression line (black) shows the correlation between β -ENaC and CFTR mRNA expression. A positive correlation between β -ENaC mRNA expression and CFTR mRNA expression was determined in surrounding lung parenchyma ($R^2 = 0.06$, $p=0.01$) but not in the whole small airways.

6.2 Gene expression studies of small airway epithelium

6.2.1 Absolute quantification

6.2.1.1 Verification of size of vectors, inserts, and plasmids by 0.7% agarose gel electrophoresis

Restriction endonuclease digestion of the recombinant plasmids carrying the cDNAs of interest confirmed the presence of fragments of the following expected sizes (Figures 6.4, 6.5 and 6.6). The 2.5 kb and 2.0 kb fragments representing β -ENaC and β -actin cDNAs, respectively, were present (Figure 6.4 and 6.5). Since β -ENaC and β -actin plasmids used the same vector, pCMV6-XL4, they both showed a 4.7 kb fragment after restriction enzyme digestion (Figure 6.4 and 6.5). For CFTR digested with Pst I, a 6.2 kb CFTR cDNA and 3.0 kb vector DNA were present (Figure 6.6).

The size of the cDNAs cloned into the plasmids is slightly different from the length of the mRNAs reported in NCBI (refer to Section 5.2.2.4.2). For β -ENaC and β -actin plasmids purchased from OriGene Technologies, Inc, 5' and 3' untranslated regions included in the cDNA differ from the reported NCBI transcript size. However, DNA sequence analysis of the inserts showed that the open reading frames of β -ENaC and β -actin cDNAs are full-length and match the reference sequences posted at NCBI (data not shown). For CFTR plasmid, 6.2 kb length for the insert is an estimation. CFTR cDNA is 6.129 kb long [64] which is the same as the NCBI sequence. However, addition of linker sequences to the CFTR cDNA during recombinant DNA synthesis has increased the size of the insert.

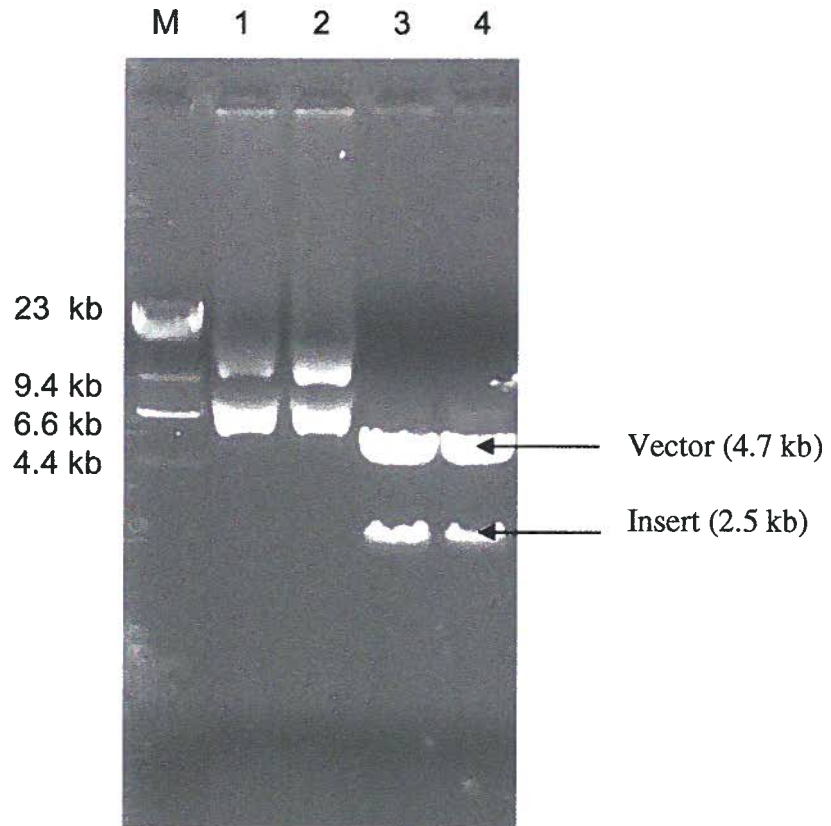


Figure 6.4: Verification of full-length human β -ENaC cDNA in the recombinant pCMV6-XL6 plasmid using 0.7% agarose gel electrophoresis. Lane M is λ DNA digested with Hind III (DNA ladder). Lanes 1 and 2 show full-length human β -ENaC plasmid DNA before Not I digestion. Lanes 3 and 4 show vector DNA and cDNA insert after Not I digestion.

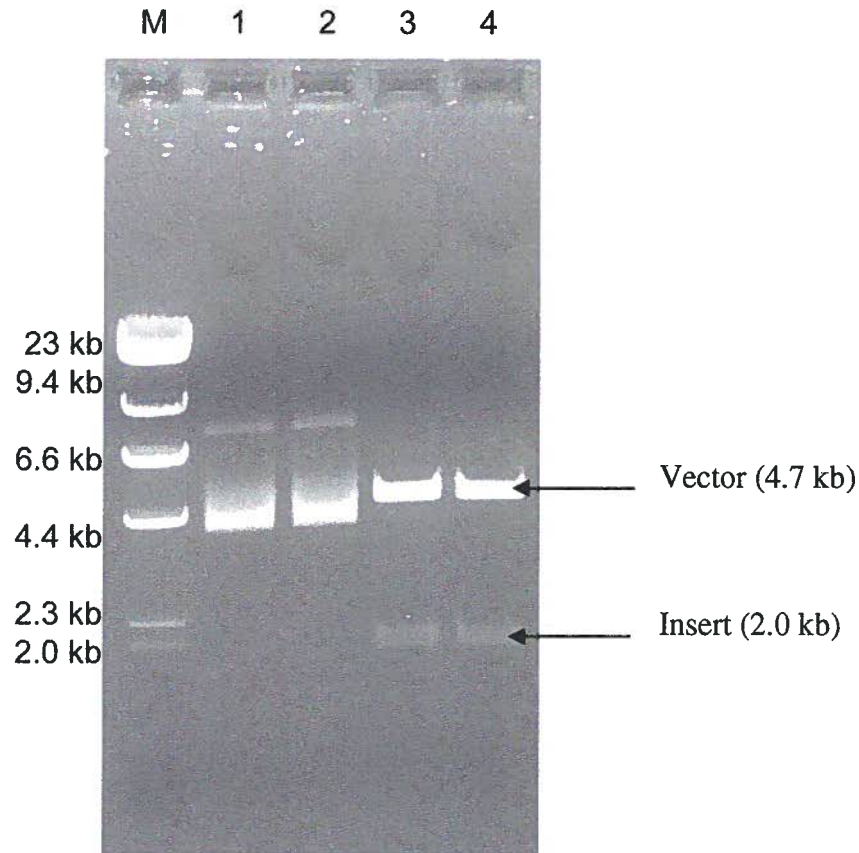


Figure 6.5: Verification of full-length human β -actin cDNA using 0.7% agarose gel electrophoresis. Lane M is λ DNA digested with Hind III (DNA ladder). Lane 1 and 2 show full-length human β -actin plasmid DNA before Not I digestion. Lane 3 and 4 show vector and insert after Not I digestion.

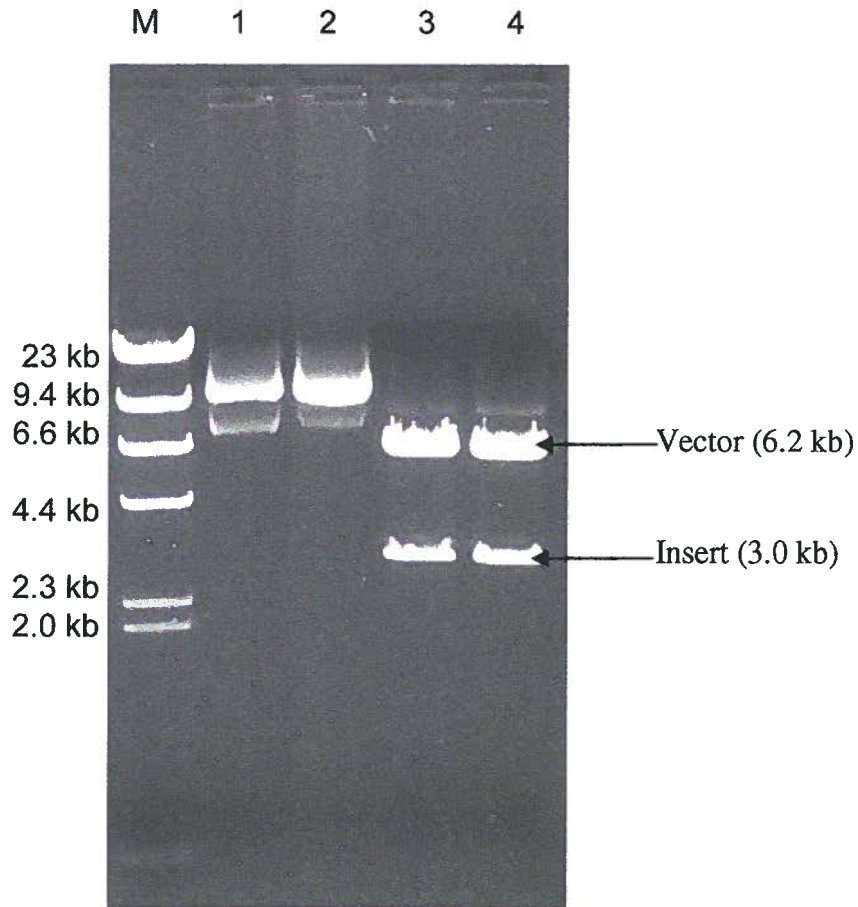


Figure 6.6: Verification of full-length human CFTR cDNA using 0.7% agarose gel electrophoresis. Lane M is λ DNA digested with Hind III (DNA ladder). Lane 1 and 2 show full-length human CFTR plasmid DNA before Pst I digestion. Lane 3 and 4 show vector and insert after Pst I digestion.

6.2.1.2 Real-time PCR standard curves of β -ENaC, CFTR and β -actin

Figures 6.7 a-c illustrate three real-time PCR standard curves prepared using 10 times serially diluted β -ENaC, CFTR or β -actin plasmid DNA standards (2×10^6 , 2×10^5 , 2×10^4 , 2×10^3 , 2×10^2 , and 2×10^1 copies). The three real-time PCR standard curves show an inverse relationship between the starting quantities of plasmid DNAs and their corresponding Ct values. The slopes of real-time PCR curves of β -ENaC, CFTR and β -actin were -3.49, -3.37, and -3.44, respectively with three R^2 values of approximately at 0.99. After applying these Ct values to the PCR efficiency formula shown in the materials and methods (Section 5.3.7.1.6), the PCR efficiencies of these three genes were calculated to be between 97% and 99%.

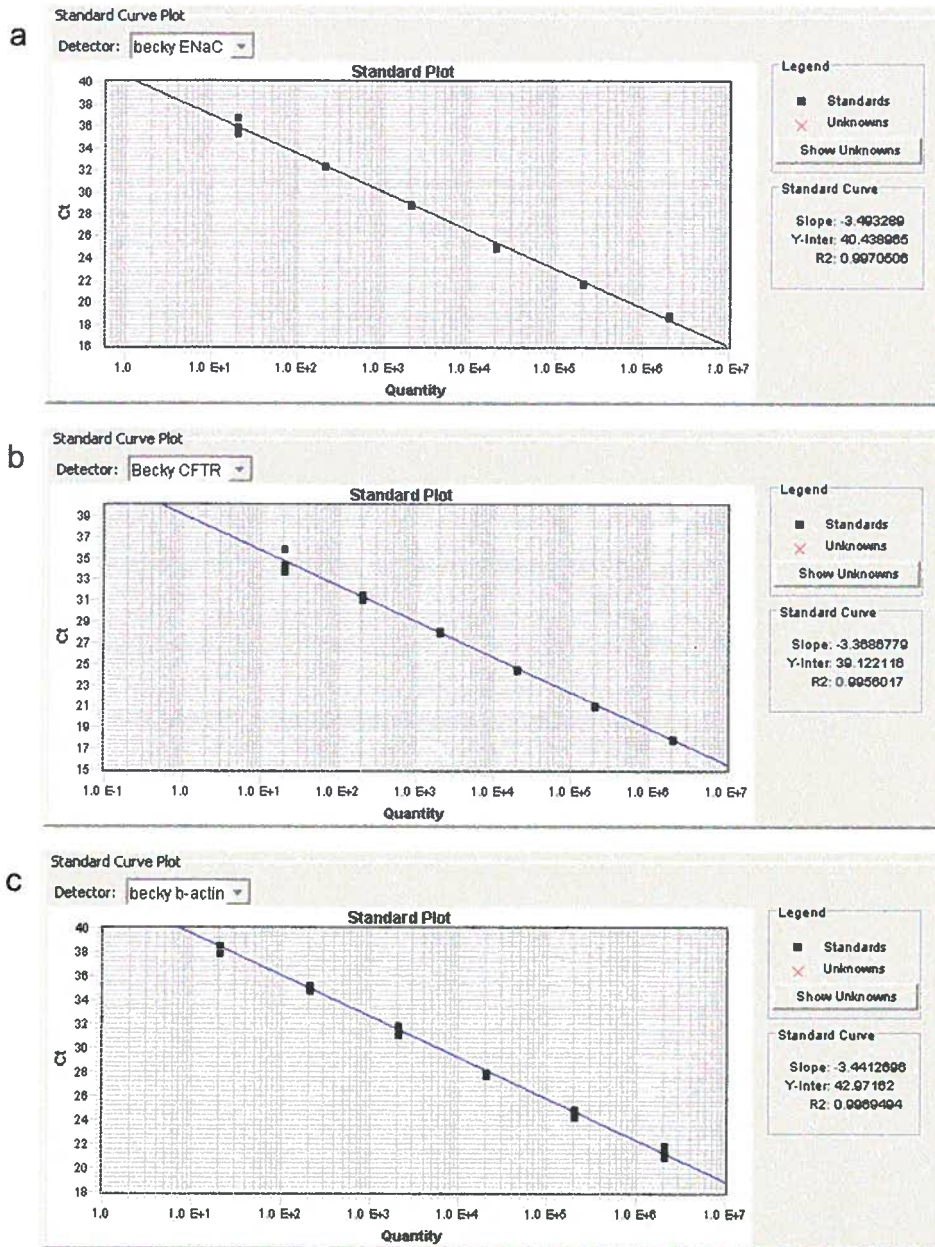


Figure 6.7: Real-time PCR standard curves. Six serially diluted plasmid DNAs of β -ENaC, CFTR, or β -actin (2×10^6 , 2×10^5 , 2×10^4 , 2×10^3 , 2×10^2 , and 2×10^1 copies) were used in the PCR reaction to generate PCR standard curves. The standard curves of a) β -ENaC, b) CFTR and c) β -actin were used for quantification of gene expression of small airway epithelium from COPD patients. Y-axis represents Ct values while x-axis represents starting quantity of plasmid DNA shown as copy number.

6.2.2 RNA quantity and quality of RNA from T84 cells

The concentration of the T84 cells grown in the 75 cm² flat culture flask and harvested in 15 ml medium was 1.74×10^7 cells/ml to give a total of 2.61×10^8 cells. RNA was extracted from 1.8×10^6 of these cells to give an average RNA yield of 0.184 ng/cell with an RIN of 8.3.

6.2.3 LCM of small airway epithelium

The epithelium of the small conducting airways on consecutive sections of frozen lung cores was isolated using LCM. Figure 6.8A shows an intact small airway which was stained with hematoxylin & eosin. Figure 6.8B shows the same section after small airway epithelium was removed. Figure 6.8C shows the captured airway epithelium on the surface of a thermoplastic cap.

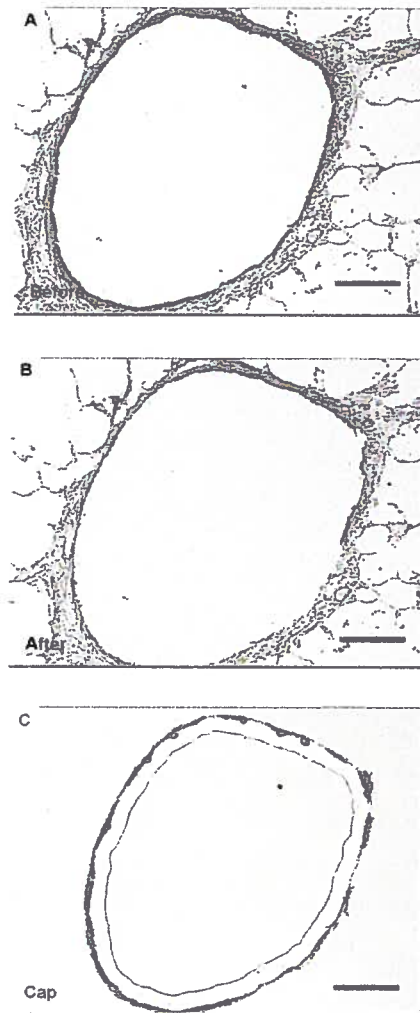


Figure 6.8: Laser capture microdissection of small airway epithelium. Small airway epithelium from a GOLD 0 patient was isolated using LCM where A is a micrograph of an intact histological section of the lung with a small airway stained with hematoxylin and eosin; B, the same section after the epithelium was removed by LCM; C, the captured epithelium. (bar = 100 μ m)

6.2.4 Determination of the amount of tissues required for LCM followed by RNA extraction to yield RNA of sufficient quantity to quantify for gene expression analyses (preliminary studies)

Table 6.3 shows the average quantity and quality of RNA of the epithelium isolated from small conducting airways from 28, 58, and 88 serial consecutive frozen lung sections from patients of undetermined GOLD category as well as 58 sections from GOLD 0 and GOLD 2 patients. In the patients of unclassified GOLD category, the average amount of total RNA extracted increased as the number of lung sections increases. The average RIN of RNA in the unclassified GOLD patients was 5.0. For the GOLD 0 and 2 patients, the average quantity and quality of total RNA extracted were 51 ng and 4.3, respectively. The average RNA quantity and RIN from 12 whole 50 μ m serial frozen lung sections with small conducting airways from GOLD 4 patients was 2750 ng and, 4.0, respectively.

Table 6.3: Quantity, quality and Ct value determined after PCR of RNA from unclassified, GOLD 0-2 and GOLD 4 patients (preliminary data).

GOLD category (# of patients)*	RNA source	Average quantity of extracted RNA (ng) \pm SD (range)	Average RIN \pm SD	RNA equivalent cDNA per PCR (ng) \pm SD (range)	Average Ct \pm S.D.		
	Airways from # of 10 μ m section				β -ENaC	CFTR	β -actin
unclassified (3)	28	71 \pm 30 (39-99)	5.0 \pm 0.8	7.1 \pm 3.0 (3.9-9.9)	36.9 \pm 1.9	37.4 \pm 1.9	33.5 \pm 2.6
	58	243 \pm 163 (65-384)		24.3 \pm 16.3 (6.5-38.4)	31.9 \pm 3.5	34.1 \pm 1.2	31.8 \pm 2.2
	88	268 \pm 43 (219-295)		26.8 \pm 4.3 (21.9-29.5)	34.3 \pm 1.7	34.7 \pm 1.4	32.8 \pm 1.7
0 (1) 2 (2)	58	51 \pm 21 (32.4-78.3)	4.3 \pm 1.3	5.1 \pm 2.1 (3.24-7.83)	29.4 \pm 1.4	33.5 \pm 0.7	30.8 \pm 1.3
4 (3)	12 whole 50μm sections	2750 \pm 793 (1850-3350)	4.0 \pm 1.4	275 \pm 79.3 (185-335)	30.4 \pm 1.4	31.4 \pm 1.6	33.1 \pm 0.4

Airways epithelium from increasing numbers of 10 μ m tissue sections from lung cores from unclassified patients was used to determining the number of sections required for generating reliable quantitative real-time PCR results for all three genes. Fifty-eight 10 μ m sections from GOLD 0-2 were used to validate the results from the unclassified patients. Twelve whole 50 μ m sections from GOLD 4 patients were used to determine if CFTR mRNA expression is detectable in severe COPD. The average quantity in ng and quality of RNA as RIN extracted from these samples is given as well as the Ct value determined after PCR using 10% of the RNA equivalent cDNA per PCR. Ct values less than 36 were considered as reliable quantitative real-time PCR results. The Kruskal-Wallis test showed no significant difference between the RIN from the three different groups of patients.

* each patient contributed to one airway except for the GOLD 0 patient whose two lung cores have one airway each.

6.2.5 TaqMan® real-time PCR on patients' samples to determine the amount of tissue required for LCM followed by RNA extraction and gene expression analysis and whether this expression could be detected in samples from GOLD 3/4 patients (preliminary studies)

After reverse transcription of the RNA from section 6.2.4, only 10% of the RNA equivalent cDNA was used in each real-time PCR reaction. For the unclassified patients, about 7.1 ng, 24.3 ng and 26.8 ng RNA equivalent cDNA from 28, 58, 88 sections was used in each of real-time PCR reaction of β -ENaC, CFTR and β -actin (Table 6.3). The average Ct values of all three genes initially decreased when the amount of cDNA added to the PCR reaction was increased from that representing the 28 sections to that from the 58 sections but then consistently decreased when more cDNA representing the 88 sections was used. From the preliminary studies done in our laboratory, Ct values lower than 36 are considered reliable for quantitative real-time PCR results. As shown in Table 6.3, Ct values of β -ENaC and CFTR were higher than 36 cycles when the RNA was limited to that representing 28 consecutive lung sections from the unclassified patients but lower with that from 58 and 88 sections from these patients. These results, indicating adequate amounts of RNA for the PCR analyses from the 58 sections, were supported by results from RNA equivalent cDNA from 58 sections of GOLD 0-2 patients which, while total RNA yields were less than a quarter of that from the unclassified patients, gave Ct values consistently below those from the same number of sections from the unclassified patients and well below our cut-off of 36 cycles (Table 6.3).

Since the hypothesis of my studies (see section 4.1) states that CFTR expression would be reduced as COPD progresses, it was important to pre-determine whether CFTR mRNA expression could be detected in patients with severe COPD. Table 6.3 shows that 275 ng of RNA equivalent cDNA representing 1/10 of the RNA from the 12 whole 50 μ m lung sections of GOLD 4 patients, gave average Ct values for all three genes that were much lower than the cut-off of 36 cycles. Therefore, CFTR mRNA expression was detectable and quantifiable in whole lung sections of severe COPD patients when adequate RNA was available.

6.2.6 Yield and quality of RNA of epithelia from 83 small conducting airways

Results from the preliminary study determined that at least 58 consecutive lung sections (10 μ m) with small airway(s) from a lung core were required for studying gene expression of β -ENaC, CFTR and β -actin in small airway epithelium. In addition, since an average of 51 ng of total RNA was extracted from the 58 sections from the GOLD 0 and 2 patients to achieve acceptable Ct values (Table 6.3), a minimum of 50 ng total RNA from these epithelial layers of each small conducting airway was set as a limit for these expression studies.

Table 6.4 shows the average quantity and quality of total RNA extracted from epithelial layers from 58 sections of each of 31 airways from 14 GOLD 0 patients, 28 airways from 13 GOLD 2 patients and 24 airways from 12 GOLD 3/4 patients. The average yield of total RNA from GOLD 0, 2, and 3/4 was 68, 157, and 160 ng, respectively. The average RIN

was 6.6, 6.8 and 7.4, respectively. The Kruskal-Wallis analysis showed significant increase in the RNA yield from GOLD 0 compared to 2 ($p=0.004$) and from GOLD 0 to 3/4 ($p=0.01$).

Table 6.4: The quantity and quality of RNA extracted from the epithelium of 83 small airways.

GOLD category	# of cases	# of cores	# of airways	Average quantity of extracted RNA (ng) ±SD (range)	Average RIN ±SD (range)
0	14	28	31	68±51 (7.4-173.9)	6.6±2.0 (3.8-8.9)
2	13	27	28	157±144* (10.5-786.3)	6.8±1.4 (4.2-9.3)
3/4	12	23	24	160±137† (7.5-365.7)	7.4±1.4 (2.9-9.1)

* comparison between GOLD 0 and 2 (p=0.004)

† comparison between GOLD 0 and 4 (p=0.01)

The quantity and quality of RNA extracted from epithelial layers of 58 consecutive serial sections (10 µm thick) from GOLD 0 GOLD 2, and GOLD 3/4 patients. The average quantity of total RNA extracted is represented in ng while the average RNA quality is expressed as RIN, where n = 83 airways. The Kruskal-Wallis test showed significant increase between the RNA yield from GOLD 0 to 2 and from GOLD 0 to 3/4. No significant difference between the RIN from the three different groups of patients.

Figure 6.9 demonstrates the frequency distribution of the amount of total RNA extracted from epithelia isolated from the 83 small conducting airways. The amount of total RNA extracted was between 7.4 and 786 ng (Table 6.4). Most epithelial samples (64/83) had a total RNA yield greater than 50 ng. Based on the criteria of at least a 50 ng RNA yield and this frequency distribution curve (Figure 6.9), 64 out of the possible 83 airway epithelial samples had sufficient amounts of RNA to study the genes of interest in the small airway epithelium. These 64 airways represented a total of 37 patients.

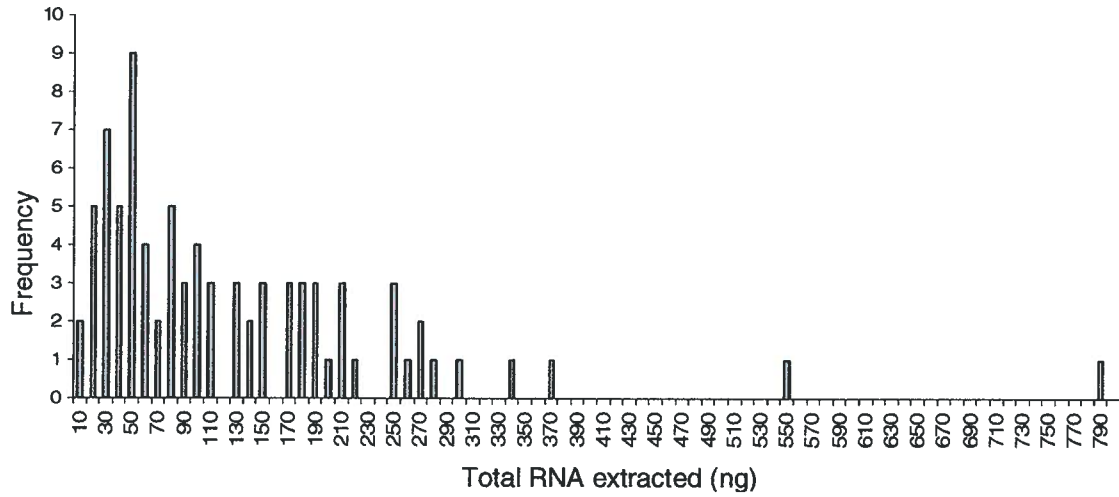


Figure 6.9: Frequency distribution of the amount of total RNA extracted from epithelium of 83 small airways. The amount of extracted total RNA ranged between 7.4 and 786 ng with 64 out of the 83 epithelial samples having greater than 50 ng.

6.2.7 PCR results from T84 RNA and total human placenta RNA and Gene expression of β -ENaC and CFTR in small airway epithelium

50 ng total RNA from each of T84 cells and human placenta served as the controls of CFTR and β -ENaC in RT, respectively. The normalized CFTR mRNA expression of T84 cells was 6.51 while the normalized β -ENaC mRNA expression was 4.82.

In the first of two PCR analyses performed on the RNA from the small airway epithelium, five ng total RNA from each of the 64 small airway epithelia that met the criterium for further PCR analysis was used in each of PCR reactions of β -ENaC, CFTR and β -actin. Since expression of β -ENaC, CFTR and β -actin could not be detected in most of these epithelial samples (data not shown), the remaining RNA from the epithelium isolated from 64 small conducting airways of lung tissue cores from the 37 patients was re-evaluated for use in a second PCR analysis. The concentration of the remaining RNA was measured by Agilent Bioanalyzer 2100 again. The quantity of the remaining RNA was calculated by multiplying the concentration of remaining RNA by the remaining volume of RNA. Only 36 out of the 64 small airway epithelial samples had sufficient quantities of RNA remaining for the second PCR analysis (Table 6.5 and data not shown). The average quantities in GOLD 0, 2, and 3/4 patients were 107, 151 and 141 ng, respectively and the average RIN, 7.9, 6.6 and 6.5, respectively (Table 6.5). These 36 airways represented 26 patients.

Table 6.5: The quantity and quality of the remaining RNA from epithelium of 36 small airways.

GOLD category	# of cases	# of cores	# of airways	Average quantity of remaining RNA (ng) (Mean±SD)	Average RIN (Mean±SD)
0	5	6	6	107±28 (58-136)	7.9±0.3 (7.5-8.4)
2	10	16	17	151±123 (60-601)	6.6±1.7 (2.9-8.0)
3/4	11	13	13	141±43 (45-195)	6.5±1.8 (3.0-8.5)

Bioanalyzer results of the RNA remaining in the 64 small airways epithelial samples after the first PCR series determined that 36 of these had sufficient RNA for a further PCR analysis. The average quantity of the RNA samples is represented in ng while the average RNA quality is expressed as RIN. The Kruskal-Wallis test showed no significant difference between the quantity of remaining RNA or the RIN from the three different groups of patients.

In the second PCR analysis, expression of β -ENaC, CFTR and β -actin in four epithelial samples from two GOLD 2 as well as two GOLD 3/4 patients could not be detected (data not shown). Therefore, gene expression could only be detected in 32 epithelial samples and these samples represent 32 airways from 24 patients (Table 6.6).

Table 6.6: The quantity and quality of the remaining RNA from the epithelium of 32 small airways with detectable gene expression.

GOLD category	# of cases	# of cores	# of airways	Average quantity of remaining RNA (ng) (Mean±SD)	Average RIN (Mean±SD)
0	5	6	6	107±28 (58-136)	7.9±0.3 (7.5-8.4)
2	9	14	15	153±132 (60-601)	6.5±1.8 (2.9-7.8)
3/4	10	11	11	141±43 (45-191)	6.4±1.9 (3.0-8.5)

Bioanalyzer results of the RNA remaining in the 64 small airways epithelial samples after the first PCR series determined that 36 of these had sufficient RNA for a further PCR analysis. Only 32 airway samples generated reliable PCR results. The average quantity of the remaining RNA is represented in ng while the average RNA quality is expressed as RIN. The Kruskal-Wallis analysis showed no significant difference between the quantity of remaining RNA or the RIN from the three different groups of patients.

Figure 6.10 shows the normalized mRNA expression of β -ENaC or CFTR against GOLD category in small airway epithelium of the 24 COPD patients. The Kruskal-Wallis test was used to analyze the difference in mRNA expression among GOLD categories. Unfortunately, there was no significant change in mRNA expression of β -ENaC or CFTR among the three GOLD categories.

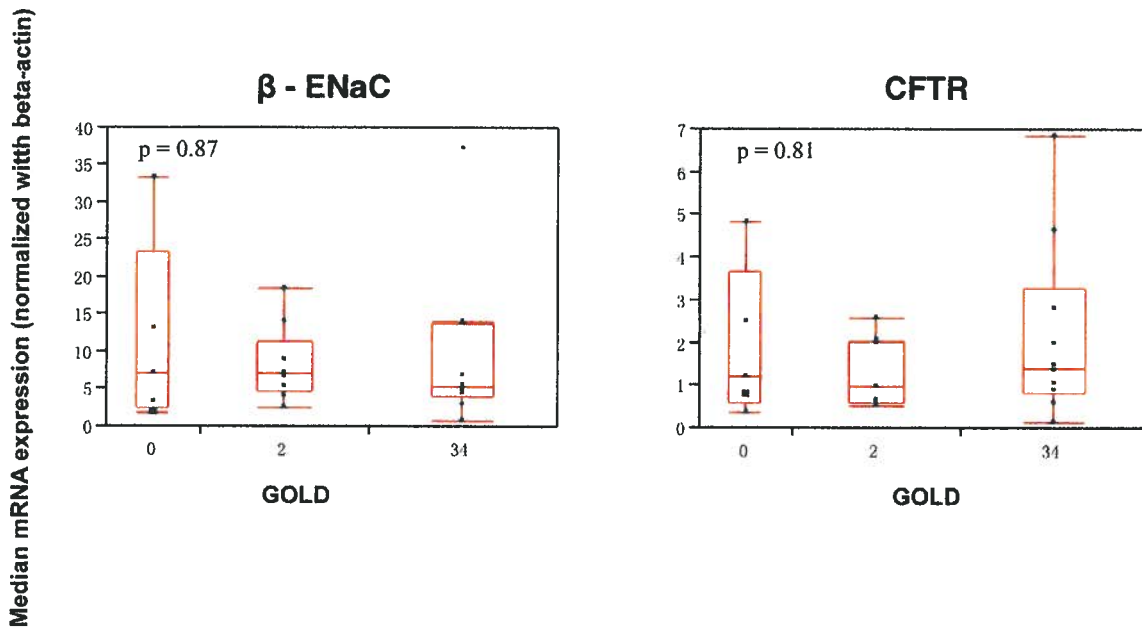


Figure 6.10: Gene expression versus GOLD stage in small airway epithelium of 24 COPD patients. The median β -ENaC (left panel) and CFTR (right panel) mRNA expression normalized with that of β -actin of each patient is on the y-axis and the different GOLD stages are on the x-axis. The data are expressed as box plots. The red line inside the box represents median mRNA expression in each GOLD stage and the boxes denote the lower and higher quantiles while the tails represent the range of the data with the exception of data outside the tails that are possible outliers. P values are from the Kruskal-Wallis test used to analyze the difference in mRNA expression among the three GOLD stages.

The correlation between median mRNA expression of β -ENaC or CFTR and FEV_{1pp} in small airway epithelium of the 24 COPD patients is shown in figure 6.11. Linear regression was used to analyze the relationship between these two variables. However, there was no correlation between mRNA expression of β -ENaC or CFTR and FEV_{1pp} in these patients.

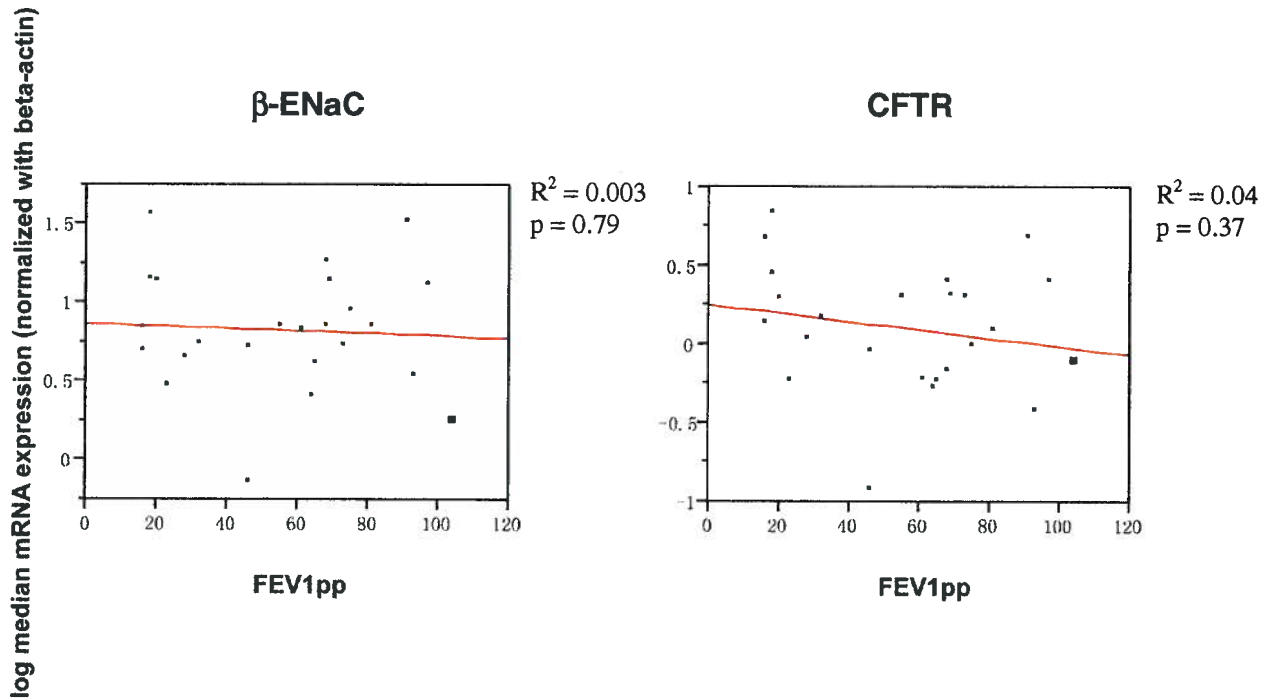


Figure 6.11: Gene expression versus FEV₁pp in small airway epithelium of 24 COPD patients. The median β-ENaC (left panel) and CFTR (right panel) mRNA expression normalized with that of β-actin for each patient of was transformed into a log scale and plotted against FEV₁pp, a parameter to measure lung function shown as a percentage of the predicted value. Linear regression (red line) was used to analyze the correlation between these two variables.

Figure 6.12 shows the relationship between β -ENaC and CFTR mRNA expression in 32 small airway epithelia from the 24 COPD patients. Linear regression was used to analyze the correlation between these two variables. A strong positive correlation was found in small airway epithelia ($R^2 = 0.7$, $p < 0.0001$).

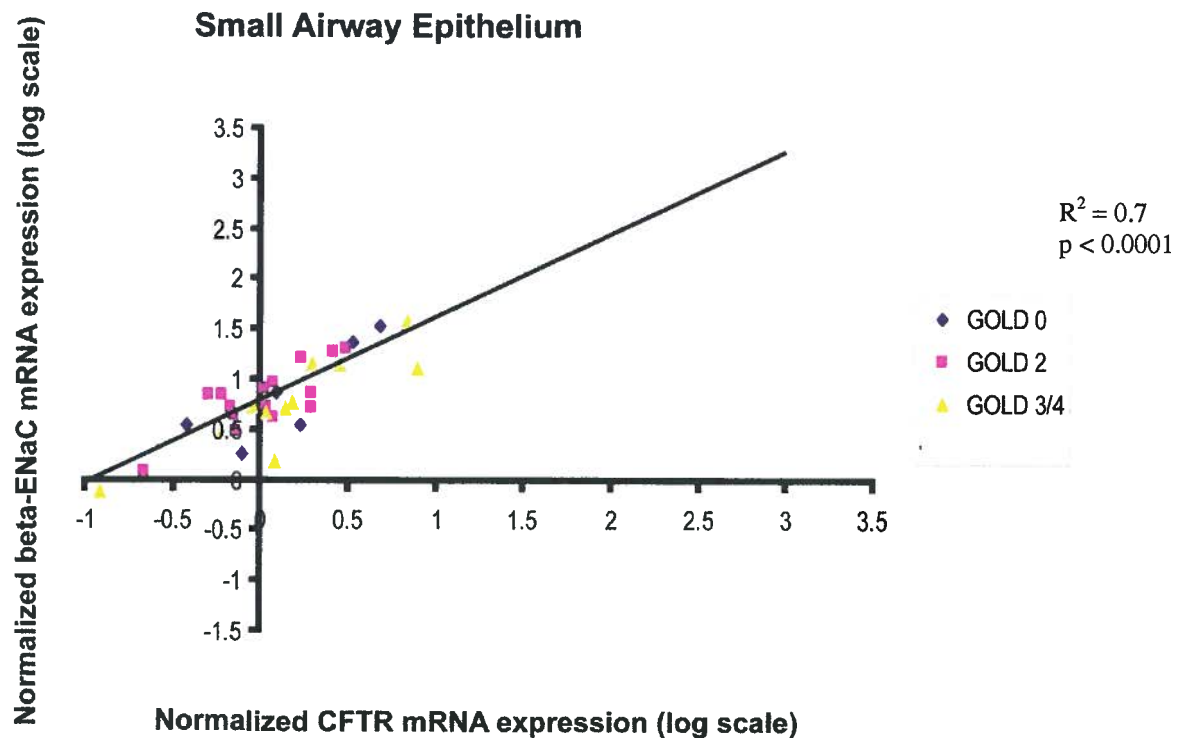


Figure 6.12: Scatterplot showing the correlation between β -ENaC mRNA expression and CFTR mRNA expression in small airway epithelium. The log transformed value of the normalized β -ENaC mRNA expression was plotted against that of the respective CFTR mRNA in 32 small airway epithelium from 24 COPD patients. These airway epithelial samples are coded according to the GOLD categories the patient represent with GOLD 0 (◆), GOLD 2 (■), and GOLD 3/4 (▲). The linear regression line (black) shows the correlation between β -ENaC and CFTR mRNA expression. A strong positive correlation between β -ENaC mRNA expression and CFTR mRNA expression was determined ($R^2 = 0.7$, $p < 0.0001$).

6.2.8 Variability of background information of patients used for gene expression of small airway epithelium and whole small airways as well as lung parenchyma

Table 6.7 compares the variability of background history of the patients providing the small airway epithelial samples to those providing whole airways and lung parenchymal samples, where the latter came from the same patients. Student t-test was used to analyze the differences in FEV_{1pp}, FEV₁/FVC, age, and smoking history and showed that there were no differences between epithelial samples and airway/parenchymal samples with respect to the patients' background history.

Table 6.7: Variability of background information of patients in small airway epithelium and whole small airways as well as lung parenchyma.

Parameter	GOLD	Patients providing small airway epithelium	Patients providing whole small airways / Lung parenchyma	p-value
		Mean \pm SD	Mean \pm SD	
FEV ₁ pp	0	94.4 \pm 7.3	96.2 \pm 8.5	0.54
	2	67.1 \pm 6.7	65.6 \pm 6.7	0.55
	3/4	27.8 \pm 12.0	27.7 \pm 12.0	1.00
FEV ₁ /FVC	0	77.6 \pm 4.0	78.2 \pm 4.1	0.68
	2	58.4 \pm 6.8	58.8 \pm 6.2	0.87
	3/4	41.0 \pm 12.9	46.0 \pm 12.8	1.00
Age	0	66.6 \pm 6.8	64.7 \pm 8.5	0.50
	2	60.8 \pm 9.2	60.8 \pm 9.0	0.98
	3/4	59.6 \pm 6.0	60.0 \pm 6.0	1.00
Pack Years	0	39.6 \pm 16.7	37.0 \pm 17.4	0.69
	2	43.1 \pm 20.7	50.7 \pm 30.6	0.45
	3/4	49.3 \pm 14.5	49.3 \pm 14.5	1.00

The background information includes FEV₁pp, FEV₁/FVC, age and smoking history in pack years. The student t-test was carried out to compare the differences in this information from patients in three the GOLD categories that provided samples of the small airway epithelium to those providing whole airways and lung parenchymal samples where the small airway epithelium came from 37 COPD patients (14 GOLD 0, 13 GOLD 2 and 12 GOLD 3/4 and whole airways and lung parenchymal samples from 45 COPD patients (16 GOLD 0, 17 GOLD 2 and 12 GOLD 3/4).

6.3 Protein expression

6.3.1 Localization of β -ENaC protein in small conducting airways

The β -ENaC protein detected with rabbit polyclonal β -ENaC antibody is shown in purple colour (Figure 6.13A-B). The magnified image (Figure 6.13B) shows clearly that β -ENaC protein is located in the apical area of airway epithelium while no staining of a similar region from an adjacent section was observed with the negative control, a pre-immune serum (Figure 6.13C).

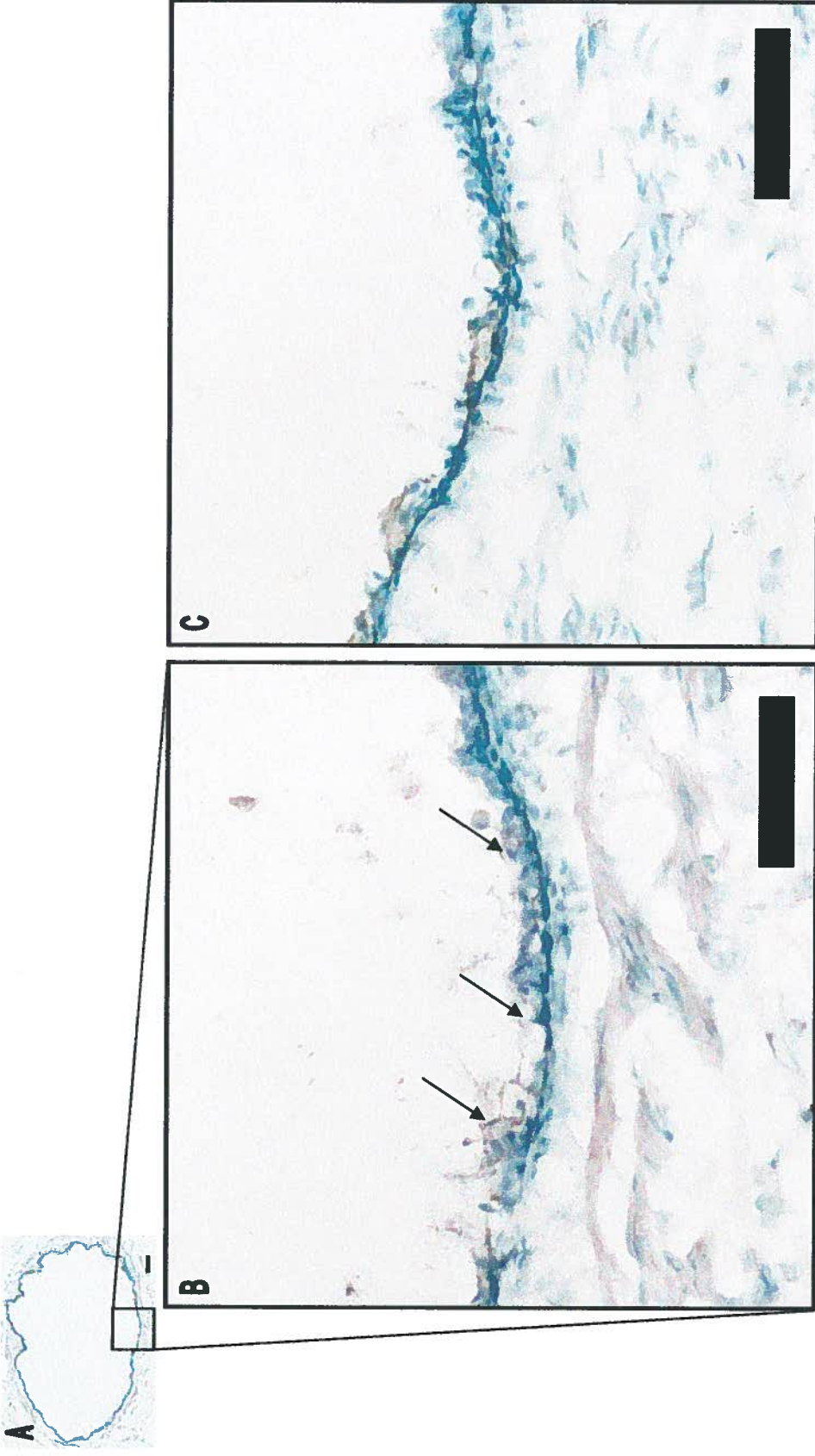


Figure 6.13: Light micrographs showing β -ENaC protein expression in the small airway epithelium. Rabbit polyclonal β -ENaC antibody was used as a primary antibody to detect human β -ENaC protein in the small airway epithelium. A) A whole small airway from a GOLD 2 patient showing β -ENaC protein staining in purple with the epithelium staining green. B) The closer view of the boxed region on A with the airway epithelium staining for β -ENaC protein (arrows). C) The negative control (pre-immune serum) was applied instead of β -ENaC antibody (bar = 100 μ m)

6.3.2 Protein expression of β -ENaC versus GOLD category, FEV_{1pp}, and β -ENaC or CFTR mRNA expression in small airway epithelium

After immunostaining for β -ENaC protein, sections with small conducting airways from 37 patients from the three GOLD categories were analyzed for β -ENaC expression in the small airway epithelium (Figure 6.14). β -ENaC protein expression was calculated as the ratio of area of positive staining in the airway epithelium to the perimeter of basement membrane of that airway. The data shows that there is significant increase of β -ENaC protein expression from GOLD 0 to 2 ($p = 0.01$) as well as from GOLD 0 to 3/4 ($p = 0.01$).

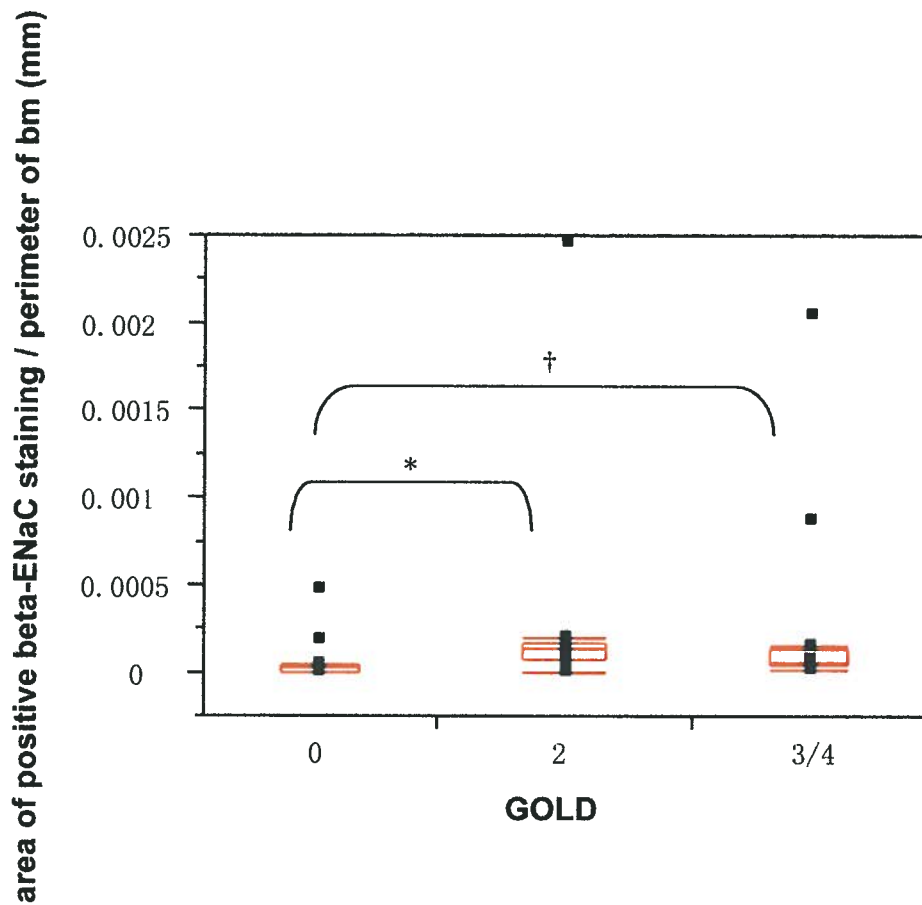


Figure 6.14: β -ENaC protein expression versus GOLD category in 37 COPD patients. β -ENaC protein expression was calculated as the ratio of area of positive staining in the airway epithelium to the perimeter of basement (bm) membrane of the airway. The data are expressed as box plots. The red line inside the box represents median β -ENaC protein expression in each GOLD stage and the boxes denote the lower and higher quantiles while the tails represent the range of the data with the exception of data outside the tails that are possible outliers. The Kruskal-Wallis test was carried out to analyze the difference in β -ENaC protein expression among three GOLD categories.

* significant increase of β -ENaC protein expression between GOLD 0 (n=12) and 2 (n=13)(p = 0.01).

† significant increase of β -ENaC protein expression between GOLD 0 (n=12) and 3/4 (n=12) (p = 0.01).

When the correlation between β -ENaC protein expression and FEV_{1pp} in 37 COPD patients was analyzed (Figure 6.15), the result showed that there was a trend for protein expression to decrease with increasing FEV_{1pp} ($\rho = -0.29$, $p = 0.09$).

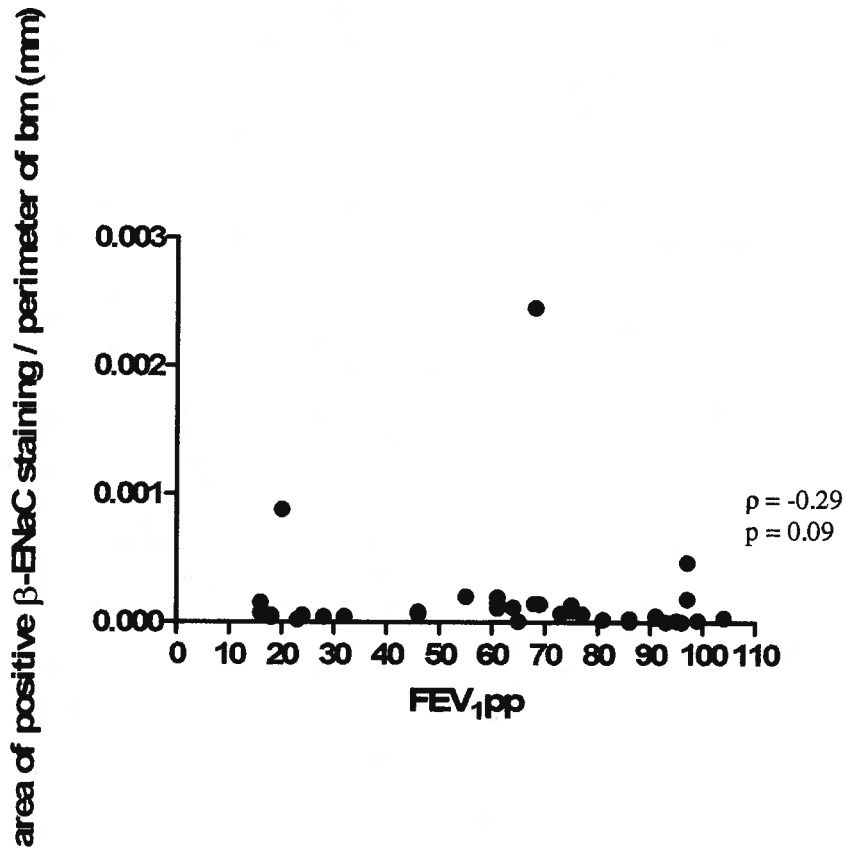


Figure 6.15: β -ENaC protein expression versus FEV_{1pp} in 37 COPD patients. β -ENaC protein expression was calculated as described in Figure 6.14. FEV_{1pp} is a parameter to measure the lung function and is shown in percentage of the predicted value. Spearman's rank correlation coefficient (ρ) was applied to analyze the correlation between these two variables. There is a trend for β -ENaC protein expression to decrease with increasing FEV_{1pp} ($\rho = -0.29$, $p = 0.09$).

The correlation between β -ENaC protein expression and β -ENaC or CFTR mRNA expression was analyzed using Spearman's rank correlation. When this analysis was based on the number of patients (Figure 6.16 A and B, respectively), a significant positive correlation between β -ENaC protein and its mRNA expression ($\rho = 0.40$, $p = 0.05$) but no correlation with CFTR mRNA expression was found. When based on individual airways, no correlations were found (Figure 6.16 C and D).

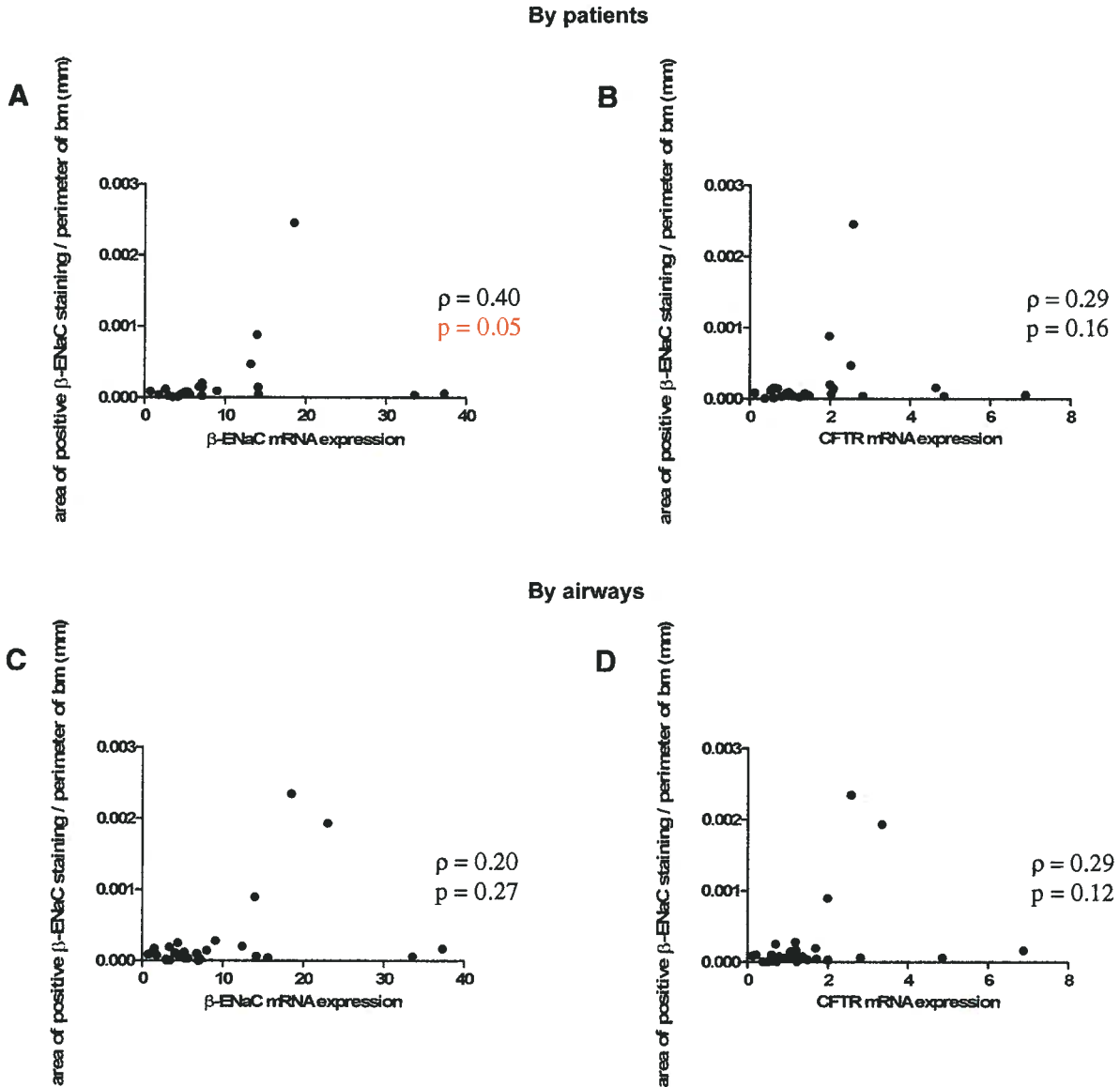


Figure 6.16: β -ENaC protein expression versus mRNA expression. β -ENaC protein expression was calculated as described in Figure 6.14. A) β -ENaC protein expression versus β -ENaC mRNA expression analyzed in 24 COPD patients. B) β -ENaC protein expression versus CFTR mRNA expression in the same patients as in (A). C) β -ENaC protein expression versus β -ENaC mRNA analyzed in 31 individual airways. D) β -ENaC protein expression versus CFTR mRNA expression in the same airways as in (C). Spearman's rank correlation coefficient (ρ) was applied to analyze the correlation between the two variables in each comparison. A significant positive correlation between β -ENaC protein expression and β -ENaC mRNA expression based on the patients was found ($\rho = 0.40$, $p = 0.05$).

6.3.3 Localization of CFTR protein in small conducting airways

Immunohistochemical staining for the CFTR protein was first tested using a mouse monoclonal CFTR antibody (L12B4). Positive staining shown in red colour (Figure 6.17A) indicates that CFTR protein is located on the apical surface of airway epithelium and inflammatory cells while no staining of the apical area of airway epithelium from an adjacent section was observed with the negative control, a mouse IgG (Figure 6.17B).

Although the mouse monoclonal antibody (L12B4) was used successfully to detect CFTR protein expression in the airways, this antibody was also being used for another project so that adequate amounts of this antibody were not available to continue the current investigation. Therefore, we tested other CFTR antibodies that were available and used the positive and specific staining provided by this mouse monoclonal antibody as a comparison for the other antibodies (see below).

When the staining for CFTR protein was tested using a goat polyclonal CFTR antibody together with ABC, no positive staining was found and, in addition, background staining was found with goat IgG as a negative control in the frozen lung tissue (data not shown). Faint positive staining was found in both the epithelium of renal tubules and the lumen of the tubules either goat polyclonal CFTR antibody or goat IgG was used (data not shown). When this same antibody was applied using the polymeric method, the whole tissue was stained in red whether the anti-CFTR antibody or goat IgG was used (data not shown). Because the two staining methods tested with this antibody could not achieved adequate specific staining,

CFTR protein expression in the small airways, in our hands, could not be quantified using the immunohistochemical procedures tested.

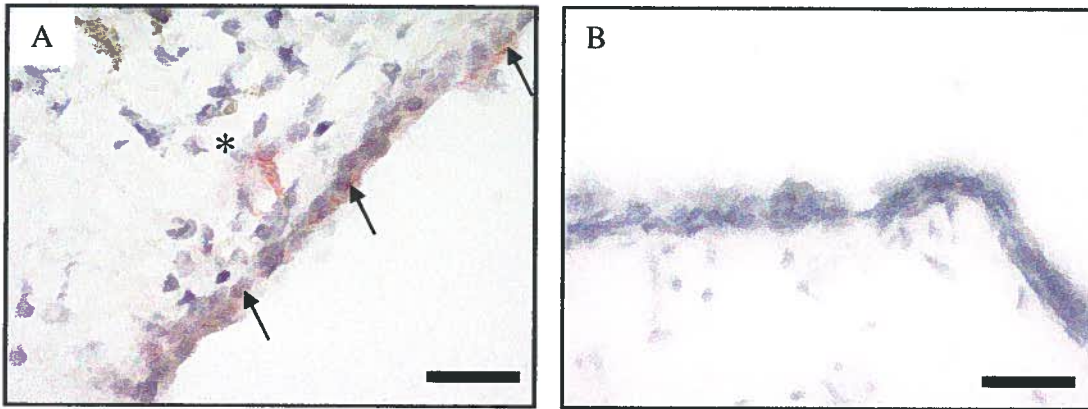


Figure 6.17: Light micrographs showing CFTR protein expression in the small airway epithelium. Mouse monoclonal CFTR antibody (L12B4) was used as a primary antibody to detect human CFTR protein in the small airway epithelium. A) airway epithelium staining for CFTR protein (arrows) from a GOLD 2 patient in red with the epithelium staining purple. The red staining next to the asterisk represents inflammatory cells. B) The negative control (mouse IgG) was applied instead of CFTR antibody (bar = 100 μ m).

6.4 Mucin studies using PAS

6.4.1 Epithelial mucin expression in small airway epithelium

Figure 6.18 shows the epithelial mucin staining in a small airway where the mucin is stained in magenta while other compartments like the airway and the alveoli are stained in purple. This light micrograph shows that mucin is mainly located in the small airway epithelium.

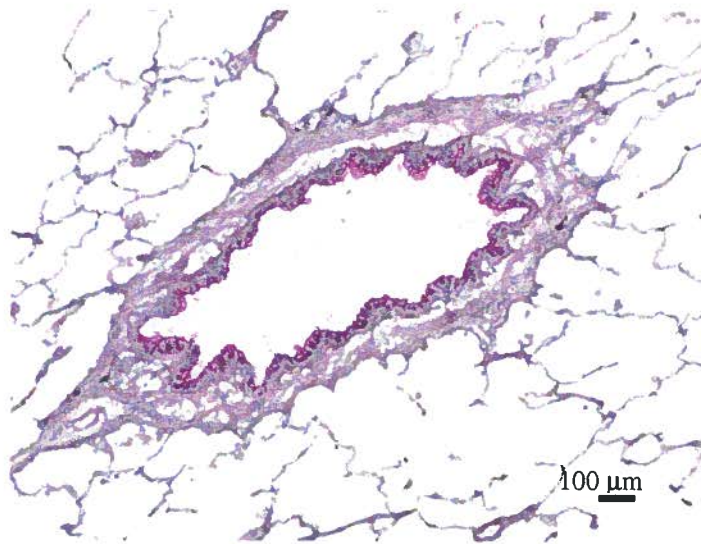


Figure 6.18: Light micrograph showing PAS staining of the epithelium in a small airway. Mucin is stained in magenta while other compartments are stained in purple in this representative micrograph from a GOLD 4 patient. (bar = 100 μm).

Figure 6.19 shows the epithelial mucin expression from 37 COPD patients in the three GOLD categories. No significant difference in epithelial mucin expression, as calculated by dividing the area of positive PAS staining in the airway epithelium by the perimeter of basement membrane of the airway, was found between the three GOLD categories. Also, no correlation was found between epithelial mucin expression and FEV_{1pp} in these 37 COPD patients (Figure 6.20).

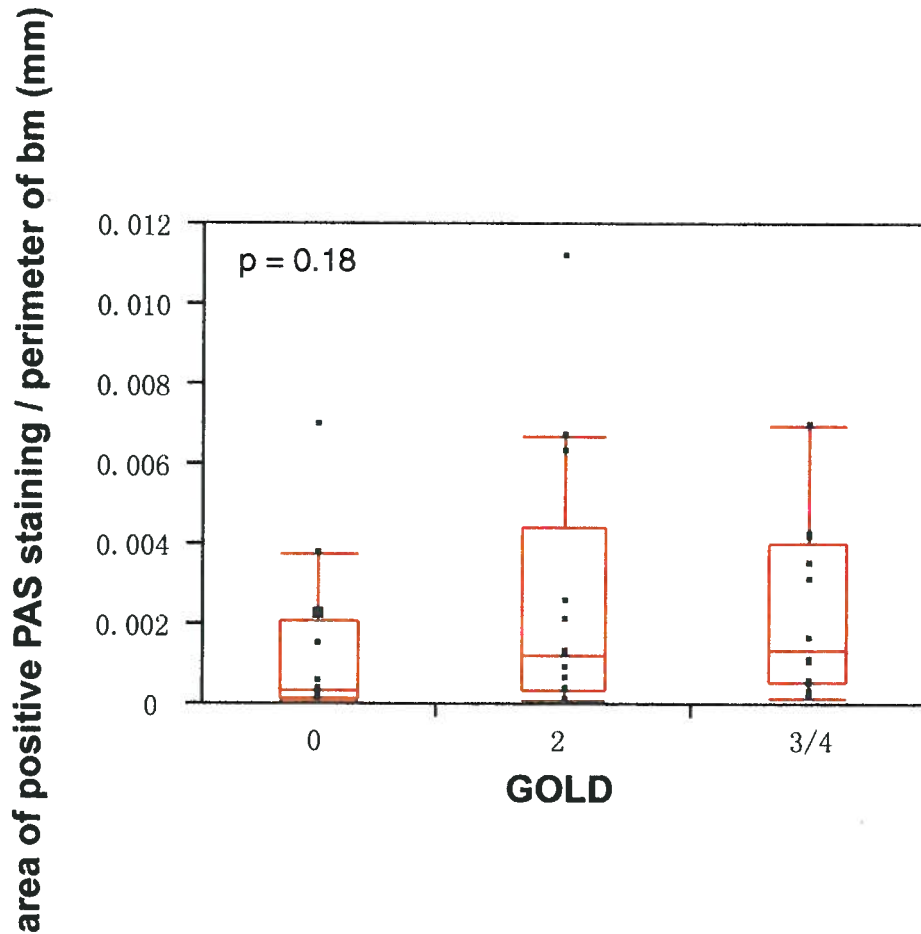


Figure 6.19: Epithelial mucin expression versus GOLD stage. Epithelial mucin expression was calculated by dividing the area of positive PAS staining in the airway epithelium by the perimeter of basement (bm) membrane of the airway in 37 COPD patients in the three different GOLD categories. The data are shown as box plots. The red line inside the box represents median epithelial mucin expression in each GOLD stage and the boxes denote the lower and higher quantiles while the tails represent the range of the data with the exception of data outside the tails that are possible outliers. The Kruskal-Wallis test was carried out to analyze the difference in epithelial mucin expression among the three GOLD categories.

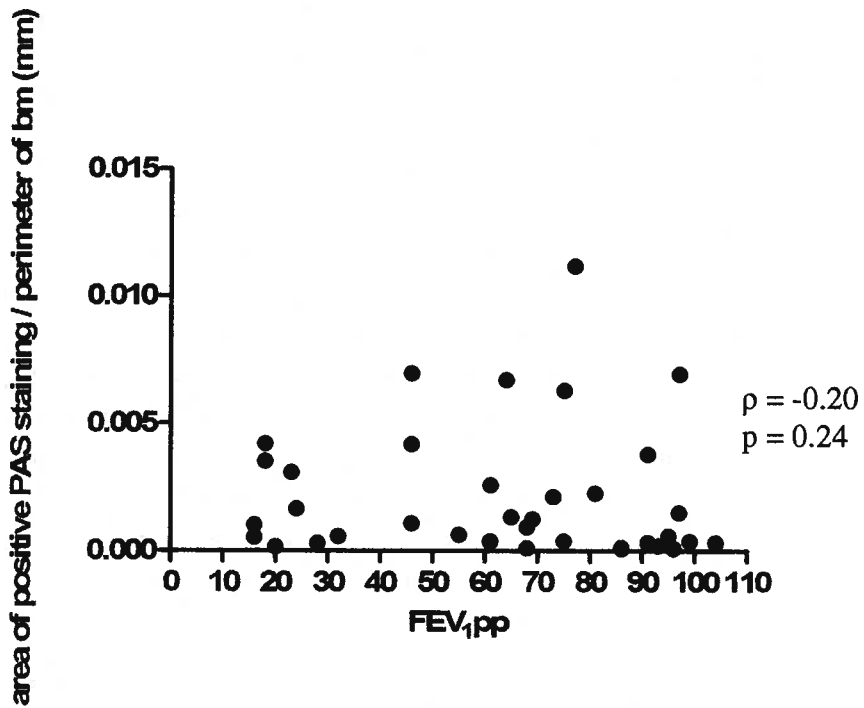


Figure 6.20: Epithelial mucin expression versus FEV₁pp. Epithelial mucin expression as measured in Figure 6.19 was correlated with the FEV₁pp of the 37 COPD patients. FEV₁pp is an indicator for lung function and is expressed in percentage of the predicted value. Spearman's rank correlation coefficient (ρ) was applied to analyze the correlation between these two variables.

The correlations between β -ENaC or CFTR mRNA expression and epithelial mucin expression in 31 small airway epithelia of 24 COPD patients are shown in Figure 6.21. When these correlations were based on expression in the patients instead of individual airways, no correlation was found for either β -ENaC or CFTR mRNA expression (Figure 6.21A and B, respectively). In contrast, when the correlations were based on the individual airways, significant positive correlations were found between both β -ENaC mRNA ($\rho = 0.38$, $p = 0.05$) and CFTR mRNA ($\rho = 0.40$, $p = 0.04$) (Figure 6.21C and D, respectively) and epithelial mucin expression.

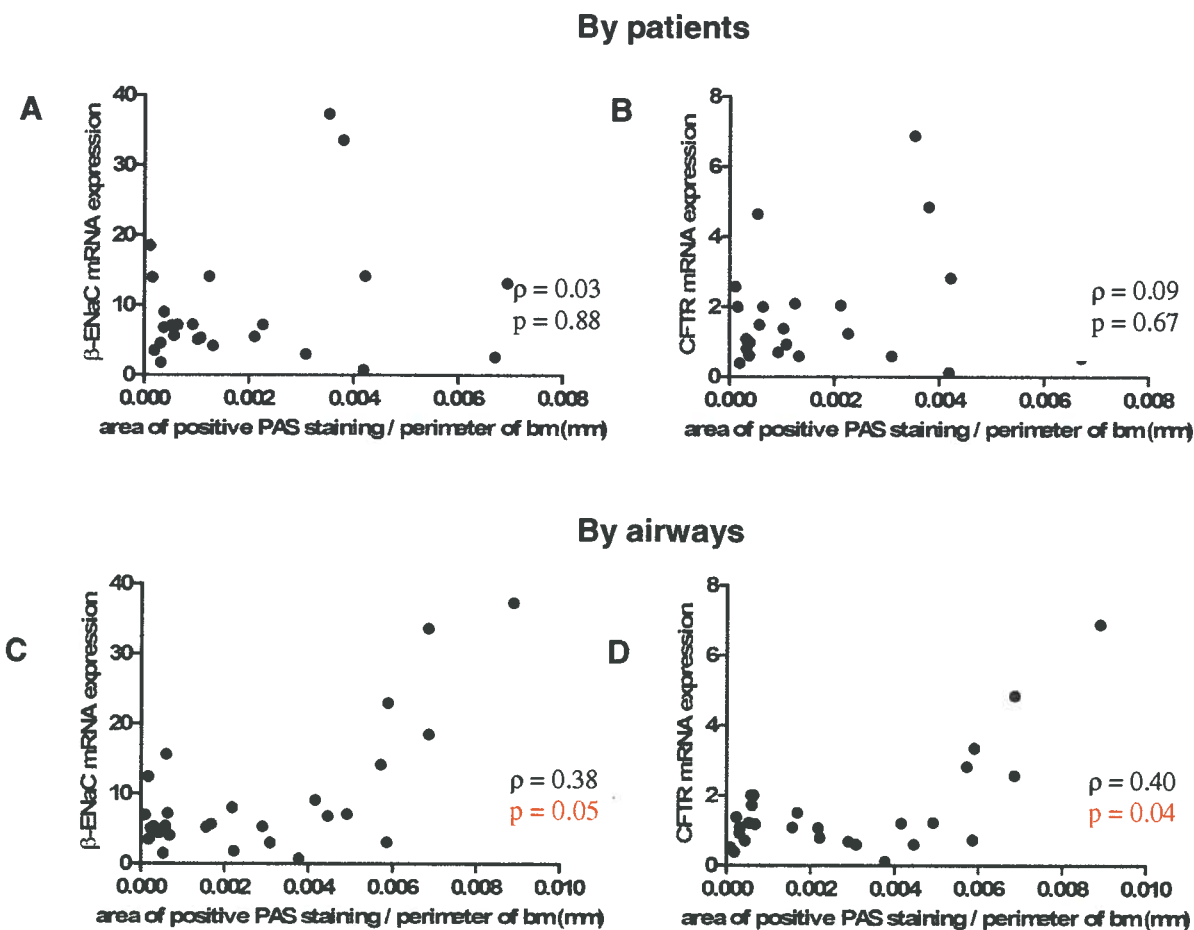


Figure 6.21: β -ENaC and CFTR mRNA expression in airway epithelium versus epithelial mucin expression. Epithelial mucin staining as measure in Figure 6.19 was correlated with the expression β -ENaC (A,C) and CFTR (B,D) mRNA normalized with β -actin expression where the correlations were based on expression in 24 COPD patients (A,B) and in 31 (no airway was available in one core of GOLD 2 patient for epithelial mucin analysis) individual airways from the 24 COPD patients (C,D). Spearman's rank correlation coefficient (ρ) was applied to analyze the correlation between these two variables. Analyses based on the individual airways showed significant positive correlations between epithelial mucin expression and both β -ENaC ($\rho = 0.38$, $p = 0.05$) and CFTR ($\rho = 0.40$, $p = 0.04$) mRNA expression.

The correlation between β -ENaC protein expression and epithelial mucin expression in 73 airways of 37 patients is shown in figure 6.22. No correlation was found in analyses based on patients (Figure 6.22A) or on individual airways (Figure 6.22B).

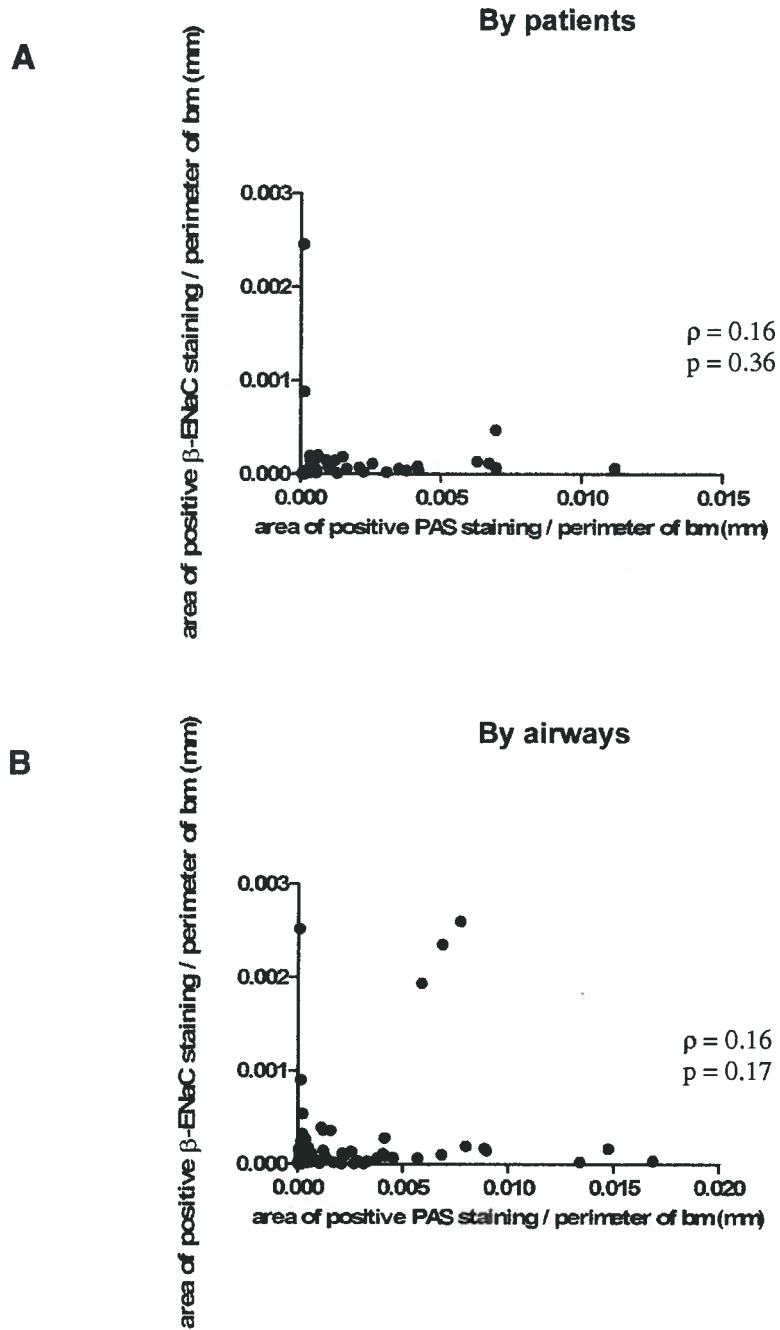


Figure 6.22: β -ENaC protein expression versus epithelial mucin expression. β -ENaC protein expression as calculated in Figure 6.14 was correlated with epithelial mucin expression as determined in Figure 6.19 from 37 COPD patients (A) and in 73 individual airways from these 37 patients (B). Spearman's rank correlation coefficient (ρ) was applied to analyze the correlation between β -ENaC protein and epithelial mucin expression.

6.4.2 Epithelial mucin expression versus β -ENaC, CFTR and Muc5ac mRNA expression in whole small conducting airways

Figure 6.23 shows β -ENaC, CFTR and Muc5ac mRNA expression against epithelial mucin expression in whole small conducting airways of 37 COPD patients. There was no correlation between epithelial mucin expression and mRNA expression.

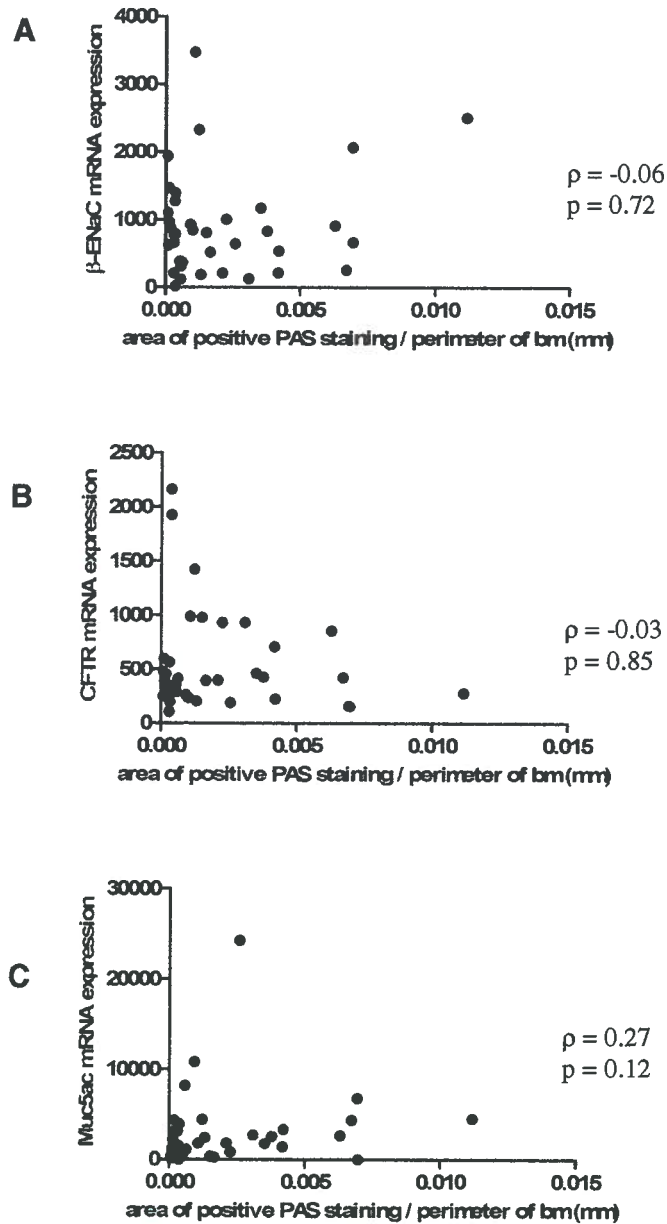


Figure 6.23: β -ENaC, CFTR and Muc5ac mRNA expression in the whole airways versus epithelial mucin expression in COPD patients. Epithelial mucin expression as determined in Figure 6.19 was correlated with β -ENaC (A), CFTR (B), and Muc5ac (C) mRNA expression as determined by relative quantification normalized with that of β -actin, β -2-M and HPRT in whole airways from 37 COPD patients. Spearman's rank correlation coefficient (ρ) was applied to analyze the correlation between expression of the mRNAs and that of mucin.

6.4.3 Mucus plugging in small conducting airways

Figure 6.24 demonstrates a mucus plug in the whole lumen of the small airway of a GOLD 4 patient. The mucus plug and epithelial mucin were stained in magenta while the airway epithelium was stained in purple. This light micrograph shows that the mucus plug contains mainly mucin and it almost completely fills the airway lumen. The magenta staining in the surrounding parenchyma may be due to a staining artifact or poor freezing/fixation process.

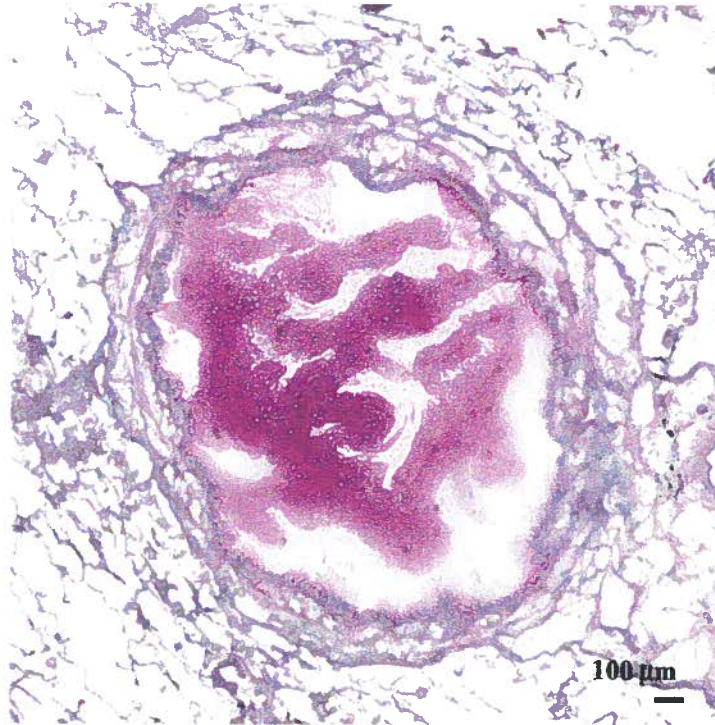


Figure 6.24: Light micrograph showing mucus plugging of small airway lumen. A mucus plug in a small airway of a GOLD 4 patient is stained in dark pink while parts of the epithelium are stained in lighter magenta and other compartments are stained in purple. The mucus plug almost occludes the whole lumen of the airway. (bar = 100 μm).

In figure 6.25 mucus plugging is plotted against the GOLD stage of 37 COPD patients whose airways were analyzed. Mucus occlusion was expressed as the ratio of plug area to the expanded luminal area. There was no significant change in mucus occlusion among the three GOLD categories. Also, no correlation was found between mucus plugging and FEV_{1pp} in these patients (Figure 6.26).

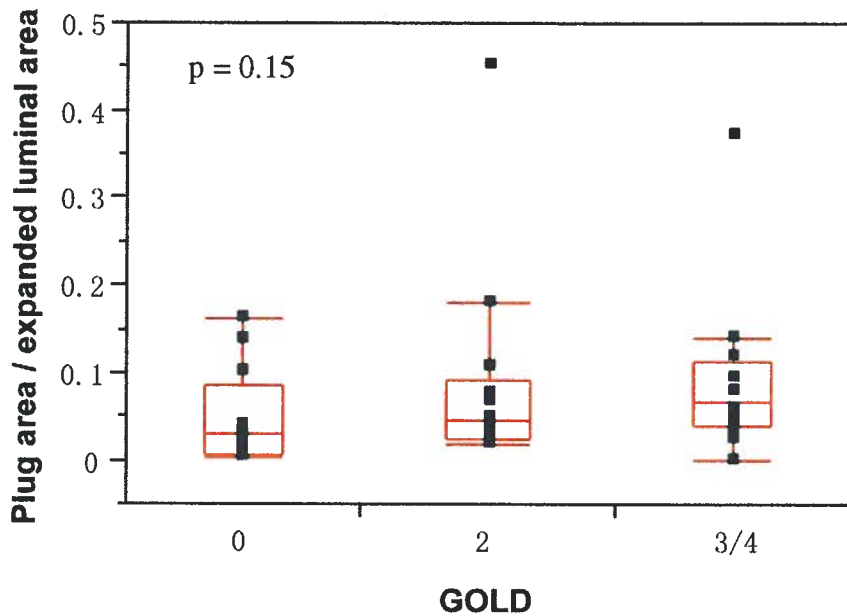


Figure 6.25: Mucus plugging versus GOLD stage. Mucus plugging as expressed as the ratio of plug area to the expanded luminal area was compared in the three GOLD categories of the 37 COPD patients in which airways were analyzed. The data are expressed as box plots. The red line inside the box represents median epithelial mucin expression in each GOLD stage and the boxes denote the lower and higher quantiles while the tails represent the range of the data with the exception of data outside the tails that are possible outliers. The Kruskal-Wallis test was used to analyze the differences in mucus plugging among three GOLD categories.

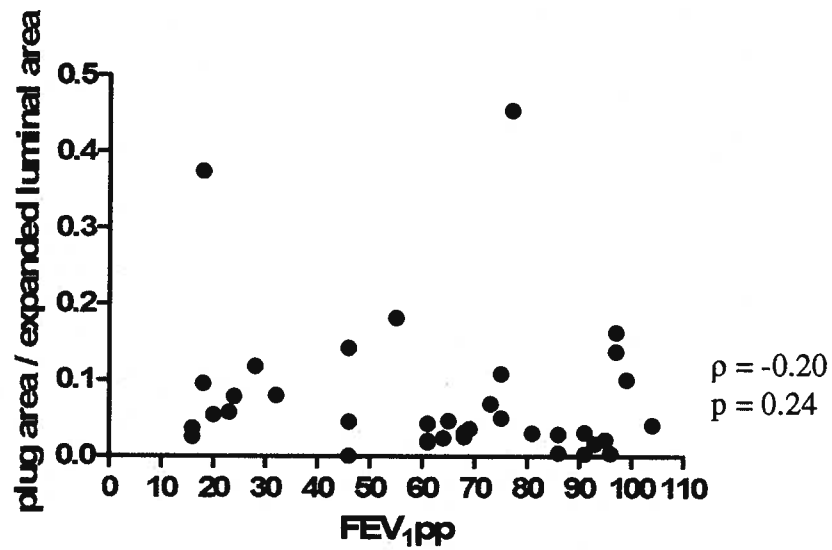


Figure 6.26: Mucus plugging versus FEV_{1pp}. Mucus plugging as determined in Figure 6.25 was plotted against FEV_{1pp}, an indicator for lung function which is expressed as a percent of the predicted value in 37 COPD patients. Spearman's rank correlation coefficient (ρ) was applied to analyze the correlation between these two variables.

Figure 6.27 shows the correlation between mRNA expression of β -ENaC or CFTR and mucus plugging in 31 small airway epithelia of 24 COPD patients. When the analysis was based on patients, no significant correlation was found between β -ENaC mRNA expression and mucus plugging (Figure 6.27A) while, interestingly, a strong positive correlation between CFTR mRNA expression and mucus plugging was found ($\rho = 0.48$, $p = 0.02$)(Figure 6.27B). Analysis on the basis of individual airways showed no significant correlations (Figure 6.27C-D).

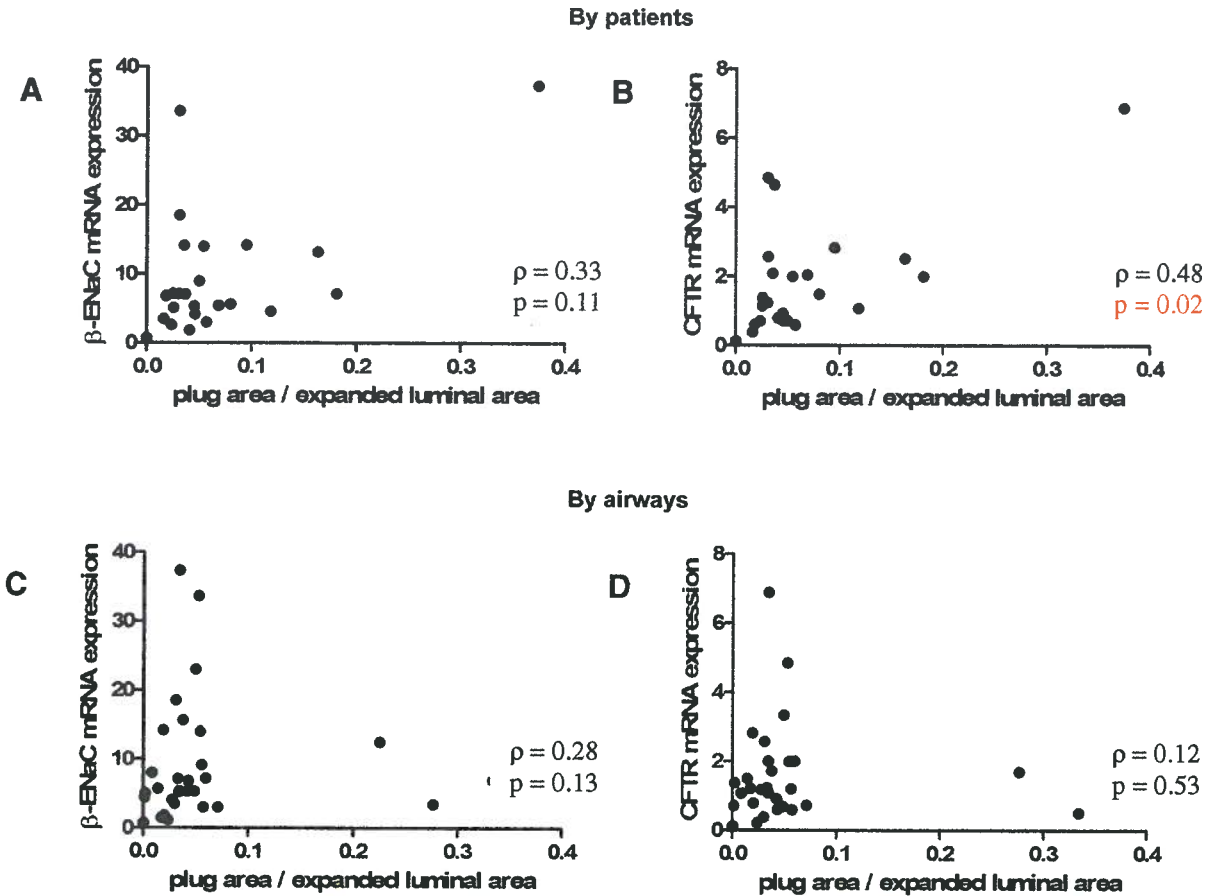


Figure 6.27: β -ENaC and CFTR mRNA expression in small airway epithelium versus mucus plugging. Expression of β -ENaC (A,C) and CFTR (B,D) mRNA normalized with β -actin was plotted against mucus plugging as measured in Figure 6.25 in 24 COPD patients (A,B) and in 31 individual airways from these patients (C,D). Spearman's rank correlation coefficient (ρ) was applied to analyze the correlation between each pair of variables. A significant correlation between CFTR mRNA expression and mucus plugging when analyzed on the basis of patients ($\rho = 0.48$, $p = 0.02$).

In whole small airways of 37 COPD patients no significant correlation between mRNA expression of β -ENaC (Figure 6.28A), CFTR (Figure 6.28B) or Muc5ac (Figure 6.28C) and mucus occlusion could be determined.

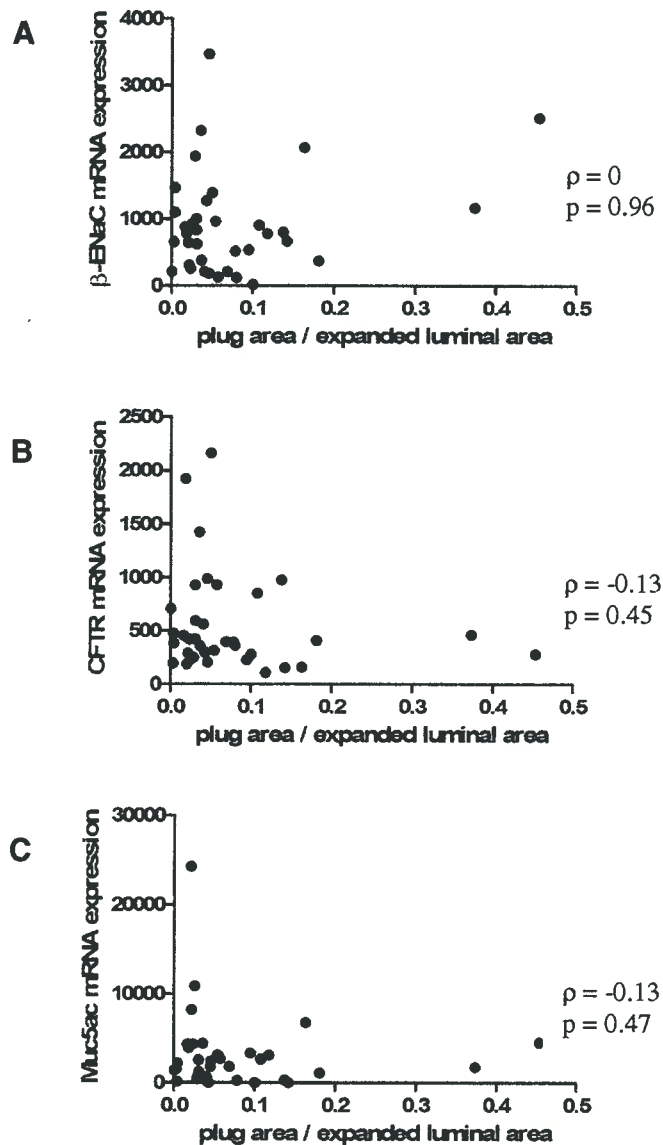


Figure 6.28: β -ENaC, CFTR, and Muc5ac mRNA expression in the whole airways versus mucus plugging. β -ENaC (A), CFTR (B), and Muc5ac (C) mRNA expression as determined by relative quantification normalized with that of β -actin, β -2-M and HPRT in whole airways from 37 COPD patients was correlated with mucus plugging as measured in Figure 6.25 in these patients. Spearman's rank correlation coefficient (ρ) was applied to analyze the correlation between each pair of variables.

An analysis of β -ENaC protein expression versus mucus plugging in 73 airways of 37 patients showed no correlation when based on patients or on individual airways (Figures 6.29 A and B, respectively). An analysis of epithelial mucin expression versus mucus plugging in these same airways showed a significant positive correlation ($\rho = 0.43$, $p = 0.0002$)(Figure 6.30).

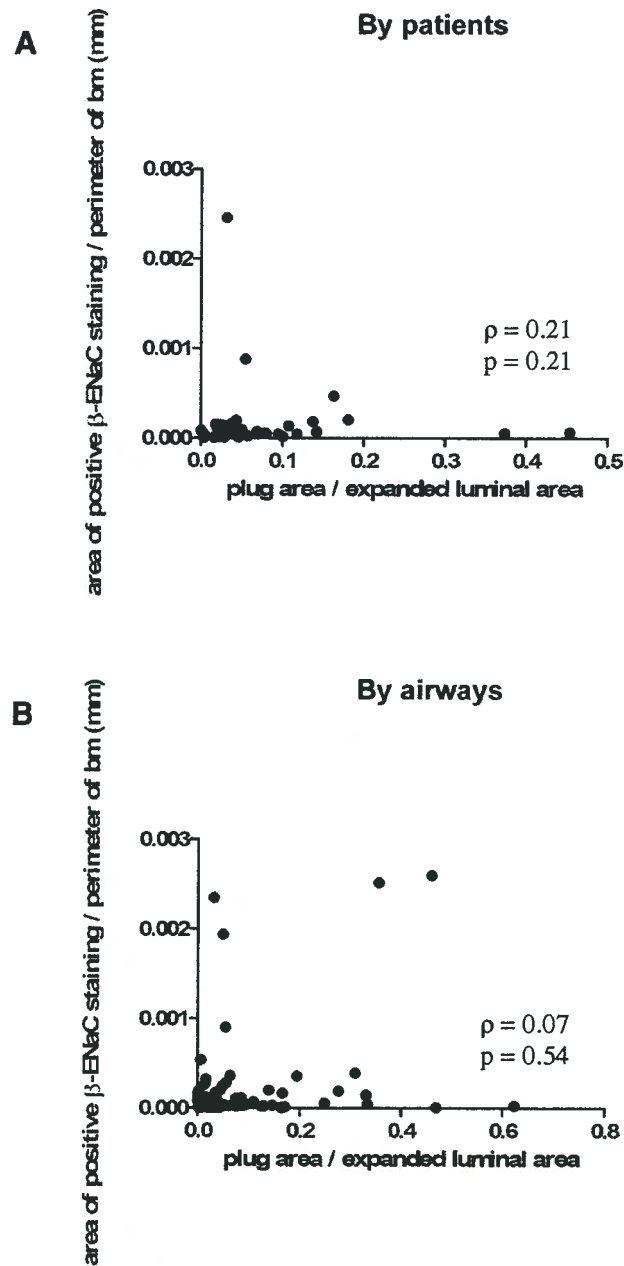


Figure 6.29: β -ENaC protein expression versus mucus plugging. β -ENaC protein expression as calculated in Figure 6.14 was plotted against mucus plugging as measured in Figure 6.25 in 37 COPD patients (A) and in 73 individual airways from these patients (B). Spearman's rank correlation coefficient (ρ) was applied to analyze the correlation between these two variables.

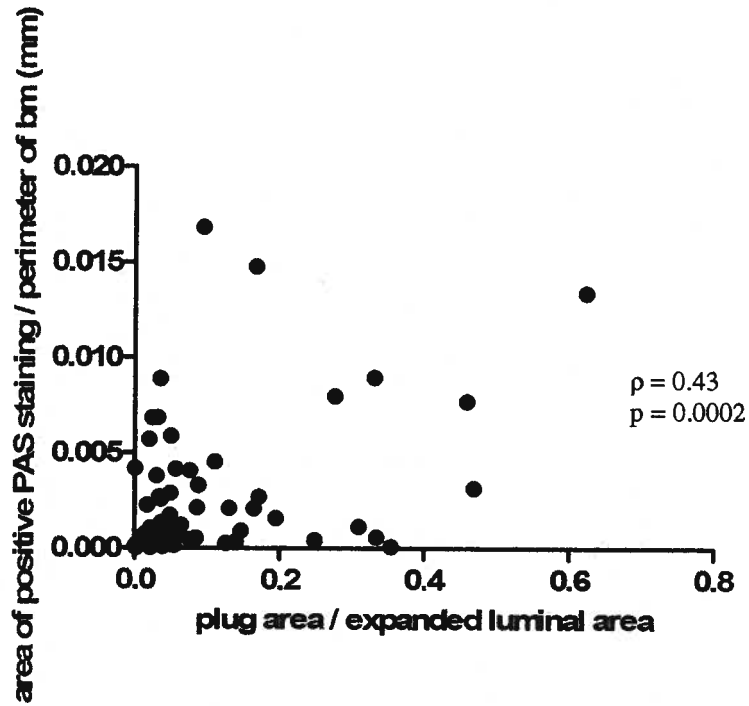


Figure 6.30: Epithelial mucin expression versus mucus plugging from 73 airways of 37 COPD patients. Epithelial mucin expression as determined in Figure 6.19 was plotted against mucus plugging as measured in Figure 6.25. Spearman's rank correlation coefficient (ρ) was applied and showed significant positive correlation between these two variables ($\rho = 0.43$, $p = 0.0002$).

6.5 Summary of Results

In summary (Table 6.8), our results showed that β -ENaC mRNA and CFTR mRNA expression positively correlated with each other in the lung parenchyma and small airway epithelium. In other words, if the mRNA expression of β -ENaC was high, the mRNA expression of CFTR was high as well. Also β -ENaC mRNA expression positively correlated with its protein expression meaning that if β -ENaC mRNA expression was high, its protein expression was also high. β -ENaC protein expression was significantly different between GOLD stages, being higher in the higher GOLD categories compared to GOLD 0. Our results further demonstrated that β -ENaC mRNA and CFTR mRNA positively correlated with epithelial mucin expression. Also, CFTR mRNA expression and mucin expression were positively correlated with mucus plugging. For this study, a total of 44 combinations of comparisons and/or analyses were conducted, and 8 significant findings were found without adjustment with Bonferroni correction. These 8 findings account for about 18% of the total analyses that were performed. However, after Bonferroni correction was applied to adjust for multiple comparisons, only β – ENaC and CFTR mRNA expression was still significantly correlated with each other.

Table 6.8: Summary of significant results.

Tissue	Dependent Variable	Independent Variable	R ² or ρ	p-value
Lung parenchyma	β – ENaC mRNA	CFTR mRNA	0.06	0.01
Small airway epithelium	β – ENaC mRNA	CFTR mRNA	0.70	< 0.0001†
Small airway epithelium	β – ENaC protein (P)*	β – ENaC mRNA	0.40	0.05
Small airway epithelium	β – ENaC protein	GOLD	N/A	0.01**
Small airway epithelium	β – ENaC mRNA (A*)	Epithelial mucin	0.38	0.05
Small airway epithelium	CFTR mRNA (A*)	Epithelial mucin	0.40	0.04
Small airway epithelium	CFTR mRNA (P)*	Mucus plugging	0.48	0.02
Small airway epithelium	Epithelial mucin	Mucus plugging	0.43	0.0002

* P – analysis based on patients, A- analysis based on individual airways

† the significant value after Bonferroni correction was made

** significant value did not require correction for multiple comparison

This table summarizes statistically significant results ($p \leq 0.05$) obtained in this study. Linear regression (R^2) and Spearman's rank correlation (ρ) were used to analyze the correlation between the two variables. The Kruskal-Wallis test used to analyze the differences of β – ENaC protein between GOLD stages. After Bonferroni correction was used to adjust for the multiple comparisons, only β – ENaC and CFTR mRNA expression was still significantly correlated with each other.

Chapter 7: Discussion

The hypothesis that was tested in this study was that the accumulation of mucus exudates observed with progression of COPD is related to excess airway epithelial sodium re-absorption as a result of over-expression of β -ENaC and reduced expression of CFTR by small airway epithelial cells. The rationale for this hypothesis is that COPD and cystic fibrosis have similar pulmonary pathologies such as mucus accumulation and airways obstruction. Previous studies used cell culture to show that α -ENaC is a functional unit that is able to induce the Na^+ current by itself [26, 29]. However, the transgenic mouse model studies [22] showed that the β -mENaC subunit is rate limiting for airway Na^+ absorption *in vivo*. They showed that even though the expression of α -mENaC transcripts were higher than that of β -mENaC and γ -mENaC, only elevated β -mENaC was associated with increased Na^+ channel activity, decrease PCL height, and mucus obstruction of the airways and led to cystic fibrosis-like disease. CFTR was shown to negatively regulate ENaC activity [72]. Because of the time limit in this thesis, it was difficult to study both α and β -ENaC at the same time. The mouse model showing that β -ENaC expression is related to mucus plugging which is a more convincing model of human disease than the cell culture studies. Therefore, this thesis focused on β -ENaC expression.

The sources of tissues used in the thesis are more suitable for COPD studies compared to others that used tissue cultures or animal models. It is relatively easy to obtain tissue cultures or animals and treat them in a manner similar to that which occurs in the disease. However, the tissues used in this thesis are directly involved in chronic bronchitis and emphysema in COPD and are from human sources.

The results showed that the gene expression of β -ENaC or CFTR as well as epithelial mucin expression or mucus plugging did not correlate with disease severity in whole small airways, the surrounding lung parenchyma and small airway epithelium. A significant positive correlation was found between β -ENaC and CFTR mRNA expression in both surrounding lung parenchyma and small airway epithelium. β -ENaC mRNA positively correlated with protein expression of β -ENaC while no correlation of CFTR mRNA expression with that of β -ENaC protein was found. Protein expression of β -ENaC was found to be significantly different between GOLD stages. In addition, the results showed that both β -ENaC and CFTR mRNA in the small airway epithelium positively correlated with epithelial mucin expression. However, expression of these two genes and that of Muc5ac in whole small airways did not correlate with mucin expression in the airway epithelium or mucus plugging. Only CFTR mRNA in the airway epithelium was positively correlated with mucus plugging. Neither epithelial mucin expression nor mucus plugging correlated with β -ENaC protein expression. Finally, epithelial mucin and mucus plugging positively correlated with each other.

7.1 Results supporting the working hypothesis:

The working hypothesis was that “the accumulation of mucus exudates observed with progression of COPD is related to excess airway epithelial sodium re-absorption as a result of over-expression of β -ENaC and reduced expression of CFTR by small airway epithelial cells”. β -ENaC mRNA positively correlated with protein expression of β -ENaC. In turn, the results from immunohistochemistry showed a significant increase in β -ENaC protein

expression between GOLD stages of COPD disease severity. This last result was further supported by a trend of decreased β -ENaC protein with increasing FEV_{1pp}. These findings suggesting an increase in β -ENaC protein expression as a consequence of β -ENaC mRNA support the working hypothesis that over-expression of β -ENaC in small airway epithelial cells is related to progression of COPD. Why β -ENaC mRNA itself did not correlate with disease severity could be due to the numbers of patients and airways tested by immunohistochemistry was greater than that tested by gene expression, that is, 37 patients providing 73 airways versus 24 patients providing 32 airways, respectively, and so the sample size might have been greater. Others have also had a similar finding in the nasal epithelium of CF patients [132] where the α and β subunits of ENaC increased while the γ subunit decreased with disease severity. Bangel et al. suggested that dysregulated expression of the different ENaC subunits may contribute to altered ENaC function [132].

Our result of β -ENaC mRNA expression being positively correlated with epithelial mucin expression supports the report of Mall et al. (2004) who used Alcian Blue-PAS staining to demonstrate mucus adhesion to airway epithelia of β -ENaC over-expressing mice [22]. Furthermore, the positive correlation between epithelial mucin and mucus plugging that we found for our experiment is similar to the findings from this mouse model [22]. Here, mucus occlusion was associated with PCL height depletion and mucus adhesion to the airway surface in the β -ENaC transgenic mice that β -ENaC over-expression led to increased Na⁺ transport, reduced PCL height, and increased mucus concentration and, in turn impaired mucus clearance in the airway, leading to mucus occlusion in the airway lumen.

7.2 Results against the working hypothesis:

Our hypothesis predicted an increase in β -ENaC and reduced CFTR mRNA expression as well as increased mucin expression in the airway epithelium and mucus plugging of the airways with decreased lung function but the results failed to show any correlation between either mucin expression or mucus plugging and lung function, measured according to either GOLD stage or FEV_{1pp}. Selection bias may be a possible explanation for the negative results. For example, all the cores in each of the GOLD 3/4 patients were screened for small airways. Since there was only a limited number of GOLD 3/4 patients, it is possible that two or more airways from a similar anatomic level of the lung from one patient were used in order to provide sufficient numbers for analysis. In this manner we may have imposed a selection bias among the GOLD 3/4 patients. Selection bias could affect the outcome from the analysis of correlation between gene expression and lung function, in particular, but also indirectly between mucin expression and lung function.

The small sample size used for our studies may be another explanation for the lack of correlation between both β -ENaC and CFTR mRNA expression and lung function decline. Before analyzing β -ENaC and CFTR gene expression in the airway epithelium, the minimum amount of RNA required for these gene studies was determined in a preliminary study. After a minimum amount of RNA of 50 ng per sample for qPCR was determined, only 64 out of the 83 samples were used in the initial PCR analysis. Also, because of difficulties in PCR analysis, only 32 airway epithelial samples were able to generate the reliable PCR data which were used for the final analysis of gene expression in the airway epithelium. This is less than half (32/83) of the number of samples that were originally planned to be analyzed.

Moreover, this sample size is also only one third of the number of whole airways and lung parenchymal samples used in the same studies. Circumstances that may have interfered with the PCR analysis including insufficient amounts of RNA used for the initial PCR on the airway epithelial samples, may have contributed to the lack of correlation. Contamination of the RNA sample by genomic DNA despite DNase I treatment during the RNA purification step, or other contaminants that were not removed during the RNA purification step that inhibit RT and PCR could result in undetectable qPCR or non-reliable qPCR data [106, 133].

Besides providing the minimum amount of RNA required PCR which in turn led to problems of inadequate sample size, the preliminary studies showed that the average RNA yield from the 58 sections from the unclassified patients was five times greater than that from the same number of sections from the GOLD 0-2 patients but generated Ct values of β -ENaC, CFTR and β -actin similar to those from the lesser RNA yielding GOLD 0-2 patients. A likely problem is one of overloading the system with the larger amount of RNA from the unclassified patients, not only in the RNA extraction step so that more contaminants came through and thus compromised the RT as well as the PCR step, but also in the PCR step by upsetting the balances required for this reaction (number of Taq polymerase molecules, concentrations of primer and dNTPs available or Mg^{2+} concentration compared to the target number of cDNAs). These reasons that the use of too much RNA from the 58 sections from unclassified patients could decrease RT or PCR “efficiency” is supported by the results from the 88 sections from these same patients that gave even more RNA but the respective Ct values are even higher than those from the 58 sections from these patients. However, an explanation for why the same number of sections from the unclassified patients yielded more

RNA than the same number from the GOLD 0-2 is difficult to find. Possibly, on the day the unclassified samples were processed, the RNA extraction was more efficient than otherwise.

Sample size may also be a concern in the difference in results from the analysis of mucin expression and mucus plugging in our studies and that of mucus plugging from Hogg et al. [9]. We analyzed the results from 37 patients while Hogg et al., reported the results from 159 patients which is four times the number used in the current study. Therefore, our study may have been under-powered to detect the changes reported by Hogg et al., 2004.

Hogg et al. (2007) [88] showed mucus occlusion is related to premature death of COPD patients, and his study in 2004 [9] demonstrated that mucus plugging is positively associated with lung function decline in terms of FEV_{1pp}. The difference in tissue processing between our study and Dr. Hogg's previous studies may be another issue causing the failure to show a correlation between mucus plugging and lung function in the current study. In the present study, the resected lungs from the GOLD 3/4 patients were inflated with OCT flushing before fixation while the lungs in Dr. Hogg's studies were either fixed by immersion in formalin or first inflated and then fixed. The addition of the OCT flushing step may have flushed the space in the lung to fill up the airways with OCT. OCT and other materials such as mucus would be able to flow back out through the bronchi making it possible to lose mucus in this way. Therefore, in our case, even if mucus plugging were present in airways of patients with severe COPD before the processing the lungs, it may have been difficult to detect after processing. Also, without inflating the lung, as was the case in lungs from the GOLD 4 patients studied by Hogg et al. 2004, it is possible that there was an over-estimate

of mucus plugging, as reported in the frequency distribution curve of 562 airways of 42 GOLD 4 patients [9], even after a process termed “expansion” was applied to correct for airway size where “the maximal luminal area was calculated by determining the area enclosed by a circle formed by the full length of the basement membrane minus the area taken up by the epithelium”. Thus, differences in tissue processing and over-diagnosis may have influenced the results from both analyses.

The positive correlation that we found between CFTR mRNA expression and either epithelial mucin expression or mucus plugging does not support our hypothesis since a reduction in CFTR mRNA expression and an increase in mucin expression and mucus plugging of the airways was expected. However, a previous study from Gray et al. [134] showed that normal human tracheobronchial epithelial cells incubated with IL-1 β transiently increased their Muc5ac mRNA expression. IL-1 β also increased CFTR mRNA expression but decreased ENaC mRNA expression [134], meaning that CFTR and Muc5ac expression increase in the same direction. But these results are in contrast to our finding of a positive correlation between β -ENaC or CFTR mRNA in the airway epithelium with epithelial mucin expression. Although we measured Muc5ac mRNA in whole small airways, because this expression did not correlate with epithelial mucin expression or mucus plugging, we did not extend this comparison to that of β -ENaC or CFTR mRNA.

An inverse relationship between CFTR protein expression and mucus plugging might have been observed. “However, and unfortunately, there were difficulties in measuring protein expression of CFTR by immunohistochemistry, including the fact that the availability of

mouse monoclonal antibody that gave specific staining was limited. Despite the use of various conditions of tissue fixation and concentrations of the goat polyclonal antibody to CFTR together with the application of both the ABC and the polymeric methods of staining, we were still unable to localize and quantify the CFTR protein in the small airway epithelium. Successful staining was achieved using mouse monoclonal antibody that is directed at the nucleotide binding domain, of which there are two per CFTR molecule, and that is located in the cytoplasm but not with the goat polyclonal directed at the C-terminus of this protein also located in the cytoplasm (refer to Figure 2.7). Therefore, we suspect that the main source of our problems lies with the goat antibody, either in the epitope it targets or the fact that it is polyclonal so that antibody specific for the effective epitope may be diluted, in contrast to the monoclonal with its single epitope that occurs twice on each CFTR molecule. The difference between the results using the ABC and the polymeric methods with the goat polyclonal, with no staining and excess non-specific staining, respectively, could be due to others factors including the addition of a tertiary rabbit/mouse antibody in the latter, but uncovering the cause this aberrant staining would not be critical if the primary goat polyclonal could not detect the target protein. For these reasons we could not make a correlation between CFTR protein expression and disease severity, gene expression, mucin staining or mucus plugging.

As mentioned in the previous paragraph, our results showed that Muc5ac mRNA expression did not correlate with epithelial mucin expression and mucus plugging. Caramori et al. [86] used immunohistochemistry of MUC5AC and PAS staining to show that the number of goblet cells in bronchiolar epithelium was not significantly different between COPD patients,

smokers and non-smokers. However, they found more mucus plugging in COPD patients compared with smokers with normal lung function and non-smokers. The expression of Muc5ac protein was higher in COPD patients than controls. Voynow et al. (1999) showed that both Muc5ac mRNA and its protein expression were upregulated in A549 cells (human lung carcinoma cell line) by neutrophil elastase [135]. Since it has not been previously shown *in vivo* whether Muc5ac mRNA expression results in similar levels of its protein, it is difficult to compare our results directly with those of Camamori et al. (2004).

There was no correlation between β -ENaC mRNA or β -ENaC protein expression and mucus plugging. Although mucus hypersecretion was found in the airway of β -ENaC over-expressing neonatal mice [23], β -ENaC mRNA or β -ENaC protein expression may not reflect the increase in ENaC activity in obstructive lung disease [136].

Although possible explanations were provided above on why the data did not support our hypothesis, it is possible that the working hypothesis needs to be modified. The gene or protein expression may not have been the appropriate target. Burch et al. [136] showed that mRNA expression of ENaC or the number of ENaC protein in the airway epithelia did not reflect the increase in Na^+ absorption in CF airway epithelia. The activities of these ion channels would be a more useful end-point because it might be more important in, and thus relate more directly, to the disease progression. Ion channel studies including some signaling pathways such as PKA, c-src kinase, or p38 MAPK (refer to section 2.4.4, 2.5 and 2.6.3) may be a good direction to further examine the correlation of ENaC or CFTR and disease severity as well as mucus plugging. On the other hand, many previous studies

showed that the α subunit is a functional channel for ENaC [26, 29], so an investigation of whether the α , or even the γ , subunit of ENaC correlates with disease severity or mucus plugging might be more appropriate.

7.3 Novel finding from this project

Our finding of a highly significant positive correlation between β -ENaC and CFTR mRNA expression in surrounding lung parenchyma and small airway epithelium is novel but somewhat contradictory to those reported in previous studies [137, 138] that showed an inverse relationship between CFTR protein expression and ENaC activity, where a lack of CFTR resulted in increased Na^+ reabsorption. As we did not study β -ENaC activity, which could be different from its mRNA expression, and could not measure CFTR protein effectively, a direct comparison of our results and theirs cannot be made. Lu et al. [139] transfected CFTR into the MDCK cell line expressing $\alpha\beta\gamma$ -ENaC to demonstrate that the stabilizing effect of CFTR on ENaC at plasma membrane is dose dependent, meaning that a certain number of CFTR molecules is required to control ENaC expression at the membrane. These results of parallel levels of protein expression are more in line with ours on mRNA expression. With respect to the transcriptional control of these genes, there are common binding sites for the transcription factors Sp1, AP-1, CREB and GR (glucocorticoid receptor that binds to GRE) in the promoter region of both β -ENaC and CFTR genes (Figure 2.2 and Figure 2.6, respectively) suggesting that their expression may be regulated in a similar way. It is possible that for the control of β -ENaC activity by CFTR [137, 138] to be effective, both proteins need to be present at similar levels on the airway epithelium in agreement with

results from Lu et al. [139] and this may rely on the similar levels of mRNA expression that we found for the two genes in these cells.

7.4 General conclusion

This project focuses on the associations between gene expression, protein expression, epithelial mucin expression, mucus plugging, and disease severity in COPD. The results show a positive correlation between β -ENaC and CFTR mRNA expression, a positive correlation between β -ENaC mRNA and its protein expression, and a significant increase in β -ENaC protein expression with disease severity. These findings suggest that control of β -ENaC activity in the small airway epithelium may differ from its gene expression. Also, there are significant positive correlations between epithelial mucin and CFTR mRNA expression, between mucus plugging and CFTR mRNA expression, even in the absence of a relationship between mucin or mucus plugging and COPD disease severity as well as β -ENaC protein expression in the small airway epithelium. These findings suggest that CFTR may regulate mucin at this site independently of β -ENaC expression. In general, many of our results support the working hypothesis in that β -ENaC mRNA is correlated with its protein expression and that higher protein expression of β -ENaC is seen in more severe COPD. However, further studies should be carried out to address whether other ENaC subunits like α or γ have an effect on the pathogenesis of mucus plugging in COPD or whether mRNA expression of β -ENaC and CFTR are co-regulated.

COPD is a major disease in the world that is caused by inhalation of toxic particles in the indoor and outdoor environment and by tobacco smoking. The airflow limitation in COPD is due to airway obstruction of the small conducting airways. Basically, alteration in lung function can be detected by simple spirometry. However, the clinical signs and symptoms manifest when the disease is in the moderate or advance stages. Since the pattern of expression of β -ENaC and CFTR genes may precede the presence of mucus plugging, early detection of these changes may suggest an alternative more effective treatment for COPD.

References:

1. Petty, T.L., *The history of COPD*. Int J Chron Obstruct Pulmon Dis, 2006. **1**(1): p. 3-14.
2. Petty, T.L., *COPD in perspective*. Chest, 2002. **121**(5 Suppl): p. 116S-120S.
3. Pauwels, R.A., et al., *Global strategy for the diagnosis, management, and prevention of chronic obstructive pulmonary disease. NHLBI/WHO Global Initiative for Chronic Obstructive Lung Disease (GOLD) Workshop summary*. Am J Respir Crit Care Med, 2001. **163**(5): p. 1256-76.
4. Murray, C.J. and A.D. Lopez, *Alternative projections of mortality and disability by cause 1990-2020: Global Burden of Disease Study*. Lancet, 1997. **349**(9064): p. 1498-504.
5. *COPD*. 2008 November 20, 2007 [cited 2008 July 2]; Available from: http://www.lung.ca/diseases-maladies/copd-mpoc/what-quoi/index_e.php.
6. Voelkel, N. and W. MacNee, *Chronic Obstructive Lung Disease*. 2002, Hamilton, Ontario: BC Decker. 428.
7. Silverman, E.K., et al., *Gender-related differences in severe, early-onset chronic obstructive pulmonary disease*. Am J Respir Crit Care Med, 2000. **162**(6): p. 2152-8.
8. Chapman, K.R., *Chronic obstructive pulmonary disease: are women more susceptible than men?* Clin Chest Med, 2004. **25**(2): p. 331-41.
9. Hogg, J.C., et al., *The nature of small-airway obstruction in chronic obstructive pulmonary disease*. N Engl J Med, 2004. **350**(26): p. 2645-53.
10. *Global Strategy for Diagnosis, Management, and Prevention of COPD (updated 2007)*. 2007 [cited; Available from: <http://www.goldcopd.org>].
11. Hogg, J.C., P.T. Macklem, and W.M. Thurlbeck, *Site and nature of airway obstruction in chronic obstructive lung disease*. N Engl J Med, 1968. **278**(25): p. 1355-60.
12. Barnes, P.J., *Chronic obstructive pulmonary disease*. N Engl J Med, 2000. **343**(4): p. 269-80.
13. Hogg, J.C., *Pathophysiology of airflow limitation in chronic obstructive pulmonary disease*. Lancet, 2004. **364**(9435): p. 709-21.
14. Kim, W.D., et al., *The association between small airway obstruction and emphysema phenotypes in COPD*. Chest, 2007. **131**(5): p. 1372-8.
15. Davies, J.C., *Ion transport in lung disease*. Pediatr Pulmonol Suppl, 2004. **26**: p. 147-8.
16. Li, W., Y.J. Xu, and Z.X. Zhang, *[Detection of the mRNA level of the subunits of amiloride-sensitive Na⁺ channel in human bronchial epithelium cells from patients with chronic obstructive pulmonary disease]*. Zhonghua Jie He He Hu Xi Za Zhi, 2004. **27**(8): p. 533-6.
17. Joos, L., P.D. Pare, and A.J. Sandford, *Genetic risk factors of chronic obstructive pulmonary disease*. Swiss Med Wkly, 2002. **132**(3-4): p. 27-37.
18. Gonzalez, J.E., J. Worley, and F. von Goor, *Ion channel assays based on ion and voltage-sensitive fluorescent probes*. 1 ed. Expression and analysis of recombinant ion channels: from structural studies to pharmacological screening ed. J.J. Clare and D.J. Trezise. 2006, Stevenage: Wiley-VCH Verlag GmbH & Co. 187-210.

19. Stryer, L., *Biochemistry*. 4 ed. 2000, New York: W.H. Freeman and Company. 291-300.
20. Dubin, D., *Ion adventure in the heartland*. Vol. 1. 2003, Lancaster: Cover Publishing Co. 376.
21. Cordell, J.L., et al., *Immunoenzymatic labeling of monoclonal antibodies using immune complexes of alkaline phosphatase and monoclonal anti-alkaline phosphatase (APAAP complexes)*. J Histochem Cytochem, 1984. **32**(2): p. 219-29.
22. Mall, M., et al., *Increased airway epithelial Na⁺ absorption produces cystic fibrosis-like lung disease in mice*. Nat Med, 2004. **10**(5): p. 487-93.
23. Mall, M.A., et al., *Development of chronic bronchitis and emphysema in beta-epithelial Na⁺ channel-overexpressing mice*. Am J Respir Crit Care Med, 2008. **177**(7): p. 730-42.
24. Rossier, B.C., et al., *Epithelial sodium channel and the control of sodium balance: interaction between genetic and environmental factors*. Annu Rev Physiol, 2002. **64**: p. 877-97.
25. Kellenberger, S. and L. Schild, *Epithelial sodium channel/degenerin family of ion channels: a variety of functions for a shared structure*. Physiol Rev, 2002. **82**(3): p. 735-67.
26. Canessa, C.M., et al., *Amiloride-sensitive epithelial Na⁺ channel is made of three homologous subunits*. Nature, 1994. **367**(6462): p. 463-7.
27. Lingueglia, E., et al., *Expression cloning of an epithelial amiloride-sensitive Na⁺ channel. A new channel type with homologies to Caenorhabditis elegans degenerins*. FEBS Lett, 1993. **318**(1): p. 95-9.
28. Voilley, N., et al., *The amiloride-sensitive Na⁺ channel: from primary structure to function*. Comp Biochem Physiol A Physiol, 1997. **118**(2): p. 193-200.
29. McDonald, F.J., et al., *Cloning and expression of the beta- and gamma-subunits of the human epithelial sodium channel*. Am J Physiol, 1995. **268**(5 Pt 1): p. C1157-63.
30. Canessa, C.M., J.D. Horisberger, and B.C. Rossier, *Epithelial sodium channel related to proteins involved in neurodegeneration*. Nature, 1993. **361**(6411): p. 467-70.
31. Barbry, P. and P. Hofman, *Molecular biology of Na⁺ absorption*. Am J Physiol, 1997. **273**(3 Pt 1): p. G571-85.
32. Voilley, N., et al., *Cloning, chromosomal localization, and physical linkage of the beta and gamma subunits (SCNN1B and SCNN1G) of the human epithelial amiloride-sensitive sodium channel*. Genomics, 1995. **28**(3): p. 560-5.
33. Thomas, C.P., et al., *Genomic organization of the 5' end of human beta-ENaC and preliminary characterization of its promoter*. Am J Physiol Renal Physiol, 2002. **282**(5): p. F898-909.
34. Thomas, C.P., et al., *5' heterogeneity in epithelial sodium channel alpha-subunit mRNA leads to distinct NH2-terminal variant proteins*. Am J Physiol, 1998. **274**(5 Pt 1): p. C1312-23.
35. Chow, Y.H., et al., *Hormonal regulation and genomic organization of the human amiloride-sensitive epithelial sodium channel alpha subunit gene*. Pediatr Res, 1999. **46**(2): p. 208-14.
36. Thomas, C.P., et al., *Genomic organization and the 5' flanking region of the gamma subunit of the human amiloride-sensitive epithelial sodium channel*. J Biol Chem, 1996. **271**(42): p. 26062-6.

37. Saxena, A., et al., *Gene structure of the human amiloride-sensitive epithelial sodium channel beta subunit*. Biochem Biophys Res Commun, 1998. **252**(1): p. 208-13.
38. Benos, D.J. and B.A. Stanton, *Functional domains within the degenerin/epithelial sodium channel (Deg/ENaC) superfamily of ion channels*. J Physiol, 1999. **520 Pt 3**: p. 631-44.
39. Rao, U.S., et al., *Role of intracellular Ca²⁺ in the expression of the amiloride-sensitive epithelial sodium channel*. Cell Calcium, 2004. **35**(1): p. 21-8.
40. Shimkets, R.A., R. Lifton, and C.M. Canessa, *In vivo phosphorylation of the epithelial sodium channel*. Proc Natl Acad Sci U S A, 1998. **95**(6): p. 3301-5.
41. Ji, H.L., et al., *The cytosolic termini of the beta- and gamma-ENaC subunits are involved in the functional interactions between cystic fibrosis transmembrane conductance regulator and epithelial sodium channel*. J Biol Chem, 2000. **275**(36): p. 27947-56.
42. Johnson, M.D., et al., *Functional ion channels in pulmonary alveolar type I cells support a role for type I cells in lung ion transport*. Proc Natl Acad Sci U S A, 2006. **103**(13): p. 4964-9.
43. Talbot, C.L., et al., *Quantitation and localization of ENaC subunit expression in fetal, newborn, and adult mouse lung*. Am J Respir Cell Mol Biol, 1999. **20**(3): p. 398-406.
44. Champigny, G., et al., *Regulation of expression of the lung amiloride-sensitive Na⁺ channel by steroid hormones*. Embo J, 1994. **13**(9): p. 2177-81.
45. Roux, J., et al., *Interleukin-1beta decreases expression of the epithelial sodium channel alpha-subunit in alveolar epithelial cells via a p38 MAPK-dependent signaling pathway*. J Biol Chem, 2005. **280**(19): p. 18579-89.
46. Itani, O.A., et al., *Glucocorticoid-stimulated lung epithelial Na⁽⁺⁾ transport is associated with regulated ENaC and sgkl expression*. Am J Physiol Lung Cell Mol Physiol, 2002. **282**(4): p. L631-41.
47. Huang, P., et al., *Local regulation of cystic fibrosis transmembrane regulator and epithelial sodium channel in airway epithelium*. Proc Am Thorac Soc, 2004. **1**(1): p. 33-7.
48. Pochynyuk, O., et al., *Regulation of the epithelial Na⁺ channel (ENaC) by phosphatidylinositides*. Am J Physiol Renal Physiol, 2006. **290**(5): p. F949-57.
49. Kunzelmann, K., et al., *Purinergic inhibition of the epithelial Na⁺ transport via hydrolysis of PIP₂*. Faseb J, 2005. **19**(1): p. 142-3.
50. Yue, G., et al., *Phosphatidylinositol 4,5-bisphosphate (PIP₂) stimulates epithelial sodium channel activity in A6 cells*. J Biol Chem, 2002. **277**(14): p. 11965-9.
51. Caldwell, R.A., R.C. Boucher, and M.J. Stutts, *Neutrophil elastase activates near-silent epithelial Na⁺ channels and increases airway epithelial Na⁺ transport*. Am J Physiol Lung Cell Mol Physiol, 2005. **288**(5): p. L813-9.
52. Hughey, R.P., et al., *Epithelial sodium channels are activated by furin-dependent proteolysis*. J Biol Chem, 2004. **279**(18): p. 18111-4.
53. Hughey, R.P., et al., *Distinct pools of epithelial sodium channels are expressed at the plasma membrane*. J Biol Chem, 2004. **279**(47): p. 48491-4.
54. Kleyman, T.R. and E.J. Cragoe, Jr., *The mechanism of action of amiloride*. Semin Nephrol, 1988. **8**(3): p. 242-8.
55. Kleyman, T.R., et al., *Mechanism of action of amiloride: a molecular prospective*. Semin Nephrol, 1999. **19**(6): p. 524-32.

56. Staub, O., et al., *Regulation of stability and function of the epithelial Na⁺ channel (ENaC) by ubiquitination*. *Embo J*, 1997. **16**(21): p. 6325-36.
57. Wiemuth, D., et al., *Epithelial sodium channel (ENaC) is multi-ubiquitinated at the cell surface*. *Biochem J*, 2007. **405**(1): p. 147-55.
58. Malik, B., et al., *Regulation of epithelial sodium channels by the ubiquitin-proteasome proteolytic pathway*. *Am J Physiol Renal Physiol*, 2006. **290**(6): p. F1285-94.
59. Staub, O., et al., *Immunolocalization of the ubiquitin-protein ligase Nedd4 in tissues expressing the epithelial Na⁺ channel (ENaC)*. *Am J Physiol*, 1997. **272**(6 Pt 1): p. C1871-80.
60. Staub, O., et al., *Regulation of the epithelial Na⁺ channel by Nedd4 and ubiquitination*. *Kidney Int*, 2000. **57**(3): p. 809-15.
61. Staub, O., et al., *WW domains of Nedd4 bind to the proline-rich PY motifs in the epithelial Na⁺ channel deleted in Liddle's syndrome*. *Embo J*, 1996. **15**(10): p. 2371-80.
62. Peters, K.W., et al., *Role of snare proteins in CFTR and ENaC trafficking*. *Pflugers Arch*, 2001. **443 Suppl 1**: p. S65-9.
63. Ungar, D. and F.M. Hughson, *SNARE protein structure and function*. *Annu Rev Cell Dev Biol*, 2003. **19**: p. 493-517.
64. Riordan, J.R., et al., *Identification of the cystic fibrosis gene: cloning and characterization of complementary DNA*. *Science*, 1989. **245**(4922): p. 1066-73.
65. Schwiebert, E.M., et al., *CFTR is a conductance regulator as well as a chloride channel*. *Physiol Rev*, 1999. **79**(1 Suppl): p. S145-66.
66. Chou, J.L., R. Rozmahel, and L.C. Tsui, *Characterization of the promoter region of the cystic fibrosis transmembrane conductance regulator gene*. *J Biol Chem*, 1991. **266**(36): p. 24471-6.
67. McCarthy, V.A. and A. Harris, *The CFTR gene and regulation of its expression*. *Pediatr Pulmonol*, 2005. **40**(1): p. 1-8.
68. Li, H., et al., *The cystic fibrosis transmembrane conductance regulator Cl⁻ channel: a versatile engine for transepithelial ion transport*. *Sheng Li Xue Bao*, 2007. **59**(4): p. 416-430.
69. Dahan, D., et al., *Regulation of the CFTR channel by phosphorylation*. *Pflugers Arch*, 2001. **443 Suppl 1**: p. S92-6.
70. Engelhardt, J.F., et al., *Submucosal glands are the predominant site of CFTR expression in the human bronchus*. *Nat Genet*, 1992. **2**(3): p. 240-8.
71. Engelhardt, J.F., et al., *Expression of the cystic fibrosis gene in adult human lung*. *J Clin Invest*, 1994. **93**(2): p. 737-49.
72. Stutts, M.J., et al., *CFTR as a cAMP-dependent regulator of sodium channels*. *Science*, 1995. **269**(5225): p. 847-50.
73. Li, S., et al., *Transcriptional repression of the cystic fibrosis transmembrane conductance regulator gene, mediated by CCAAT displacement protein/cut homolog, is associated with histone deacetylation*. *J Biol Chem*, 1999. **274**(12): p. 7803-15.
74. Li, S., et al., *Regulation of the homeodomain CCAAT displacement/cut protein function by histone acetyltransferases p300/CREB-binding protein (CBP)-associated factor and CBP*. *Proc Natl Acad Sci U S A*, 2000. **97**(13): p. 7166-71.

75. Guggino, W.B. and B.A. Stanton, *New insights into cystic fibrosis: molecular switches that regulate CFTR*. Nat Rev Mol Cell Biol, 2006. **7**(6): p. 426-36.
76. Heda, G.D., M. Tanwani, and C.R. Marino, *The Delta F508 mutation shortens the biochemical half-life of plasma membrane CFTR in polarized epithelial cells*. Am J Physiol Cell Physiol, 2001. **280**(1): p. C166-74.
77. Farinha, C.M., et al., *Biochemical methods to assess CFTR expression and membrane localization*. J Cyst Fibros, 2004. **3 Suppl 2**: p. 73-7.
78. Ward, C.L., S. Omura, and R.R. Kopito, *Degradation of CFTR by the ubiquitin-proteasome pathway*. Cell, 1995. **83**(1): p. 121-7.
79. Meacham, G.C., et al., *The Hsc70 co-chaperone CHIP targets immature CFTR for proteasomal degradation*. Nat Cell Biol, 2001. **3**(1): p. 100-5.
80. Randell, S.H. and R.C. Boucher, *Effective mucus clearance is essential for respiratory health*. Am J Respir Cell Mol Biol, 2006. **35**(1): p. 20-8.
81. Konig, J., et al., *The cystic fibrosis transmembrane conductance regulator (CFTR) inhibits ENaC through an increase in the intracellular Cl⁻ concentration*. EMBO Rep, 2001. **2**(11): p. 1047-51.
82. Kunzelmann, K., *ENaC is inhibited by an increase in the intracellular Cl⁻ concentration mediated through activation of Cl⁻ channels*. Pflugers Arch, 2003. **445**(4): p. 504-12.
83. Wine, J.J., *The genesis of cystic fibrosis lung disease*. J Clin Invest, 1999. **103**(3): p. 309-12.
84. Kunzelmann, K., et al., *Inhibition of epithelial Na⁺ currents by intracellular domains of the cystic fibrosis transmembrane conductance regulator*. FEBS Lett, 1997. **400**(3): p. 341-4.
85. Boucher, R.C., *Relationship of airway epithelial ion transport to chronic bronchitis*. Proc Am Thorac Soc, 2004. **1**(1): p. 66-70.
86. Caramori, G., et al., *Mucin expression in peripheral airways of patients with chronic obstructive pulmonary disease*. Histopathology, 2004. **45**(5): p. 477-84.
87. Williams, O.W., et al., *Airway mucus: From production to secretion*. Am J Respir Cell Mol Biol, 2006. **34**(5): p. 527-36.
88. Hogg, J.C., et al., *Survival after lung volume reduction in chronic obstructive pulmonary disease: insights from small airway pathology*. Am J Respir Crit Care Med, 2007. **176**(5): p. 454-9.
89. Kim, K.C., et al., *Airway goblet cell mucin: its structure and regulation of secretion*. Eur Respir J, 1997. **10**(11): p. 2644-9.
90. Voynow, J.A., S.J. Gendler, and M.C. Rose, *Regulation of mucin genes in chronic inflammatory airway diseases*. Am J Respir Cell Mol Biol, 2006. **34**(6): p. 661-5.
91. Fujisawa, T., et al., *Involvement of the p38 MAPK pathway in IL-13-induced mucous cell metaplasia in mouse tracheal epithelial cells*. Respirology, 2008. **13**(2): p. 191-202.
92. Li, D., et al., *Cloning of the amino-terminal and 5'-flanking region of the human MUC5AC mucin gene and transcriptional up-regulation by bacterial exoproducts*. J Biol Chem, 1998. **273**(12): p. 6812-20.
93. Woolley, A.T. and R.A. Mathies, *Ultra-high-speed DNA fragment separations using microfabricated capillary array electrophoresis chips*. Proc Natl Acad Sci U S A, 1994. **91**(24): p. 11348-52.

94. Salowsky, R. and A. Henger, *High sensitivity quality control of RNA samples using the RNA 6000 Pico LabChip kit*. 2001.
95. Effenhauser, C.S., et al., *High-speed separation of antisense oligonucleotides on a micromachined capillary electrophoresis device*. *Anal Chem*, 1994. **66**: p. 2949-53.
96. Kuschel, M., *Analysis of total RNA using Agilent 2100 bioanalyzer and the RNA 6000 LabChip kit*. 2002.
97. Lightfoot, S., *Quantitation comparison of total RNA using the Agilent 2100 bioanalyzer, ribogreen analysis and UV spectrometry*. 2002.
98. Mueller, O., S. Lightfoot, and A. Schroeder, *RNA integrity number (RIN)-standardization of RNA quality control*. 2004.
99. Imbeaud, S., et al., *Towards standardization of RNA quality assessment using user-independent classifiers of microcapillary electrophoresis traces*. *Nucleic Acids Res*, 2005. **33**(6): p. e56.
100. Matz, M., et al., *Amplification of cDNA ends based on template-switching effect and step-out PCR*. *Nucleic Acids Res*, 1999. **27**(6): p. 1558-60.
101. Cheng, S., et al., *Effective amplification of long targets from cloned inserts and human genomic DNA*. *Proc Natl Acad Sci U S A*, 1994. **91**(12): p. 5695-9.
102. Zhu, Y.Y., et al., *Reverse transcriptase template switching: a SMART approach for full-length cDNA library construction*. *Biotechniques*, 2001. **30**(4): p. 892-7.
103. Kellogg, D.E., et al., *TaqStart Antibody: "hot start" PCR facilitated by a neutralizing monoclonal antibody directed against Taq DNA polymerase*. *Biotechniques*, 1994. **16**(6): p. 1134-7.
104. Mackay, I.M., K.E. Arden, and A. Nitsche, *Real-time PCR in virology*. *Nucleic Acids Res*, 2002. **30**(6): p. 1292-305.
105. Bustin, S.A., et al., *Quantitative real-time RT-PCR--a perspective*. *J Mol Endocrinol*, 2005. **34**(3): p. 597-601.
106. Wong, M.L. and J.F. Medrano, *Real-time PCR for mRNA quantitation*. *Biotechniques*, 2005. **39**(1): p. 75-85.
107. Dorak, T., *Real Time PCR (BIOS Advanced Methods) Relative quantification*, ed. M.W. Pfaffl. 2006, New York: Taylor & Francis Group. 329.
108. Hellems, J., et al., *qBase relative quantification framework and software for management and automated analysis of real-time quantitative PCR data*. *Genome Biol*, 2007. **8**(2): p. R19.
109. Bustin, S.A., *Absolute quantification of mRNA using real-time reverse transcription polymerase chain reaction assays*. *J Mol Endocrinol*, 2000. **25**(2): p. 169-93.
110. Pfaffl, M.W. and M. Hageleit, *Validities of mRNA quantification using recombinant RNA and recombinant DNA external calibration curves in real-time RT-PCR*. *Biotechnol Lett*, 2001. **23**: p. 275-82.
111. Kiernan, J., *Histological & Histochemical Methods Theory and Practice*. Third ed. 2002, London: Arnold, a member of the Hodder Headline Group. 502.
112. Burnett, R., Y. Guichard, and E. Barale, *Immunohistochemistry for light microscopy in safety evaluation of therapeutic agents: an overview*. *Toxicology*, 1997. **119**(1): p. 83-93.
113. Nakane, P.K. and G.B. Pierce, Jr., *Enzyme-labeled antibodies: preparation and application for the localization of antigens*. *J Histochem Cytochem*, 1966. **14**(12): p. 929-31.

114. Mason, D.Y. and R. Sammons, *Alkaline phosphatase and peroxidase for double immunoenzymatic labelling of cellular constituents*. J Clin Pathol, 1978. **31**(5): p. 454-60.
115. Hsu, S.M., L. Raine, and H. Fanger, *The use of antiavidin antibody and avidin-biotin-peroxidase complex in immunoperoxidase technics*. Am J Clin Pathol, 1981. **75**(6): p. 816-21.
116. Hsu, S.M., L. Raine, and H. Fanger, *Use of avidin-biotin-peroxidase complex (ABC) in immunoperoxidase techniques: a comparison between ABC and unlabeled antibody (PAP) procedures*. J Histochem Cytochem, 1981. **29**(4): p. 577-80.
117. Wiedorn, K.H., et al., *EnVision+, a new dextran polymer-based signal enhancement technique for in situ hybridization (ISH)*. J Histochem Cytochem, 2001. **49**(9): p. 1067-71.
118. Vosse, B.A., et al., *Background staining of visualization systems in immunohistochemistry: comparison of the Avidin-Biotin Complex system and the EnVision+ system*. Appl Immunohistochem Mol Morphol, 2007. **15**(1): p. 103-7.
119. Ding, L., et al., *A lung tissue bank for gene expression studies in chronic obstructive pulmonary disease*. Copd, 2004. **1**(2): p. 191-204.
120. Gosselink, J., et al., *Gene expression of peripheral lung remodeling in COPD*. Am J Respir Crit Care Med 2008. **177**: p. A656.
121. Emmert-Buck, M.R., et al., *Laser capture microdissection*. Science, 1996. **274**(5289): p. 998-1001.
122. Eltoun, I.A., G.P. Siegal, and A.R. Frost, *Microdissection of histologic sections: past, present, and future*. Adv Anat Pathol, 2002. **9**(5): p. 316-22.
123. Bonner, R.F., et al., *Laser capture microdissection: molecular analysis of tissue*. Science, 1997. **278**(5342): p. 1481,1483.
124. Gosselink, J.V., et al., *Evaluation of small sample cDNA amplification for microdissected airway expression profiling in COPD*. Copd, 2007. **4**(2): p. 91-105.
125. Foster, T., *Energiewanderung und Fluoreszenz*. Annalen der Physik, 1948. **2**: p. 55-75.
126. Proudnikov, D., et al., *Optimizing primer--probe design for fluorescent PCR*. J Neurosci Methods, 2003. **123**(1): p. 31-45.
127. Matthews, R.P. and G.S. McKnight, *Characterization of the cAMP response element of the cystic fibrosis transmembrane conductance regulator gene promoter*. J Biol Chem, 1996. **271**(50): p. 31869-77.
128. Ullmann, A., F. Jacob, and J. Monod, *Characterization by in vitro complementation of a peptide corresponding to an operator-proximal segment of the beta-galactosidase structural gene of Escherichia coli*. J Mol Biol, 1967. **24**(2): p. 339-43.
129. Ausubel, F.M., et al., *Current Protocols in Molecular Biology*. Selected Topics from Classical Bacterial Genetics, ed. K. Janssen. Vol. 1. 1994, Massachusetts: John Wiley & Sons. Inc.
130. Gaillard, D., et al., *Early expression of beta- and gamma-subunits of epithelial sodium channel during human airway development*. Am J Physiol Lung Cell Mol Physiol, 2000. **278**(1): p. L177-84.
131. Kartner, N. and J.R. Riordan, *Characterization of polyclonal and monoclonal antibodies to cystic fibrosis transmembrane conductance regulator*. Methods Enzymol, 1998. **292**: p. 629-52.

132. Bangel, N., et al., *Upregulated expression of ENaC in human CF nasal epithelium*. J Cyst Fibros, 2008. **7**(3): p. 197-205.
133. Fleige, S. and M.W. Pfaffl, *RNA integrity and the effect on the real-time qRT-PCR performance*. Mol Aspects Med, 2006. **27**(2-3): p. 126-39.
134. Gray, T., et al., *Regulation of MUC5AC mucin secretion and airway surface liquid metabolism by IL-1beta in human bronchial epithelia*. Am J Physiol Lung Cell Mol Physiol, 2004. **286**(2): p. L320-30.
135. Voynow, J.A., et al., *Neutrophil elastase increases MUC5AC mRNA and protein expression in respiratory epithelial cells*. Am J Physiol, 1999. **276**(5 Pt 1): p. L835-43.
136. Burch, L.H., et al., *Relative expression of the human epithelial Na⁺ channel subunits in normal and cystic fibrosis airways*. Am J Physiol, 1995. **269**(2 Pt 1): p. C511-8.
137. Stutts, M.J., B.C. Rossier, and R.C. Boucher, *Cystic fibrosis transmembrane conductance regulator inverts protein kinase A-mediated regulation of epithelial sodium channel single channel kinetics*. J Biol Chem, 1997. **272**(22): p. 14037-40.
138. Reddy, M.M., M.J. Light, and P.M. Quinton, *Activation of the epithelial Na⁺ channel (ENaC) requires CFTR Cl⁻ channel function*. Nature, 1999. **402**(6759): p. 301-4.
139. Lu, C., et al., *CFTR stabilizes ENaC at the plasma membrane*. J Cyst Fibros, 2007. **6**(6): p. 419-22.

Appendix

UBC research ethics board certificate of approval



PROVIDENCE HEALTH CARE
Research Institute

UBC-Providence Health Care Research
Institute
Office of Research Services
11th Floor Hornby Site - SPH
c/o 1081 Burrard St.
Vancouver, BC V6Z 1Y6
Tel: (604) 806-8567
Fax: (604) 806-8568

ETHICS CERTIFICATE OF EXPEDITED APPROVAL: ANNUAL RENEWAL

PRINCIPAL INVESTIGATOR: James C. Hogg	DEPARTMENT: UBC/Medicine, Faculty of Pathology & Laboratory Medicine	UBC-PHC REB NUMBER: H05-50147
INSTITUTION(S) WHERE RESEARCH WILL BE CARRIED OUT:		
Institution Providence Health Care	Site St. Paul's Hospital	
Other locations where the research will be conducted: N/A		
CO-INVESTIGATOR(S): N/A		
SPONSORING AGENCIES: British Columbia Lung Association - "Regulation of mucous secretion and clearance in small airways in chronic obstructive pulmonary disease"		
PROJECT TITLE: Regulation of mucous secretion and clearance in small airways in chronic obstructive pulmonary disease		

EXPIRY DATE OF THIS APPROVAL: July 15, 2009

APPROVAL DATE: July 15, 2008

CERTIFICATION:

1. The membership of the UBC-PHC REB complies with the membership requirements for research ethics boards defined in Part C Division 5 of the Food and Drug Regulations of Canada.
2. The UBC-PHC REB carries out its functions in a manner fully consistent with Good Clinical Practices.
3. The UBC-PHC REB has reviewed and approved the research project named on this Certificate of Approval including any associated consent form and taken the action noted above. This research project is to be conducted by the principal investigator named above at the specified research site(s). This review of the UBC-PHC REB have been documented in writing.

The UBC-PHC Research Ethics Board Chair or Associate Chair, has reviewed the documentation for the above named project. The research study, as presented in the documentation, was found to be acceptable on ethical grounds for research involving human subjects and was approved for renewal.

Approval of the UBC-PHC Research Ethics Board or Associate Chair, verified by the signature of one of the following:

Dr. I. Fedoroff,
Chair

Dr. J. Kernahan,
Associate Chair

Dr. Kuo-Hsing Kuo,
Associate Chair